

POLITECNICO DI MILANO  
School of Industrial and Information Engineering  
M. Sc. Programme in Automation and Control Engineering

# Comparative Assessment and Improvement of Pneumatic Artificial Muscles Modelling

Master Thesis

**Branislav Stojanović**

Matr. 858716

Supervision: Prof. Dr. Gianantonio Magnani, Politecnico di Milano  
Dr. Dragoljub Šurdilović, Fraunhofer IPK

2017/2018

Correspondence:

[branislav.v.s@gmail.com](mailto:branislav.v.s@gmail.com)



**POLITECNICO**  
MILANO 1863

 **Fraunhofer**  
IPK



*"The Earth has music for those who listen."*

---

George Santayana



# Acknowledgments

I would first like to thank my tutor Dr. Dragoljub Šurdilović, for sharing his expertise and valuable guidance, leading me in the right direction throughout this venture. The ideas, useful critiques and advises that I received about and, as well, apart from this work, inspired me to further explore this scientific field, showing me the meaning of the word "tutor".

Furthermore, I am deeply grateful to my academic supervisor Prof. Dr. Gianantonio Magnani, from Politecnico di Milano ([POLIMI](#)), for giving me the chance of working on my thesis in Fraunhofer Institute for Production Systems and Design Technology ([IPK](#)).

I want to thank Jelena Radojičić for her willingness and effort in assistance in keeping my progress on schedule and making accurate and useful corrections while reading the thesis.

I would also like to extend thanks to all my friends from Milan, for being my family abroad and for making these two years memorable. Special thanks to my best friend Jovana, without whose moral support I wouldn't be there.

Finally, I must express profound gratitude to my parents, my brother and to my sister for giving me unfailing support, continuous encouragement and love during the years of my study and through the process of working on this thesis. This accomplishment would not be possible without them.



# Abstract

In the last two decades, a lot of attention has been focused on Pneumatic Artificial Muscles (PAM) because of their clear advantages, such as inherent compliance, structural flexibility to working environments, compactness, low cost and excellent power to weight ratio compared to other, of the same kind, actuators. Having all the advantages of traditional pneumatic actuators (cylinders) without the main drawback (power/weight ratio) some researchers were euphoric with the idea to replace pneumatic cylinders with PAMs in many applications. Against big expectations, however, pneumatic muscles bring many difficulties as well. The need for a pair of them to have a degree of freedom and highly variable and nonlinear characteristics, which require complex modelling and sophisticated control design for achieving high system performance, have significantly reduced this plan. Still, PAMs have its application importance in the field of interactive robotic devices and rehab systems, but the common belief is that, with finding an appropriate mathematical model, this field will be much more outspread.

The main goal of this thesis is to investigate the performance of different approaches to PAM modelling, seeking for a universal model that can be used to control a cable driven robotic system (CDRS), which includes PAM actuators with various dimensions instead of cables.

Firstly, an experimental setup capable of performing all relevant examinations of fluidic muscles tests (isometric, isobaric, isotonic), including muscle's dynamic response test, has been designed. Furthermore, a set of modelling approaches has been analyzed and the comparison between them has been outlined. Therefore, the most suitable model is proposed and evaluated by implementation in the chosen control method.

The proposed strategy shows acceptable results in variables prediction, which is proven with successful control simulation. Furthermore, this mathematical model showed a tendency towards valuable results when cross-validation of model parameters, obtained from different dimensions PAMs, was done. Therefore, we believe that further development of this approach is justified, essentially improving the robustness of the model to actuators variability, as well as including real situation phenomena that in this work were not considered.



# Sommario

Nelle ultime due decadi, si è rivolta particolare attenzione ai Muscoli Artificiali Pneumatici (MAP) per gli evidenti vantaggi che presentano, tra cui intrinseca reattività, flessibilità strutturale in ambienti lavorativi, compattezza, basso costo ed ottimo rapporto peso/potenza rispetto ad altri attuatori dello stesso tipo. Dal momento che presentano tutti i vantaggi degli attuatori pneumatici tradizionali (cilindrici) senza l'inconveniente principale (rapporto potenza/peso), ad alcuni ricercatori è apparsa interessante la possibilità di sostituire i cilindri tradizionali con i MAP in svariate applicazioni. D'altra parte i muscoli pneumatici presentano varie difficoltà. A deludere notevolmente le aspettative sono il fatto che è necessaria almeno una coppia di questi muscoli per realizzare un grado di libertà e le loro caratteristiche altamente variabili e non lineari, che richiedono una modellazione complessa e un sofisticato sistema di controllo per ottenere prestazioni elevate. Tuttavia i MAP trovano importante applicazione nell'ambito dei dispositivi di robotica interattiva e dei sistemi di riabilitazione e si crede che una volta identificato un modello matematico adeguato, questo campo si possa espandere molto di più.

Il principale obiettivo di questa tesi è quello di analizzare le prestazioni dei diversi approcci alla modellazione dei MAP e cercare di identificare un modello universale che possa essere utilizzato per controllare un sistema robotico cablato (SRC) che includa attuatori MAP di varie dimensioni piuttosto che cavi. In primo luogo, è stata progettata una configurazione sperimentale in grado di eseguire tutti i test più rilevanti per i muscoli fluidici (isometrici, isobarici, isotonici), tra cui il test di risposta dinamica del muscolo. Inoltre, il modello più adeguato è proposto e valutato con la sua implementazione nel metodo di controllo scelto.

La strategia proposta mostra risultati accettabili nella predizione delle variabili, come dimostrato efficacemente mediante simulazione. Inoltre, questo modello matematico ha mostrato di fornire risultati validi in validazioni incrociate, ottenuta da MAP di diverse dimensioni, dei parametri del modello. Pertanto, crediamo in un ulteriore sviluppo di questo approccio migliorando essenzialmente la robustezza del modello rispetto alla variabilità degli attuatori, includendo fenomeni presenti in situazioni reali che in questo lavoro non sono stati considerati.



# Contents

<b>1</b>	<b>Introduction</b>	<b>1</b>
1.1	STRING-MAN	3
1.2	Diploma thesis goals and organization	5
<b>2</b>	<b>Fundamentals</b>	<b>7</b>
2.1	Fluidic Muscles	7
2.1.1	Properties	9
2.2	Classification of PAMs	12
2.2.1	Braided muscles	12
2.2.2	Pleated muscles	13
2.2.3	Netted muscles	13
2.2.4	Embedded muscles	14
2.3	FESTO fluidic muscles	16
<b>3</b>	<b>Modeling of Pneumatic Muscles</b>	<b>19</b>
3.1	Geometrical modeling	19
3.2	Empirical modeling	25
3.3	Phenomenological modeling	26
3.4	Summary	28
<b>4</b>	<b>Experimental Modeling of FESTO Fluidic Muscles</b>	<b>29</b>
4.1	Requirements and design of the experimental setup	29
4.1.1	Setup description	31
4.2	Experimental analysis of operational characteristic of PAM	36
4.2.1	Isotonic experiments	36
4.2.2	Isobaric experiments	41
4.2.3	Isometric experiments	42
4.3	Experimental implementation of different modeling methods	43
4.3.1	Empirical "Virtual Area" Model	43
4.3.2	Empirical "Spring" Model	49
4.3.3	Geometrical models	53
4.4	Dynamic experiments	65
<b>5</b>	<b>Controller Synthesis for Model Verification</b>	<b>69</b>
5.1	Model implementation	69
5.2	Model of the proportional valve	71
5.3	Controller design	71
5.4	Evaluation	74
<b>6</b>	<b>Conclusion</b>	<b>81</b>
6.1	Future Research	82
	<b>Bibliography</b>	<b>83</b>
	<b>List of Figures</b>	<b>89</b>
	<b>List of Tables</b>	<b>93</b>



# 1

## Introduction

Actuators, i.e., driving systems, represent a very important part in all automation processes and have the goal to transform one form of energy into mechanical motion. Their characteristics are expressed through indicators like power (i.e., power/weight and power/volume ratios), static and dynamic characteristic of drive force (momentum), principle of work and structure, controllability, reliability, response time, velocity, dimensions, efficiency, rigidity (i.e., compliance), price, maintenance, etc. To run a mechanical system, various technical principles have been developed: systems with internal/external combustion, hydraulic systems, electrical drives, pneumatic systems. Every of these driving techniques has a field of application in which it has proven to be particularly convenient. However, the fact, that there is still the whole series of driving systems for different use, proves difficulty or impossibility of developing actuator for universal applications in all the environments.

In traditional industrial robotics, the majority of tasks are successfully realized with electrical drives, primary, with the alternate current. With time, the field of robotic application was expanding, making new demands, imposing new constraints for actuator systems. Nowadays, robotics applications based on human interaction are of special importance, which brings moving from regular electromotor drive to novel biomimetic actuators. With this it comes to change, not only in view of energy transformation but also in material that actuator is made of, in order to realize biologically inspired, functional movement, which is in the same time safe and redundant. Having new demands, it is clear that electrical drives are losing the reputation of the universally best solution, and that the need for developing also new types is rising.

In case of a system needed to repeat simpler motions, having high power/weight ratio, self-cooling and relatively expressed temperature insensitivity, it implies as logical, to choose from many of pneumatic actuators. Besides that, compared to traditional electric and hydraulic actuators, pneumatic actuators have the high level of compliance which comes from compressibility of the gas. The mostly used pneumatic actuators are pneumatic cylinders. A large number of cylinder kinds exists, as well as applied control techniques. Although widespread, well-known and always available, pneumatic cylinders, even if fulfilling previously mentioned criteria, are not always an ideal solution even in fields where their characteristics are in advantage comparing to characteristics of some other actuators. To cover all specific practical problems, many efforts are invested in discovering new sorts of actuators, not only to improve or push down existing, rather use them together in future applications. Among such novel actuators, until now, biggest success is achieved with variations of pneumatic artificial muscles. Pneumatic artificial muscles cover field which has a good background for inventing different constructive solutions for many robotic applications. Pneumatic muscles found the biggest use in the field of Biorobotics and Medical applications [1], and some of them are presented in the figures 1.1 and 1.2:

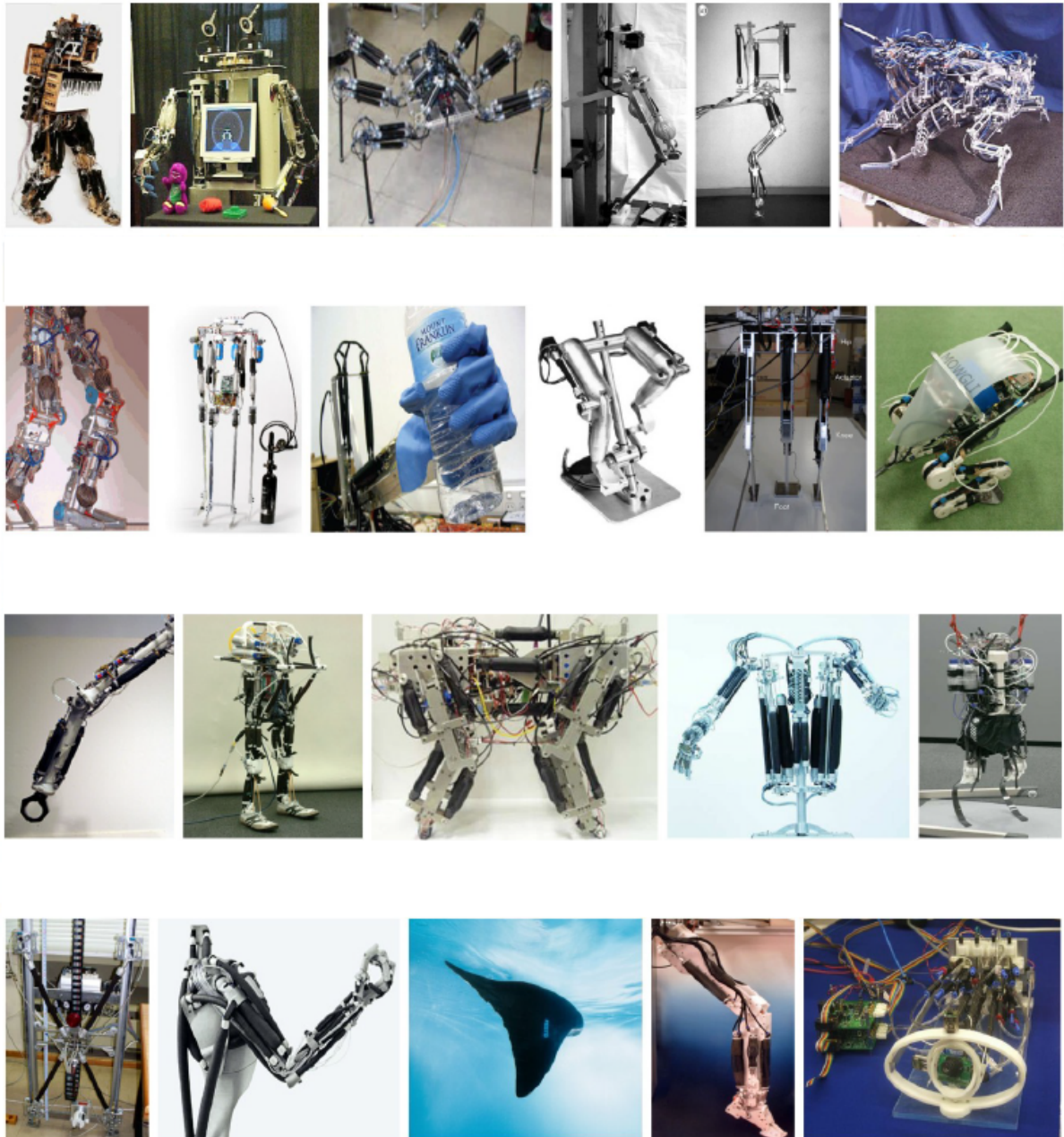


Figure 1.1: **Biorobotic applications of PAMs** (respectively): (1)Shadow biped walker; (2)Isac [2]; (3)Airbug [3]; (4)Hopping robot [4]; (5)Panther leg [5]; (6)Ajax [6]; (7)Lucy [7]; (8)Stumpy [8]; (9)Low cost humanoid hand [9]; (10)Pneumatic bicycle [10]; (11)Three-legged robot [11]; (12)Mowgli [12]; (13)Robotic arm; (14)Bipedal robot [13]; (15)Quadruped robo [14]; (16)Pneumatic torso [15]; (17)Pneumatic athlete robot [16]; (18)Pneumatic climbing robot [17]; (19)Airic's arm; (20)Aqua Ray; (21)Shadow robot leg; (22)Robotic eye with pneumatic actuation [18]

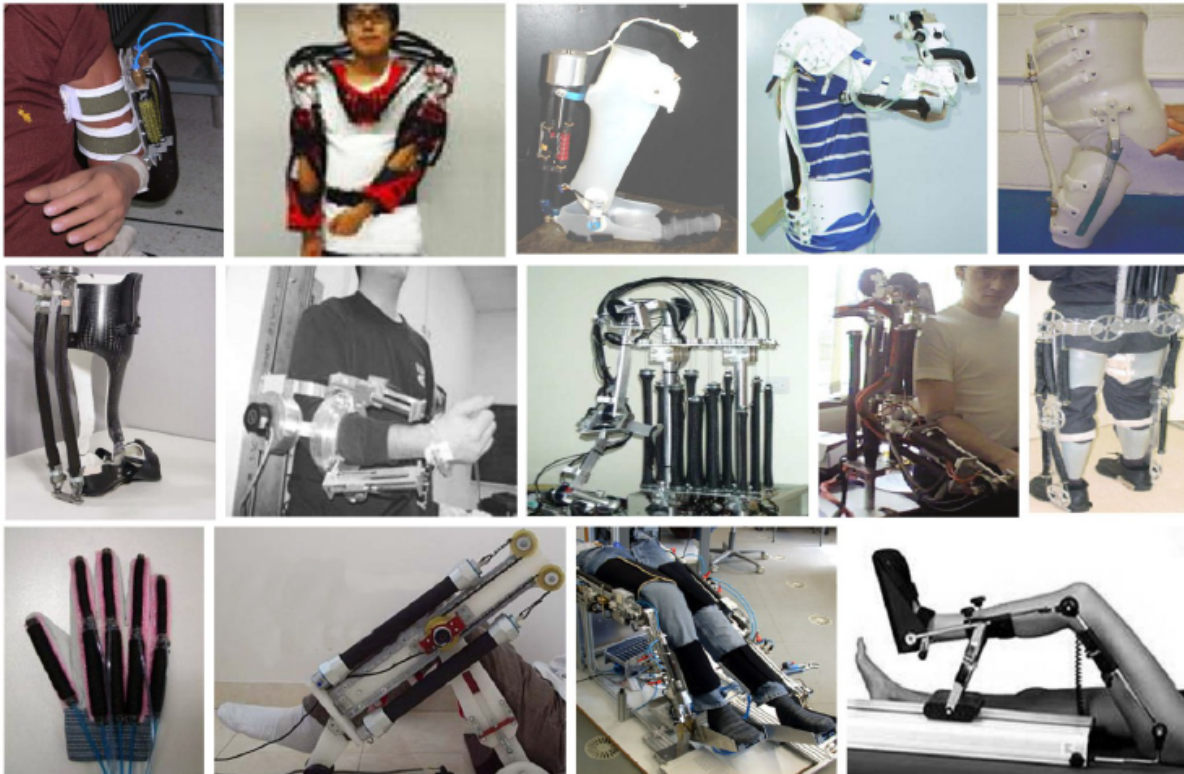


Figure 1.2: **Medical applications of PAMs** (respectively): (1)PAM-actuated forearm [19],[20]; (2)Muscle suit [21]; (3)Powered-ankle foot orthosis [22]; (4)Rupert [23],[24]; (5)Pneumatic hip orthosis [25]; (6)Pneumatic foot orthosis [26],[27],[28]; (7)Haptic arm exoskeleton [29]; (8)Upper body exoskeleton [30]; (9)Upper body exoskeleton [31]; (10)Lower body exoskeleton [32]; (11)Pneumatic power assist glove [33]; (12)Knee rehabilitation device [34]; (13)Orthosis for home training [35]; (14)Isokinetic equipment for recovery exercises [36]

## 1.1. STRING-MAN

“STRING-MAN” [37] is a rehabilitation robot designed as a cable-driven parallel robot (CDPR), which has favorable applicability because of its high dynamics and lightweights, for assisting the locomotion recovery therapy and training. This concept, established on the string-puppet idea, opens new possibilities for assisting restoration of posture balancing and gait motoric functions 1.3.

Even though “STRING-MAN” concept actuates with low-power actuators and poses robust compliance control during operation, the safety issues are still critical and require a sophisticated solution to prevent risks on the patient. The new idea utilizes PAM drives and string-puppet idea used in “STRING-MAN”, substituting wires with pneumatic muscles, where contractions of the muscle produce variations of “active wire” lengths and requested balancing motion and weight bearing. Due to the characteristic of PAMs, that with increasing of the pressure realized force is decreasing, in the case of sudden uncontrolled pressure overrun the force tends to zero, thus making the system inherently safe. The muscles provide a minimum of physical compliance, which can be further adjusted by means of compliance control, that would make redundant safety, which is, in general, the best solution. Another reason for implementing pneumatic muscles is that actuators which are used for prosthesis or orthosis should, in some way, replace muscle function, performing contractions and extensions, thereby realizing motion. Technically it is not possible to realize the fibril structure of biological muscle, but it is possible to imitate its inherent functionality. Beside pneumatic, there are application attempts of other types of actuators which are mimicking biological muscles. However, none of these did achieve motion that has “softness” of biological muscle. The concept of a novel, referred to as “SMART-STRING” module [37], under development at Fraunhofer IPK, is presented in Figure 1.4.



Figure 1.3: **STRING-MAN configuration**



Figure 1.4: **Integrated Wire-Robot – Active weight balancing and leg moving modules with 10 PAMs**

Moreover, additional modules can be applied for leg motion and integrate into an overall gait rehabilitation system (Figure 1.4). Considering that, for rehabilitation needs, it is necessary to mimic movement to some extent, and with this to accomplish movements that seem natural as possible, pneumatic artificial muscles are becoming worthy of detailed research.

## 1.2. Diploma thesis goals and organization

The main goal of the thesis is to find an appropriate model of *FESTO PAMs* to be implemented in "SMART-STRING" system. Knowing that such setup will include various muscle dimensions, the demand to develop universal and plausible model has raised, which lead to analyzing different types of model, with the aim to have a simple but physically meaningful model that is suitable for different, potentially used *PAMs*. Utilizing the developed model, a control algorithm for the actuator is also proposed.

The diploma thesis is organized into six chapters. The structure of the diploma thesis is the following:

**Chapter 1 – Introduction:** Introduces the reason of considering *PAMs* and presenting "SMART-STRING" system.

**Chapter 2 - Fundamentals:** Involves a description of the operation and properties of pneumatic muscles. The different types of pneumatic muscles are related.

**Chapter 3 - Modelling of Pneumatic Muscles:** Provides a review of the existent models for pneumatic muscles.

**Chapter 4 - Experimental Modelling of FESTO Fluidic Muscles:** Presents the set-up used to perform the tests, relates the experimental results and elaborates the experimental models, proposing one of them.

**Chapter 5 - Controller Synthesis for Model Verification:** Considers design and evaluation of a PID+Feed-Forward controller, for the purpose of proposed model validation.

**Chapter 6 - Conclusions:** Summarizes and analyses the results of the work carried out and proposes future work issues.



# 2

## Fundamentals

This chapter presents a theoretical background necessary for the understanding of the project. An introduction to the following topics is provided: Section 2.1 introduces Pneumatic Artificial muscle concept and present its fundamental properties as well as their advantages and disadvantages. Section 2.2 classifies PAMs and explains their difference, while Section 2.3 introduces actuator used for experiments in the project and presents its properties and possible applications.

### 2.1. Fluidic Muscles

The McKibben muscle, the most frequently used artificial muscle, has been introduced in the late 1950s by J. L. McKibben to actuate an orthotic device for handicapped people, and after that American scientist, Schulte analyzed its characteristics in 1961 [38]. For this reason, the braided pneumatic muscle is still referred to as a McKibben muscle in rehabilitation apparatus. However, due to problems inherent to the power storage and the bad quality of the valves, interest in these actuators decreased. During the following years, the braided pneumatic muscle was not the preferred actuator for robotic applications. As pneumatic technology improved, in 80's *Bridgestone Co.*, brought it up again by commercializing it as the *Rubbertuator* for use in robotic systems and this is the start of the McKibben pneumatic artificial muscles commercialization. Nowadays the fluidic muscles are brought up to the market by *FESTO Ag. & Co.* and *Shadow Robot Company*, which leverage significantly interest in these actuator systems.

Fluidic Muscles, called also Pneumatic Artificial Muscles (PAMs), are contractile linear actuators capable of transferring fluid work into mechanical one. Basically, PAMs are essentially made of a rubber or elastomer inner tube, which functions as an air enclosure, also called a bladder. The bladder is surrounded by a double-helix-braided sheath [39], which functions as an anti-rupture layer and used for the transmission of work, the so-called "braided shell". The entire tube is closed by two end caps, one of which has a hose for connecting the air supply and the other is available for connecting to the mechanical load. As the muscle is inflated or gas is sucked out of it, the tube/membrane counterparts bulge outward or are squeezed, respectively. Together with this radial expansion the membrane shell contracts axially and thereby exert a pulling force on a connected load. Because the braid fibers are very stiff, limiting membrane, it can just deform radially [40]: the length is getting shorter while the diameter is getting larger. In contrast, if deflated, the pneumatic artificial muscle recoils, then the diameter reduces, with the increase of the length and the reduction of contracted force. However, when under no pressure, the force of the pneumatic artificial muscle output is zero and the muscle has no bearing capacity. By this means, generated force and motion are linear and unidirectional. The energy source is a gas, normally air. Although it is possible to design an under-pressure operating muscle, PAMs usually operate at an over-pressure. The force decreases monotonically with the contraction [41]. The figures 2.1 and 2.2 illustrate the operation of a PAM:

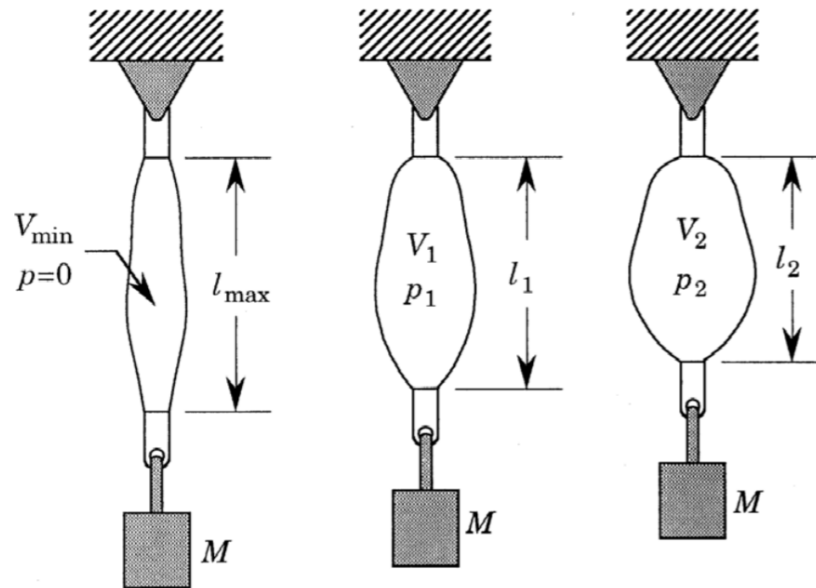


Figure 2.1: **Operation at constant load** [42]: The length decreases at a constant load with increasing pressure.

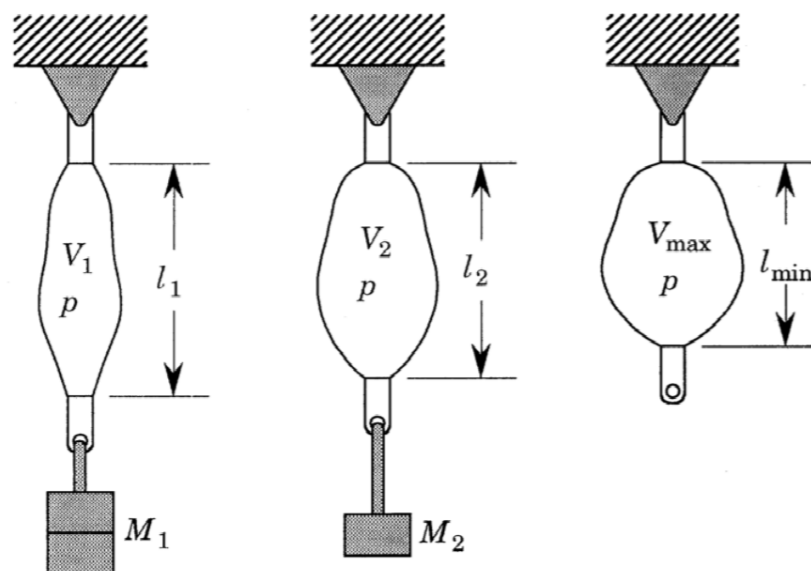


Figure 2.2: **Operation at constant pressure** [42]: At a constant pressure the length decreases with decreasing load. When the load has reached the zero value, that means that the muscle has its maximum volume and its minimum length (at a certain gauge pressure), then further shortening is only possible by compressing the muscle.

The state of particular PAM is fully determined by its length and gauge pressure. The Figure 2.3 illustrates the principle PAM force to length relationship at different pressures [41]. The force developed is monotonically decreasing with the contraction at a constant gauge pressure and nonlinear. At a fixed length, the force increases with increasing pressure.

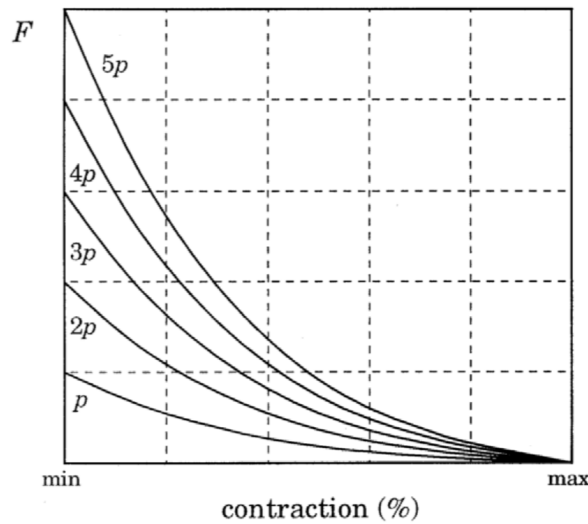


Figure 2.3: **PAM's isobaric force contraction diagrams** [41]

### 2.1.1. Properties

In human and most of the animal bodies, three kinds of muscles exist, namely skeletal, heart, and smooth muscles. Unlike the other two kinds of muscles, skeletal muscle constitutes a major part of the animal body and it is the prime mover of animal locomotion [43]. Different shapes of skeletal muscles are presented in figure 2.4:

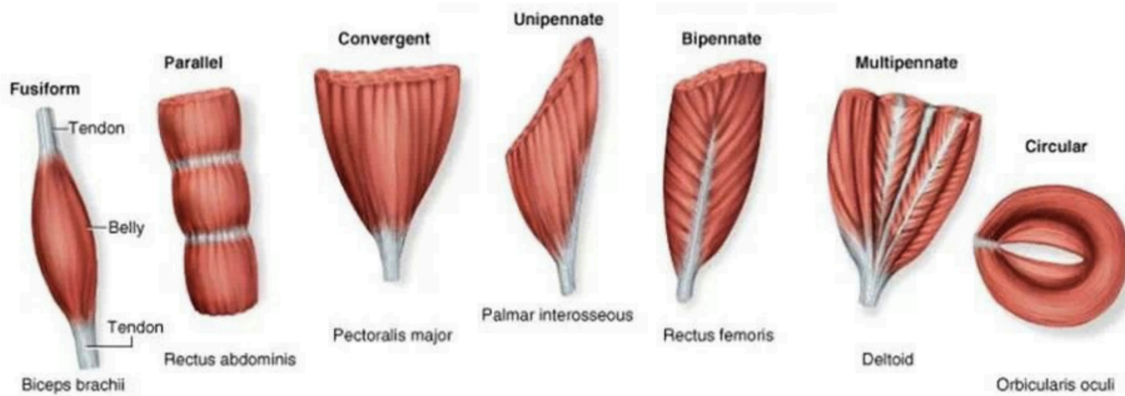


Figure 2.4: **Biological skeletal muscle shapes**

It is shown in [44] that pneumatic muscles share some properties with skeletal muscles, more precise with fusiform shape skeletal muscle (first in Figure 2.4). Both can be modelled as an actuator whose output force is a function of length, velocity, and level of activation which is equivalent to pressure in PAMs. The pneumatic muscles have similar force-length properties to human skeletal muscles. Figure 2.5, where  $L_m$  is muscle length,  $L_{m,0}$  is muscle length at rest,  $F_m$  is muscle force and  $F_{m,0}$  muscle force at rest, shows the relationships between force and length for the human muscle, for the PAM McKibben and for other animals. Skeletal muscles can stretch beyond its resting length, while pneumatic muscles cannot. However, for lengths between 1 and 0.8 times the resting length of the muscle, the McKibben actuator provides a first order approximation of the human skeletal muscle.

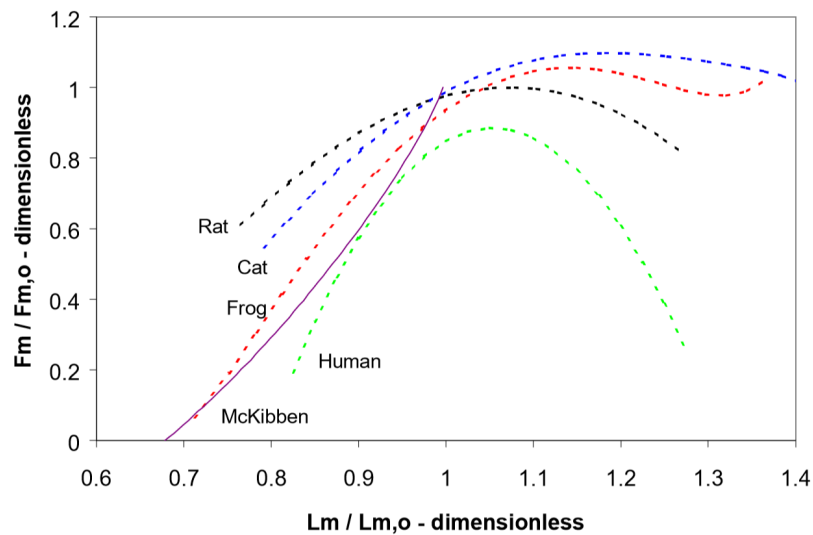


Figure 2.5: **The dimensionless relationship between force and length under isometric conditions at maximal activation for various animals and a McKibben actuator pressurize to 5 bars [44]**

At a constant level of activation, the output force of skeletal muscles drops significantly as contraction velocities increase. Similarly, in the PAM actuator's maximum force is only available under static conditions and decreases with increasing velocity. However, this decreasing (internal damping) is considerably smaller in comparison to the biological muscles.

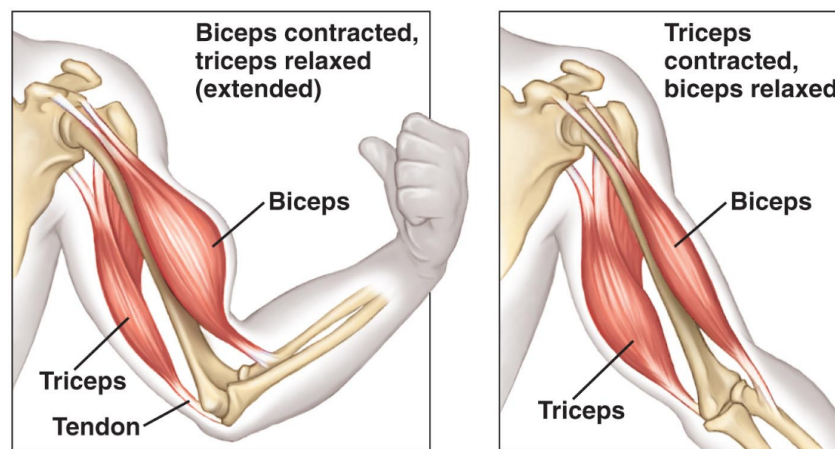


Figure 2.6: **Agonist-antagonist connection of biological muscles**

Like in biological muscles the motion generated by McKibben muscles is linear and unidirectional. Two muscles must be used to realize a bidirectional movement. One acts as a motor to move the load and the other like a brake to stop it, and vice versa. The muscles invert their operation to move the load in the other direction. This connection of the muscles to the load is known as agonist-antagonist set-up, like human muscles biceps-triceps (Figure 2.6). This set up can be used for either linear or rotational motion, as shown in the figures 2.7 and 2.8. The generated force of each muscle is proportional to the gauge pressure in each muscle and the equilibrium position is thus determined by the ratio of both pressures.

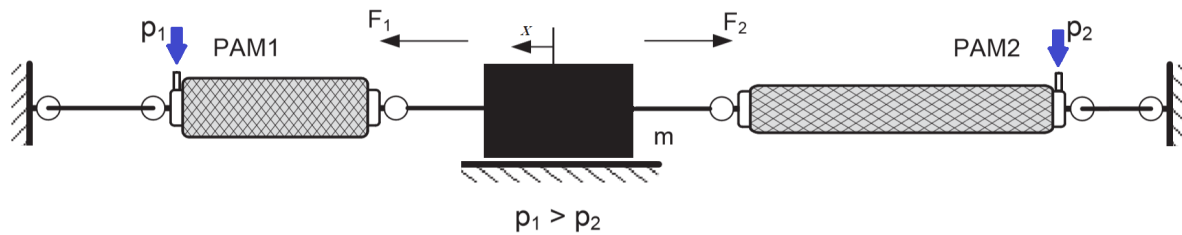


Figure 2.7: **Agonist-antagonist connection of artificial muscles for linear motion**

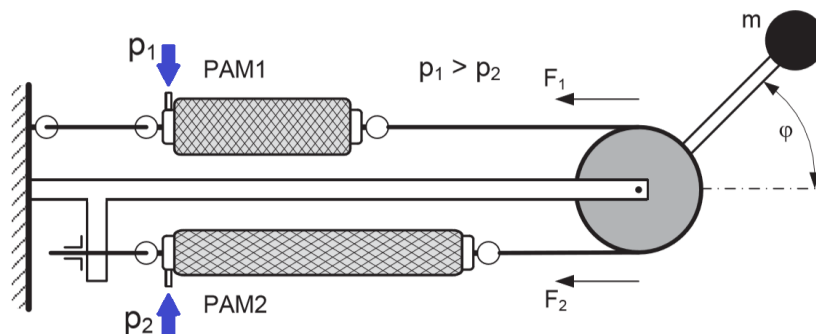


Figure 2.8: **Agonist-antagonist connection of artificial muscles for rotational motion**

Considering all descriptions in this chapter, we can mark some of the advantages of pneumatic muscles:

- Light weight and flexibility (volume to weight ratios are high)
- Relatively high contraction velocity and energy efficiency - power to weight ratio (400:1) [45]
- No need of transmission elements, they are direct drives
- Low cost and easy construction
- Possibility of use in rough environments
- No need of maintenance and facility to be replaced

Despite the above advantages, we found out that PAM has not been extensively used in the past due to its inherent drawbacks as listed below:

- Poor accuracy. It is due to the compressibility of the air and to the difficulty of handling nonlinearities in the position control of these actuators
- Somewhat loud operation of the pneumatic system in which pneumatic muscles work
- Relatively low bandwidth
- Big size of the tubes compared to the small stroke. This is due to the fact that the maximal contraction of pneumatic muscles is just 25-30% of the resting length

## 2.2. Classification of PAMs

Pneumatic artificial muscles can be classified considering various criteria. However, the most relevant criteria concern operation pressure and structural design. Considering the first criterion we can distinguish:

**Over-pressure or under-pressure operation:** If the pressure inside the muscle is bigger or smaller than outside respectively.

Considering the structural design of the membrane the following groups of PAMs may be distinguished:

**Braided, netted or embedded muscles:** This classification refers to the load carrying the element of the PAM. It can be embracing the membrane, like in braided or netted muscles or embedded into it. Regarding the way the membrane inflates there are muscles with:

**Stretching or rearranging membrane:** It refers to the manner in which the membrane inflates. Either the membrane material has to stretch or the membrane section has to change by rearranging its surface.

In the next paragraphs, the different types of muscles, according to the second classification criteria, are described.<sup>1</sup>

### 2.2.1. Braided muscles

Braided muscles operate at over-pressure and are of the stretching membrane type. They consist of an elastic tube surrounded by a braid as shown in Figure 2.9. The first braided muscles were introduced by J.L.McKibben as mentioned at the previous section in orthotics applications in the late 50's. This type has a tube and braids both connected at both ends to fittings. The permanent contact between the tube and the inextensible braid while pressurized permits transferring the tension from the fibers to the load. Typical materials used to make these muscles are latex and silicone rubber and nylon fibers. By changing its braid angle (angle between fibers and the cylinder axis) the muscle changes its length and diameter.

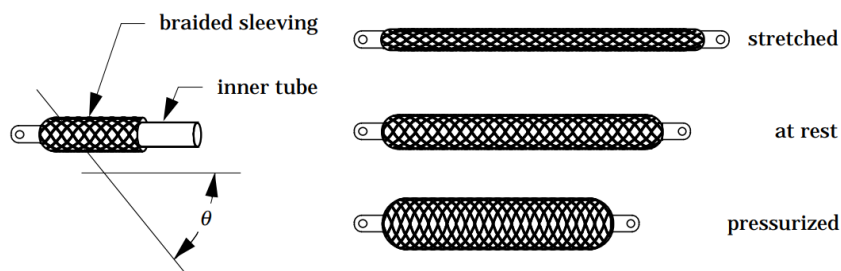


Figure 2.9: **Braided muscles**

Sleeved Bladder Muscle type (Figure 2.10) differs from the McKibben type in the design of the inner bladder that is not connected to the sleeving. The main advantage of this PAM is its extreme ease of assembly. A Sleeved Bladder Muscle is also subject of the patent of Beullens [46].

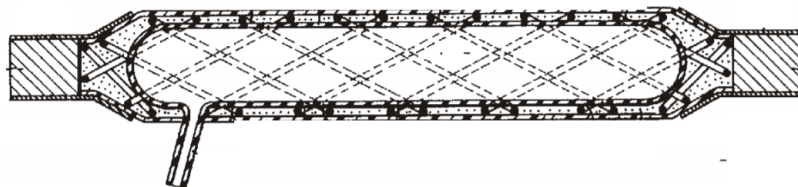


Figure 2.10: **Sleeved muscle**

<sup>1</sup>Detailed PAMs type overview can be found in [42]

### 2.2.2. Pleated muscles

This actuator is of the membrane rearranging kind. This means no material strain is involved when it is inflated. The way this is done is shown in Figure 2.11. The muscle membrane has several pleats in the axial direction and when it expands it does so by unfolding them, so there is no friction involved in this process. As a result, there is no energy needed for expanding the membrane. Because of the absence of friction this design shows no hysteresis characteristics.

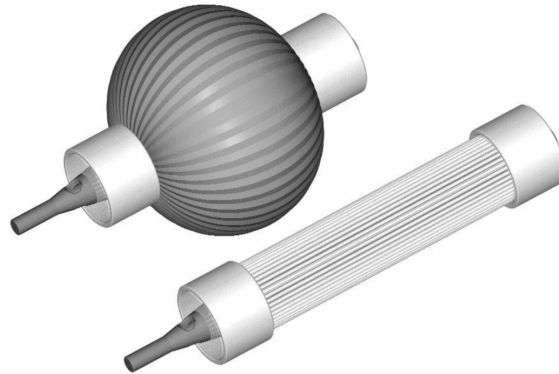


Figure 2.11: **Pleated muscle**

### 2.2.3. Netted muscles

The difference between braided and netted muscles is the density of the network surrounding the membrane; a net is a mesh with relatively large holes. Because of this, the netted muscles have often a rearranging membrane; otherwise, they can only operate at low pressures. The Yarlott [47] muscle is represented in Figure 2.12. It comprises an elastomeric bladder of a prolate spheroidal shape netted by a series of cords or strands that run axially from end to end. The bladder is radially reinforced by strands to resist elastic expansion. In its fully inflated state, this actuator takes the spheroid bladder shape.

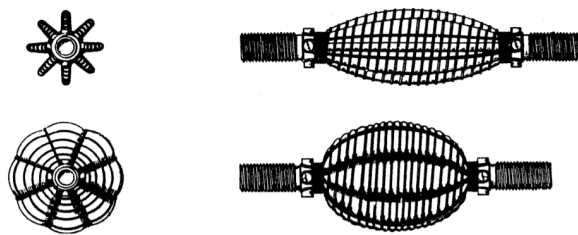
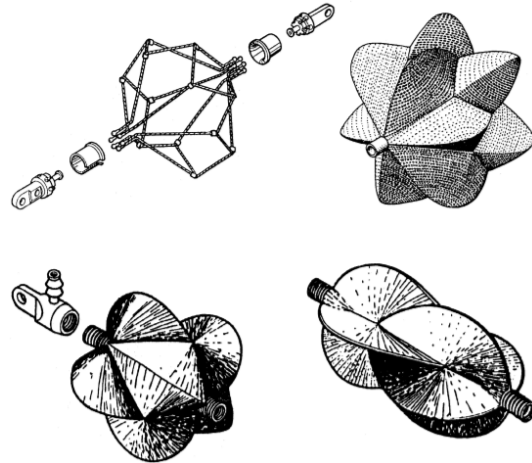
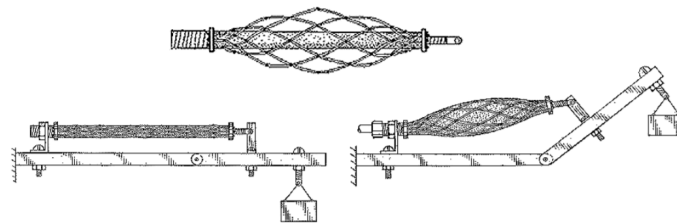


Figure 2.12: **Yarlott muscle**

ROMAC (RObotic Muscle ACtuator) [48, 49], consists of an articulating polylobe bladder harnessed by a wire netting and closed at both ends by fittings. The bladder is made of a sheath, that is characterized by its high tensile stiffness, its flexibility, and its fluid-tightness. The netting or harness is comprised of non-stretchable flexible tension links which are joined at nodes to form four-sided diamond shaped apertures in the network. The harness expands radially and contracts axially, thereby changing the base of each protruding lobe. As a result of this mechanism the enclosed volume changes.

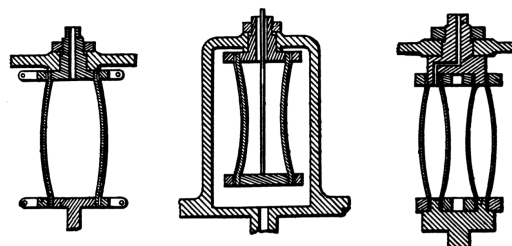
Figure 2.13: **ROMAC muscle**

Kukolj [50] is a variation of the McKibben Muscle. The main difference between them is the sleeve: McKibben Muscles have a tightly woven braid while the Kukolj design (Figure 2.14) uses an open-meshed net. In its nonloaded condition, there is a gap between the net and the membrane, which only disappears at a suitably high extending load.

Figure 2.14: **Kukolj's muscle**

#### 2.2.4. Embedded muscles

The load carrying the structure of these muscles is embedded in its membrane. These muscles can operate at over-pressure or at under-pressure. Figure 2.15 shows the Morin embedded muscle designs. The Morin muscles [51], which can operate with any fluid, are the origin for McKibben's design. In this design, a rubber tube is embedded by threads of a high tensile stiffness. These threads can be directed along the actuator's long axis or in a double helix about that axis. As fiber material, Morin cites cotton, rayon, asbestos or steel; a choice that is clearly marked by that time. The two-phase membrane is clamped by two end fittings, serving to seal and to attach the load. The full tensional load is taken by the fibers while the elastomer stretches to allow for inflation. Possible operating fluids suggested by Morin are compressed air, water, oil or even steam.

Figure 2.15: **Morin muscle**

The Baldwin muscle [52] is based on the design of Morin. It consists of an elastomeric membrane, a very thin surgical rubber, embedded by glass filaments in the axial direction. The resulting membrane has a modulus of elasticity in the fiber direction that is much higher than that in the direction perpendicular to the fibers (Figure 2.16).

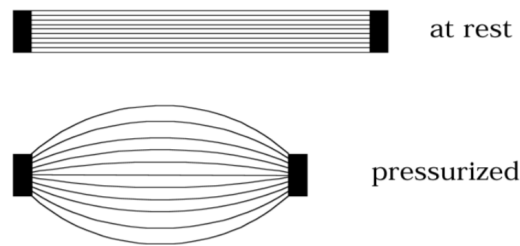


Figure 2.16: **Baldwin muscle**

Paynter [53] actuator has a spherical bladder that is reinforced by a knitted structure of strong, tough and flexible fibers. This structure is made to have the same spherical shape as the bladder so that it conforms to it and can be easily bonded to it. The bladder is made of an elastomeric material. During inflation, the bladder does not stretch as is the case for McKibben Muscles. When fully inflated the muscle takes on the shape of the original bladder and knitting sphere. If extended from thereon, it will gradually take on a fluted shape. Unpressurized, the muscle can be extended to a length equaling half the circumference of the sphere (Figure 2.17).

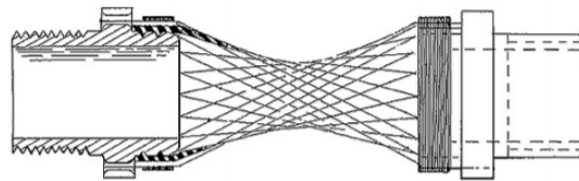


Figure 2.17: **Paynter's muscle**

Kleinwachter torsion device (Figure 2.18) has a toroid diaphragm attached at its outer edge to a ring-shaped structure and at its inner edge to a shaft. The diaphragm is embedded with stiffening filaments that run obliquely across the radial direction from the outer structure to the shaft. When inflated the membrane bulges and the filaments thereby rotate the shaft in the direction of  $\phi$ , as indicated in the figure. One-way rotation and torque are thus achieved.

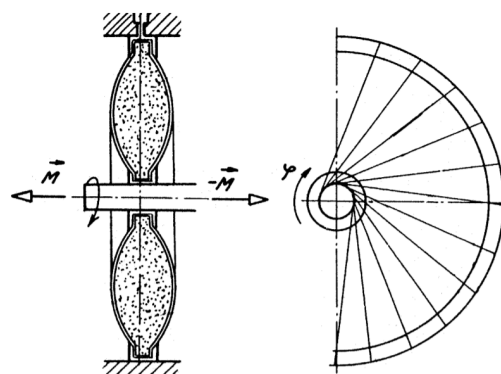


Figure 2.18: **Kleinwachter torsion device**

### 2.3. FESTO fluidic muscles

This actuator is a braided artificial muscle. It consists of an anisotropic flexible rubber tube and non-extensible fiber that contracts when the pressure inside increases. For some authors, the FESTO muscles are obviously McKibben muscles [54]. The difference between this muscle and the conventional McKibben muscle is that the fiber here is knitted in the tube itself (2.20). Friction between fiber and rubber is thus minimized reducing hysteresis and non-linearity in the operation. This artificial muscle can also be assembled easy. Figure 2.19 displays the FESTO's DMSP-muscle type.



Figure 2.19: **Pneumatic muscle manufactured by FESTO:** (1)Contraction membrane (fiber tube); (2)Connecting flange for press-form sleeve; (3)Thread for compressed air port; (4)Connecting thread

The fluidic muscles used in this work were from DMSP-40-1000N and DMSP-40-290N, (named according to its length) series. They are manufactured by *FESTO*. The two fluidic muscles (see: <http://www.festo.com/> for more information) have a maximum contraction over the nominal length of 25% and they are 290mm long and 1000mm. Other series available are DMSP-5, DMSP-10, DMSP-20 (named according to its length). The DMSP-5 can generate a maximal force of 140N at 8bar. The DMSP-10 muscle can generate a maximal force of 480N at 8bar. The DMSP-20 can generate a force of 1500N at 6bar and the maximal force produced by DMSP-40 is 600N at 6bar. They have a very long lifetime up to 10 million switching cycles [55].



Figure 2.20: **Cross-section of FESTO fluidic muscle [56]:** (1)PAM bladder; (2)First layer of fibres; (3)Second layer of fibres

Producer recommends some successful applications of *FESTO* pneumatic muscle (Figure 2.21):

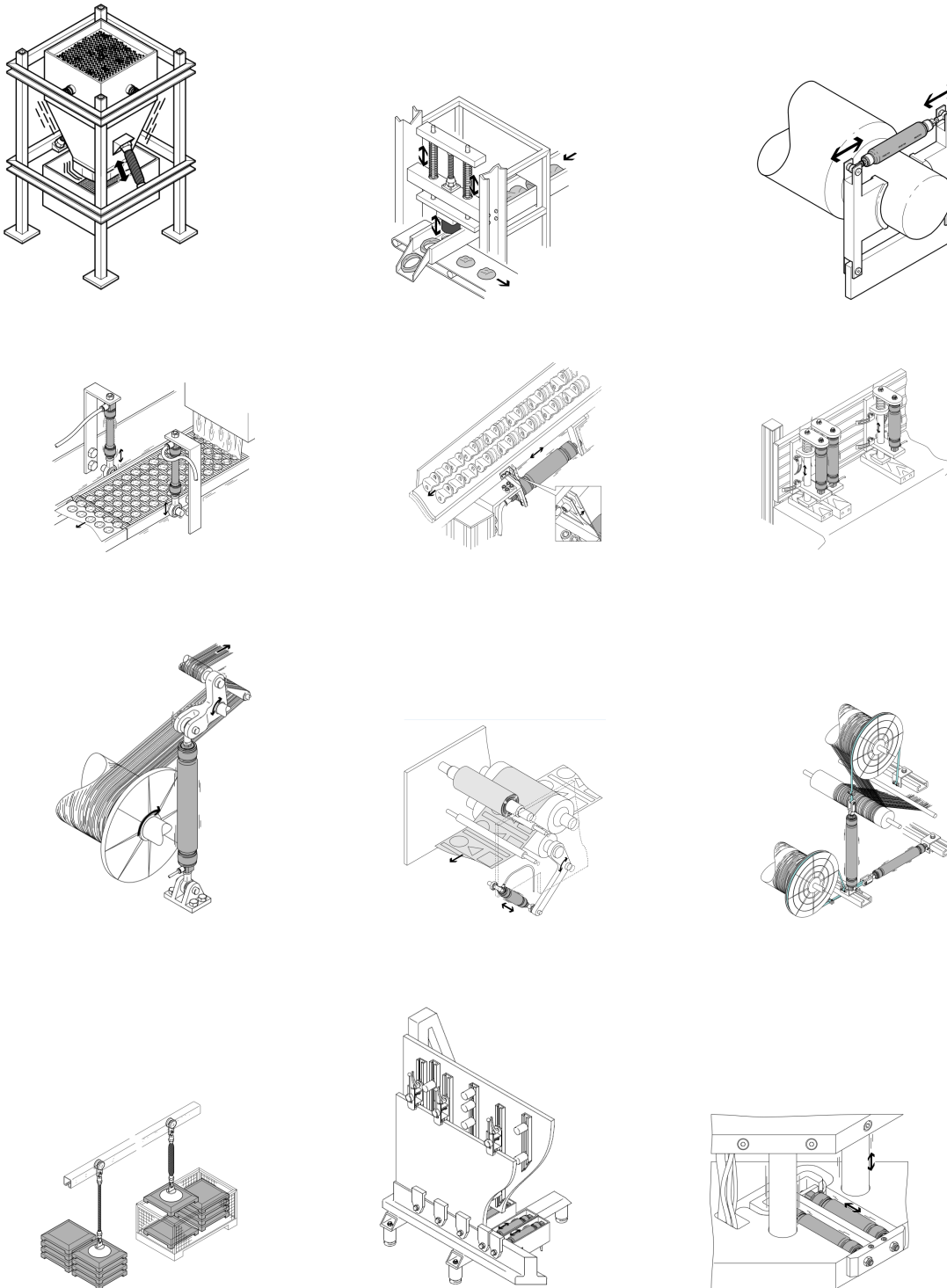


Figure 2.21: **Some applications of FESTO pneumatic muscle recommended from producer [55]** (respectively): (1)Releasing; (2)Punching; (3)Emergency stop device; (4)Disturbing; (5)Conveying; (6)Clamping work-pieces; (7)Stress equalization; (8)Adjustable contact pressure; (9)Brakes for tension regulation; (10)Lifting aid; (11)Clamping metal sheets; (12)Clamping parts to be joined



# 3

## Modeling of Pneumatic Muscles

This chapter gives an overview of the main ideas for modelling of PAMs. The chapter starts with a static force modeling approach that is considered as fundamental, since it is based on the basic properties of the PAMs geometric description. Furthermore, this section also outlines a couple of upgrades to basic geometrical modeling. Section 3.2 proposes two empirical methods for modeling, while 3.3 presents phenomenological approaches to modeling.

For control synthesis, i.e., realizing desired control results it is needed to understand a mathematical model of the system. In some cases, getting model is possible through using basic physical laws, but in most of the situations, these relations are much more complex, meaning that there is a big number of conditions that are describing the behavior of a system. Pneumatic artificial muscle is a highly nonlinear element which is, in many authors papers, observed differently, where more or less successful results are achieved. Approaches based on theory only (from simpler ones to very complex dependencies with a big number of variables) exists, but also models established based on experimental results. In general, synthesizing of models can be divided in two big groups, static and dynamic modeling.

### 3.1. Geometrical modeling

These models are derived on basis of simplified energy transformation of the system. Applying law of energy conservation, it is possible to determine the force of PAM as a function of pressure and length of the actuator. During arbitrary short time interval  $dt$  and difference between pressures of the muscle and the environment, feeding with infinitely small gas mass ( $dm$ ), the volume of the mesh is increasing with  $dV$ , realizing input work  $dW_{in}$ . This change can be mathematically described as:

$$dW_{in} = \int_{S_i} (p - p_0) dl_i = (p - p_0) \int_{S_i} dL_i \cdot ds_i = p' dV \quad (3.1)$$

Where  $p$  is absolute pressure of gas inside of mesh,  $p_0$  is pressure of environment ( $1atm=1.0336bar$ ),  $p'$  relative pressure,  $S_i$  total inside surface area,  $dL_i$  moving of inside surface area,  $dV$  relative volume. These changes cause axial moving, i.e. changing of actuator's length, whereby load, i.e., external axial force ( $F$ ) realizes mechanical (output) work:

$$dW_{out} = F dL \quad (3.2)$$

From the view of energy conservation, the input work should be equal to the output work if a system is loss-less and without energy storage. That yields:

$$F = -p \frac{dV}{dL} \quad (3.3)$$

In the mid-90s, Chou and Hannaford [45] built an ideal model of the pneumatic artificial muscle with the theory of energy conservation previously explained. With this approach the PAM actuator can be modeled as a cylinder, depicted in 3.1, with actuating length  $L$ , thread length  $b$ , the internal diameter  $D$ ,  $t$  the thickness of the elastic tube and number of thread turns  $n$ . The angle  $\theta$  is defined as the angle of the threads with the longitudinal axis.

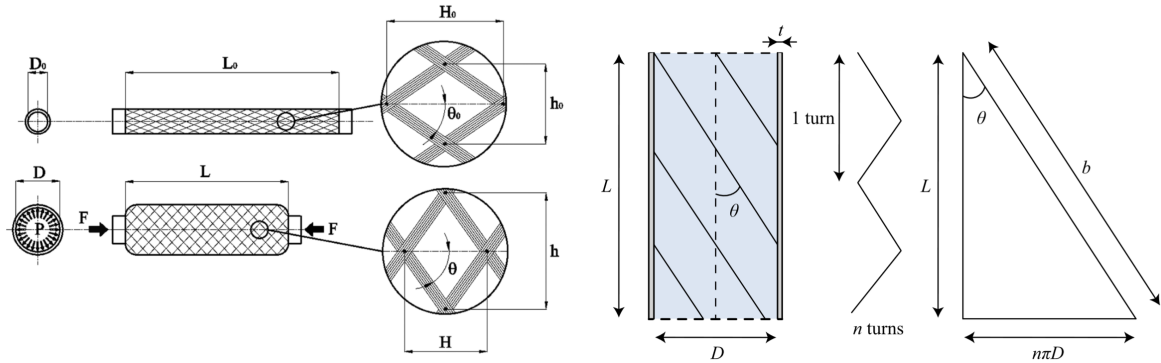


Figure 3.1: Schematic of geometrical relations of braided muscle [57]

With this approach, the expressions for the PAM's length and diameter are formulated as:

$$L = b \cos \theta, \quad D = \frac{b \sin \theta}{n\pi} \quad (3.4)$$

$$b = \sqrt{L^2 + D^2 n^2 \pi^2} \quad (3.5)$$

Equation 3.5 is referred in the literature as the geometric relationship of PAM, while its volume is provided by:

$$V = \frac{b^3 \cos \theta \sin^2 \theta}{4n^2 \pi} \quad (3.6)$$

Utilizing the energy conservation principle with previous expression, the PAM geometric force is formulated as the gauge relative pressure  $P$  multiplied by the change in volume with respect to length:

$$F = \frac{P b^2 (\cos^2 \theta - 1)}{4\pi n^2} \quad (3.7)$$

From [57], by introducing unloaded state where  $L_0$ ,  $D_0$  and  $\theta_0$  are the PAM's initial values of the length, diameter, and braid angle, respectively, we can get expression for  $n$ , that is number of turns, using equations 3.4 and 3.5, that is:

$$n = \frac{(L_0^2 - L^2)^{\frac{1}{2}}}{\pi(D^2 - D_0^2)^{\frac{1}{2}}} \quad (3.8)$$

Utilization of 3.4 in the idle state leads to following geometrical expression:

$$\tan \theta_0 = \frac{n\pi D_0}{Ln} \quad (3.9)$$

The initial braid angle  $\theta_0$  analytic formulation can be derived by substitution 3.8 to 3.9:

$$\theta_0 = \arctan \frac{(L_0^2 - L^2) D_0}{(D^2 - D_0^2) L_0} \quad (3.10)$$

Incorporation of initial braid angle equation and expression for the number of turns into general geometric force equation 3.7 yields an equivalent expression of the force model:

$$F = \pi \frac{D_0^2}{4} P [\alpha(1 - \varepsilon_l)^2 - \beta] \quad (3.11)$$

Which takes the identical form of one, as well commonly used model presented by Tondu and Lopez [58], given the geometric expressions  $\alpha = \frac{3}{\tan^2 \theta_0}$ ,  $\beta = \frac{1}{\sin^2 \theta_0}$ , and the produced strain  $\varepsilon_l = \frac{x}{L_0}$  in the longitudinal  $L$  direction, where  $x = L_0 - L$  is the PAM's displacement.

Two models presented, on which many future research works are based, are valid under following assumptions: (1) the actuator is cylindrical in shape; (2) the threads in the sheath are in-extensible and always in contact with the outside diameter of the latex bladder; (3) frictional forces between the tubing and the sheath and between the fibers of the sheath are negligible; (4) latex tubing forces are negligible.

In an attempt to increase the accuracy of the static force model, authors of [58] incorporated the parameter  $k$  into 3.11 to counteract the PAM's non-cylindrical ends:

$$F = \pi \frac{D_0^2}{4} P [\alpha(1 - k\varepsilon_l)^2 - \beta] \quad (3.12)$$

Parameter  $k$  was defined as a linear function of pressure to further increase the modeling accuracy in low pressures and counteract the elasticity of the tube and the increased compressibility of the pressurized air.

Beside Tondu and Lopez, other models for improving basic geometrical model can be found in the literature. In [59] the proposed geometry includes a frustum cone that models each end-section and a cylinder to model the muscle middle section.

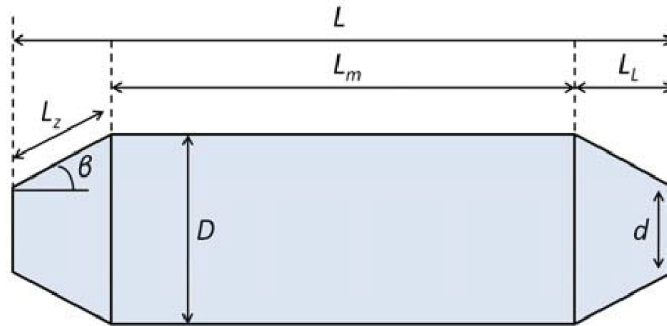


Figure 3.2: **Schematic of geometrical relations of braided muscle with frustum cone endings**

Novel geometrical relations are formulated by:

$$L_L = (L_z^2 - (\frac{D}{2} - \frac{d}{2})^2)^{\frac{1}{2}} \quad (3.13)$$

$$D = \frac{(b^2 - L_m^2)^{\frac{1}{2}}}{\pi n} \quad (3.14)$$

$$L = L_m + 2L_L \quad (3.15)$$

In the geometry of muscle modelled like this, all the parameters are a function of the muscle-contracted length, except  $L_z$  that is determined experimentally based on the muscle end diameter and maximum contracted diameter.

Another upgrade of geometrical description of the actuator is done by [60], where (from Figure 3.3, left) all ends were combined together, and the ideal shape is a cuboid, implying the volumes of the cylindrical  $V_v$ ,  $R(D = 2R)$  is radius of muscle,  $R_0$  radius of inner tube, and that the actual shape  $V_a$ :

$$V_a = \pi(R - R_0)^2 \times \left(\frac{R - R_0}{\tan \theta}\right) \times 2 = \frac{2\pi(R - R_0)^3}{\tan \theta} \quad (3.16)$$

$$V_a = \frac{2\pi}{3}[3R_L - (R - R_0)] \times (R - R_0)^2 \quad (3.17)$$

$$R_L \times \sin \theta = \frac{1}{2} \times \frac{R - R_0}{\sin \theta} \quad (3.18)$$

$$F = -p \frac{d[V - (V_v - V_a)]}{dL} = -p \frac{d[V - (V_v - V_a)]/d\theta}{dL/d\theta} = \frac{p'b^2(3 \cos^2 \theta - 1)}{4\pi n^2} + p'M \quad (3.19)$$

$$M = \frac{(R - R_0)^3 \times (2\pi - \pi \cot \theta)}{n\pi R} \quad (3.20)$$

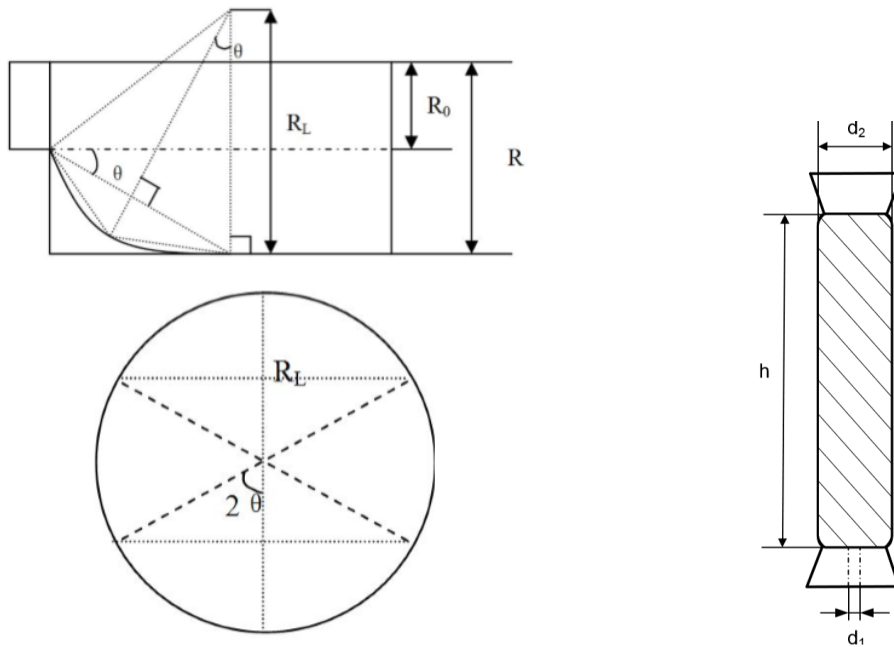


Figure 3.3: **Upgraded geometrical relations schematics:** (1)The analysis of end constrains(up-left); (2)The section of the visual sphere including all ends of the muscle(down-left); (3)Diameter variation included(right)

In [61], advanced geometric muscle model assumes that change of the pressure in the muscle and change of the diameter of the muscle varies, where  $h$  is the length of the muscle,  $d_1$  is valve diameter,  $d_2$  is muscle diameter as shown in Figure 3.3 (right), where:

$$c = \sqrt{4L^2 - h^2} \quad (3.21)$$

$$d_2 = \frac{c}{N\pi} = \frac{\sqrt{4L^2 - h^2}}{N\pi} \quad (3.22)$$

$$V = \frac{h[3d_1^2\pi^2N^2 + 4d_1\pi N\sqrt{4L^2 - h^2} + 8(4L^2 - h^2)]}{60\pi N^2} \quad (3.23)$$

In literature not only improvements of geometrical relations are done, rather expanded energy-based approach to modeling is proposed. In Klute et.al. [62] the model is improved by adding the effects of the deformation energy of the bladder, the energy balance equation can be written as:

$$F = -p \frac{dV}{dl} - V_b \frac{dW}{dl} \quad (3.24)$$

Where  $V_b$  is volume surrounded by mesh,  $dW$  is deformation energy density difference and  $F_f$  friction force of braids in contact with the mesh. The second term of the equation 3.24 for a rubber bladder of known geometric and material properties can be defined using the relationship between the stress  $\bar{\sigma}$  and the strain  $\bar{\varepsilon}$  given by  $\bar{\sigma} = \frac{dW}{d\bar{\varepsilon}}$ , where  $W$  is the strain energy density function. Assuming initial isotropy and incompressibility,  $W$  can be described as a function of two strain invariants ( $I_1$  and  $I_2$ ):

$$W = \sum_{i=0, j=0}^{\infty} C_{ij} (I_1 - 3)^i (I_2 - 3)^j \quad (3.25)$$

$C_{ij}$  are empirical constants and for the McKibben's muscle, only two constants were necessary to obtain accurate results with natural latex rubber bladder. The solution of differential equation 3.24, formulated in terms of longitudinal stretch ratio  $\lambda_1$ , is ( $L$  is the actuator instantaneous length and  $L_0$  is the initial length):

$$\lambda_1 = \frac{L}{L_0} \quad (3.26)$$

$$F = \frac{p}{4n^2\pi} [3(\lambda_1 L_0)^2 - b^2] - V_b [S_1 + S_2 + S_3 + S_4] \quad (3.27)$$

$$S_1 = \frac{1}{2L_0^3 \lambda_1^3} 4(C_{10} + C_{01}) L_0^2 (-1 + \lambda_1^4) \quad (3.28)$$

$$S_2 = \frac{4L_0^6 (-1 + \lambda_1) \lambda_1^2 (1 + \lambda_1) (C_{10} + C_{01} \lambda_1^2)}{[-4n^2 \pi^2 R_0^2 + L_0^2 (-1 + \lambda_1^2)]^2} \quad (3.29)$$

$$S_3 = -\frac{4L_0^4 (C_{10} + C_{01} \lambda_1^4)}{-4n^2 \pi^2 R_0^2 + L_0^2 (-1 + \lambda_1^2)} \quad (3.30)$$

$$S_4 = -\frac{L_0^4 \lambda_1^4 [C_{10} + C_{01} (-1 + 2\lambda_1^2)]}{n^2 \pi^2 R_0^2} \quad (3.31)$$

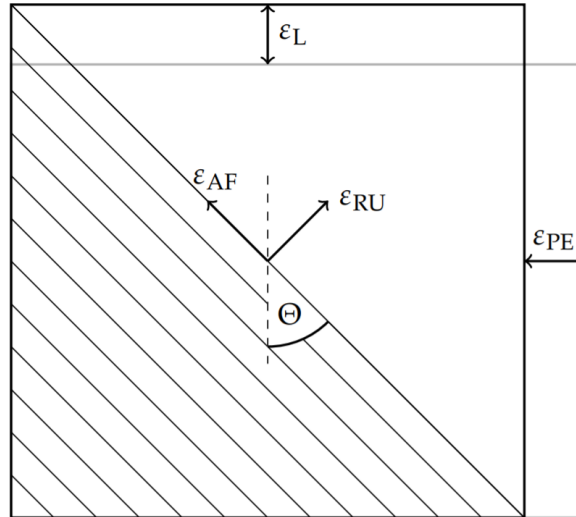
Author of [63] is proposing a similar way of expressing the energy used while the muscle is contracting, separating virtual work of the PAM in two parts. As above, first one  $W_v$  has to be done to change included air volume, and additional virtual work  $W_e$  to change the potential energy of the elastic membrane rubber:

$$W_{pam} = W_v + W_e \quad (3.32)$$

It can be considered that deformation of the membrane is a plane state strain and described by the strain in direction of the PAM length  $\varepsilon_L$  and its perimeter  $\varepsilon_{PE}$ . If we rotate coordinate system by the angle  $\theta$ , the deformation is given by the strain in fiber direction  $\varepsilon_{AF}$  and perpendicular to the fiber course, the direction of pure rubber  $\varepsilon_{RU}$  (Figure 3.4).

As nonlinear deformation is approximated with linear, one-dimensional state of stress can be assumed, and the tensions inside the rubber can be calculated with Hooke's law:

$$\sigma_{RU} = E(L) \varepsilon_{RU} \quad (3.33)$$

Figure 3.4: **Schematic of deformation strains of membrane**

Where, from Pythagoras theorem:

$$\varepsilon_{RU} = \sqrt{\left(\frac{L - L_0}{L_0}\right)^2 + \left(\frac{D - D_0}{D_0}\right)^2} \quad (3.34)$$

Rotating the tension  $\sigma$  back to initial coordinates, it is possible to calculate the tension in both directions:

$$\sigma_L = \sigma_{RU} \sin \theta = E(L) * \varepsilon_{RU} \sin \theta = E \frac{L - L_0}{L_0} \quad (3.35)$$

$$\sigma_D = \sigma_{RU} \cos \theta = E(L) * \varepsilon_{RU} \cos \theta = E \frac{D - D_0}{D_0} \quad (3.36)$$

The virtual work for membrane deformation is the sum of virtual work necessary to deform the membrane in length direction  $W_L$  and virtual work for perimeter direction membrane deformation  $W_D$ . These can be calculated by multiplying the tension with the edge surfaces (in Figure 3.5 labeled with grey color) of the unreeled membrane.

Edge surfaces are denoted with:

$$S_L = \frac{\pi D^2}{4} - \frac{\pi(D - 2\delta)^2}{4} = \frac{4\pi D\delta}{4} - \frac{4\pi\delta^2}{4} \approx \pi D\delta \quad (3.37)$$

$$S_D = DL - (D - 2\delta)L = 2\delta L \quad (3.38)$$

Utilizing equations these equations in explained way in new energy balance equation we obtain:

$$FdL = -pdV + F_L dL + F_D dD \quad (3.39)$$

$$F = -p \frac{dV}{dL} - F_L + F_D \frac{dD}{dL} \quad (3.40)$$

$$F_L = \sigma_L S_L \quad (3.41)$$

$$F_D = \sigma_D S_D \quad (3.42)$$

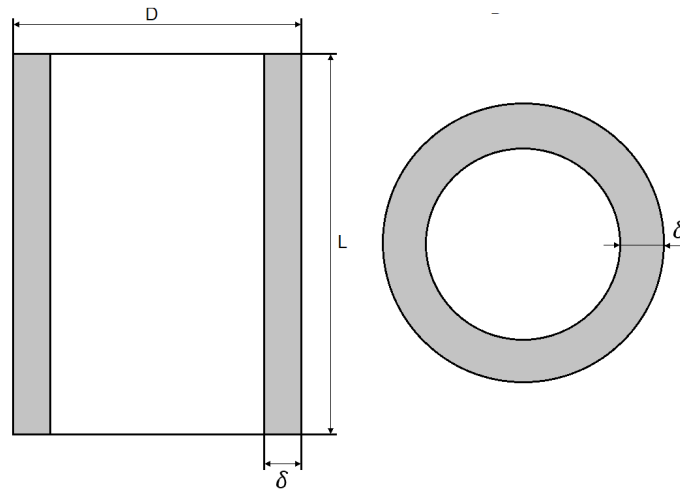


Figure 3.5: **Edge surfaces:** (1)Edge surface- $S_D$  of perimeter deformation(left); (2)Edge surface- $S_L$  of length deformation(right)

Opposite sign (for chosen positive direction of actuation) in front of  $F_D$  in equation 3.40 is necessary because an increase in the length of the PAM has to result in a decreasing diameter, what is defined to be positive. After utilizing geometrical relations mentioned above, the final form of the PAM force is:

$$F = \frac{p}{4\pi n^2} [3L^2 + b^2] + E(L)\epsilon_L \delta \pi D - E(L)\epsilon_D \frac{2\delta L^2}{Dn^2\pi^2} \tag{3.43}$$

### 3.2. Empirical modeling

Empirical modelling is kind of modelling where knowledge of some system nature is gained by means of direct and indirect observation or experience. Through experimentation, specific patterns of system behavior can be sensed and exploited as the system description even without proving with physics laws in details.

Such model is proposed by [64]. In this paper, its noticed that PAM and mechanical spring system are showing very similar characteristic when in working conditions, both with and without pulling forces applied at one end of the element.

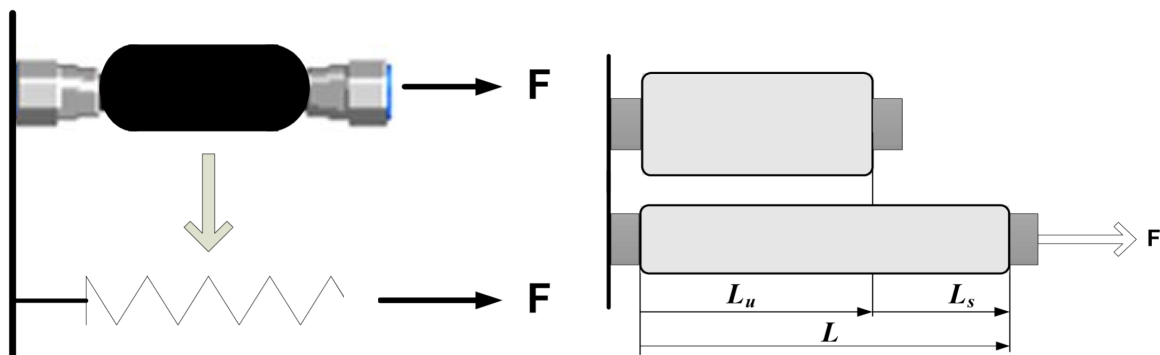


Figure 3.6: **Spring model of PAM:** (1)Equivalent system diagram of pneumatic muscle and spring; (2)Length definitions when pneumatic muscle is exerted by pulling force

In Figure 3.6 is presented physical functionality of PAM and spring system (right), together with variable notation used. Conventionally, the stiffness of the spring system is constant, and it is dependent upon the material properties and the geometry of the spring. With PAM, oppositely, the stiffness is a variable parameter and it depends upon not only the above-mentioned properties but also the operating air pressure within the actuator. Based on these considerations, the pulling forces acting on the muscle can be modeled in the same as the force acting on the mechanical spring system. The stiffness parameter of the muscle denotes as  $K$  and it is considered as a function of the operating air pressure,  $P$  and the stretched length,  $L_S$ . The elastic forces adversely generated by the muscle is denoted by  $F_{elastic}$ :

$$F_{elastic} = K(P, L_S)L_S \quad (3.44)$$

Another empirical model can be derived from energy balance laws presented in the first section of this chapter. The developed force by the fluidic muscle disregarding energy storage and energy losses can be described with equation 3.45:

$$F = -p \frac{dV}{dl} \quad (3.45)$$

The muscle can be then considered as a one-way cylinder with variable diameter. That means that the expression  $\frac{dV}{dl}$  could be interpreted as variable piston area, which is called virtual area of the fluidic muscle so the force can be expressed as the product of the relative pressure in the muscle and the virtual area. The minus sign indicates that the positive axis for length variation is chosen in the muscle extension direction. Assuming the virtual  $A(\Delta L)$  area only depends on the contraction of the muscle, which is the difference between its length at rest and its actual length,  $\Delta L = (L_0 - L)$ , implying the developed force is:

$$F(p, \Delta L) = pA(\Delta L) \quad (3.46)$$

At a considered contraction the virtual area has a constant value and the force appears to be proportional to the pressure analogously to pneumatic cylinders. Further development of this model will be presented in Chapter 4, section 4.3.1.

### 3.3. Phenomenological modeling

Phenomenological models aim to better capture the dynamic behavior of PAM and the fundamental Hill model represents a general form for skeletal muscle dynamic behavior. This phenomenological model is describing a known relationship between input and output without trying to describe the biochemical mechanisms underlying muscle force production. The base model is described in 1938. by Hill [65]. Commonly, the Hill muscle model has three components: a nonlinear spring representing the tendon (SE), a contractile element (CE) representing the active properties (actin-myosin interaction) of the muscle fibers, and a passive elastic element (PE) representing the passive properties of the muscle tissue (Figure 3.7).

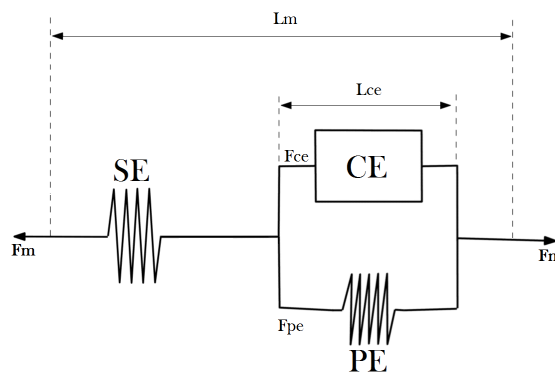


Figure 3.7: Hill model

It is shown in [66] that muscle is able to mimic the Hill Velocity-Tension model and thus can be modelled using this approach. In light of these conclusions, the Hill model was modified to the three-element model, that is more convenient for describing of actuator studied [67]. This model differs from Hill's model of skeletal muscle in that it has a single parallel spring rather than springs in series and parallel (Figure 3.8).

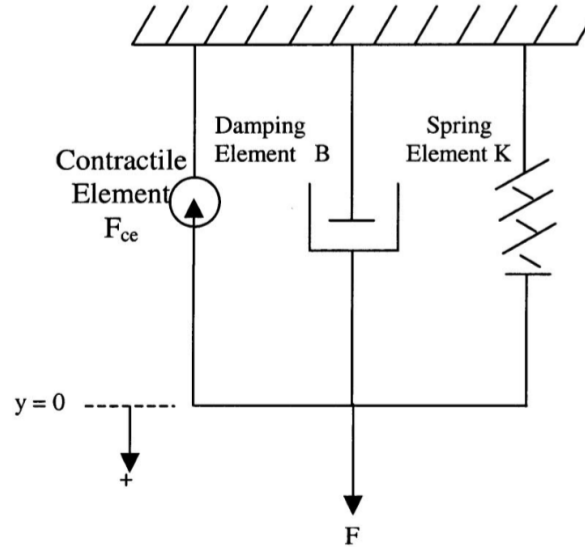


Figure 3.8: **Three-element model**

Letting  $y$  be position, the equations of motion is derived:

$$M\ddot{y} + B\dot{y} + Ky = F_{ce} - Mg \quad (3.47)$$

Where  $K$  is the spring coefficient,  $B$  is the damping coefficient, and  $F_{ce}$  is the effective force provided by the contractile element. The spring element represents the nonlinear force-length relationships, the viscous damping element models the viscous effects of the fluid flow losses in the system, and contractile element effects of the losses due to the sliding contact between the bladder and outer braided shell. In Reynolds [67], also hysteresis was introduced to this way of modeling. Two models are made for damping  $B$ , one for inflation and one for deflation. The coefficient  $B$  in deflation results smaller than in inflation because the PAM system vents against a constant atmospheric pressure and during inflation, however, it has to do it against its own pressure.

Another method for modeling that can be also understood as phenomenological is using the Hammerstein model. When the output of a system depends non-linearly on its inputs, sometimes it is possible to decompose the input-output relationship into two or more interconnected elements. In this case, it is possible to represent the dynamics by a linear transfer function and capture the nonlinearities using nonlinear functions of inputs and outputs of the linear system [68]. A block-oriented nonlinear model is a model that consist a series of blocks that represent both memory-less nonlinearity and linear dynamic of the system based on input and output measurement of the system and Hammerstein model is among them. Hammerstein model consists of a static nonlinear element and dynamic linear element in cascade [69]. It possesses a flexible structure that the mathematical formulations of nonlinear and linear blocks are free to choose, which means it is possible to have a big range of choices for bases. In Figure 3.9,  $f(\cdot)$  denotes the nonlinear element and  $G(z^{-1})$  the linear element.  $u_k$ ,  $d_k$  and  $y_k$  are input, disturbance, and output respectively.

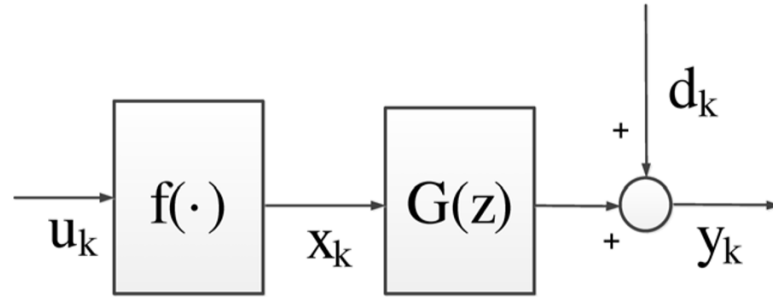


Figure 3.9: **Hammerstein model block diagram**

In case of pneumatic artificial muscle, we are dealing with a single input single output (SISO) system, and according to [69] mathematical formulations of  $f(u_k)$  and  $G(z^{-1})$  are:

$$f(u_k) = \sum_{i=1}^l a_i h_i(u_k) \quad (3.48)$$

$$G(z^{-1}) = \sum_{j=1}^m b_j P_j(z^{-1}) \quad (3.49)$$

$$y = \sum_{j=1}^m \sum_{i=1}^l b_j a_i P_j(z^{-1}) h_i(u_k) + d_k \quad (3.50)$$

Vectors of  $u_k$ ,  $y_k$  are acquired through experimental measurements, where  $u_k$  denotes the input voltage signal and  $y_k$  is the corresponding output displacement of PAM. For the static nonlinear block can be chosen polynomial functions and for the second part, acting as a dynamic linear element, Kautz bases [70] is adopted, since the bases of nonlinear and linear blocks can be chosen in a various range.

### 3.4. Summary

Summarizing modeling approaches described above we could put them in the two categories: for modeling based on mechanical/geometry characteristics PAM is usually decomposed into many components based on geometric structure, then different parameters are found through virtual work or other characteristics to figure out their relations, also including probabilistic fitting of data. The other one includes phenomenological and soft computing modeling (which in these paper are not described) that do not need a thorough knowledge of PAM, rather, it is just needed to know the basic mathematical model and a pair of input/output data from experiments. These approaches emphasize optimizing model parameters more than analyzing muscle's structure.

# 4

## Experimental Modeling of FESTO Fluidic Muscles

The previous chapters provide the description of Pneumatic Artificial Muscle and description of their modelling, the theoretical foundation for the understanding of the project, and the proposed methods for improving the mathematical model. This chapter provides the experiment description (Section 4.1), results of the baseline performance and evaluations of the proposed methods (Section 4.2) and a discussion thereon.

### 4.1. Requirements and design of the experimental setup

In order to carry out various muscle tests with variable intensity of tension, length, diameter, and pressure and record the data, the testing system was designed.

Due to the relatively high tension and available equipment configuration of the setup was chosen to be vertical. The frame and all connection elements were designed to ensure stability and easy replacement of muscles to be tested. Figure 4.1 presents the scheme of the experimental set-up.

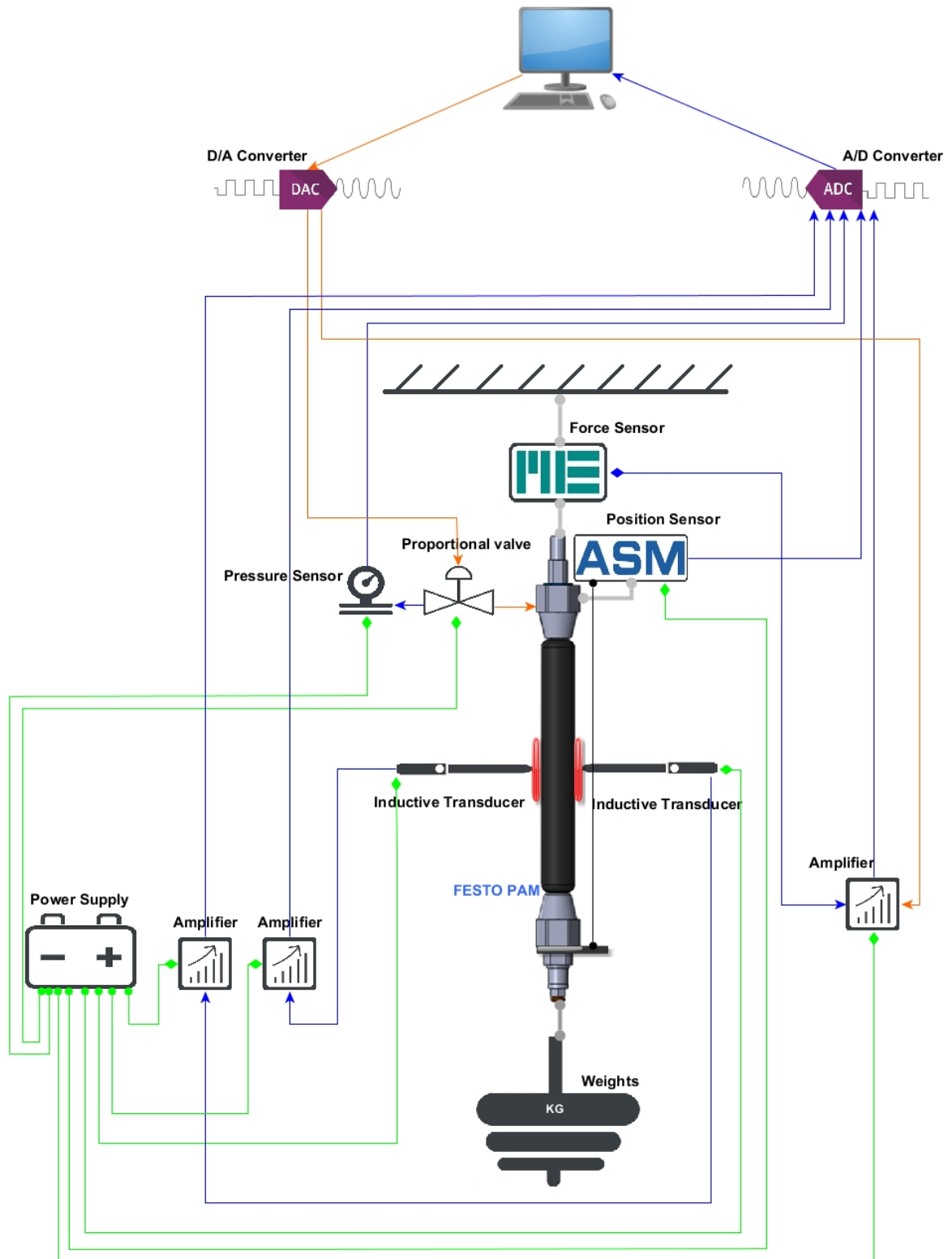


Figure 4.1: **Experimental setup draft:** Blue connections denoting data acquisition signals; Orange connections denoting control signals; Green connections denoting energy supply

#### 4.1.1. Setup description

The testing system includes a personal computer (PC) connected via PC extension bus to a rapid control prototyping *dSPACE* system with digital/analog input/output cards and control CPU card. A fluidic pneumatic muscle *FESTO* model DMSP (4.2), with inner diameter 40mm and different lengths (1000mm, 290mm), was attached vertically to the frame.



Figure 4.2: **Fluidic Muscles DMSP-40 manufactured by FESTO**

In order to realize the desired load (e.g. in isotonic experiments from 100N to 800N) different combinations of weights (20kg and 5kg) were used, which were attached to tested muscle trough manufactured rack (Figure 4.3).



Figure 4.3: **Manufactured rack for mounting weights**

The force is measured with compact tension/pressure/force sensor, the used model was KM30z manufactured *ME-Systeme* (Figure 4.4) with a maximum measured force up to 2500N.



Figure 4.4: **Force sensor**

The valve used is electronically controlled proportional pressure regulator manufactured by *HOER-BIGER* (Figure 4.5). The set pressure is constantly compared with the electronically detected actual value. If deviations occur, the electronic control system rapidly corrects the output pressure using an internal control system. An analog input signal ( $1\text{ V}/\text{bar}$ ) is realized by *dSPACE* control system. Other valve characteristics of interest are: operating pressure range 0-10bar and weigh of 0.6Kg.



Figure 4.5: **Proportional valve**



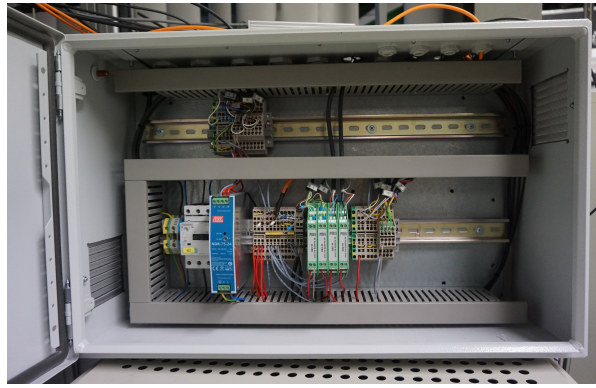


Figure 4.8: **Expansion box**

The control development system is based on *MATLAB/Simulink* environment, providing Toolboxes and Toolsets for control development and implementation, system identification, as well Real-Time Workshop providing automatic code generation. A GUI is realized in the *dSPACE(Control Desk)* supporting real-time data acquisition of selected signals. Specific functions (e.g. for reference signal generations) are implemented in C and integrated using *Simulink's* S-functions mechanisms. Utilizing these functions, as well as standard libraries, various tests, such as isotonic, dynamic testing and other tests for modelling coefficients identification, were implemented in *Simulink* and realized in the *dSPACE* system (Figure 4.9).



Figure 4.9: **dSPACE Board box**

Described setup is presented in Figure 4.10:

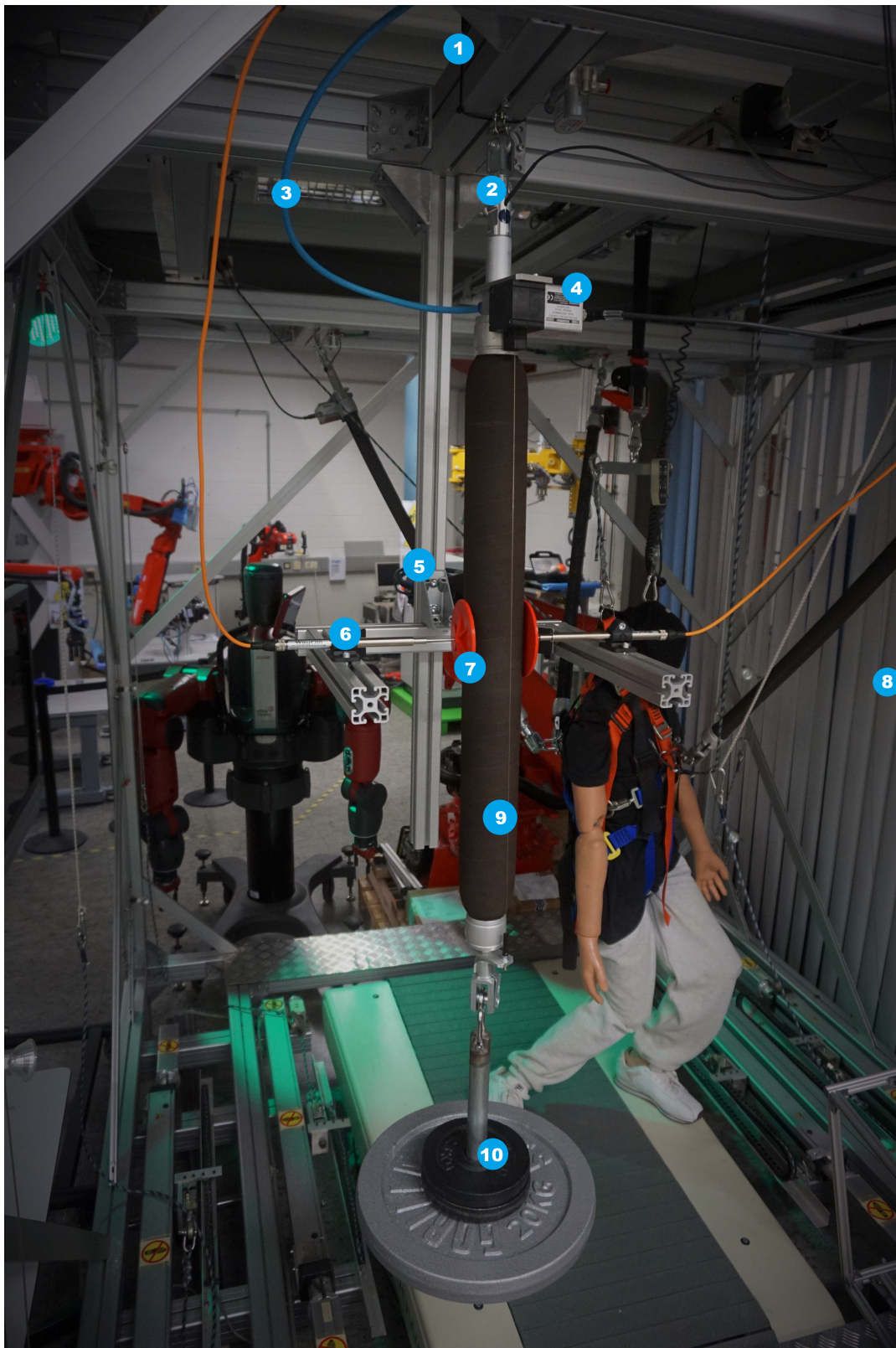


Figure 4.10: **Experimental setup:** (1)Proportional valve(not visible); (2)Force sensor; (3)Pneumatic connection; (4)Position sensor; (5)Construction; (6)Inductive sensor; (7)3D-printed extensions; (8)Expansion box(not visible); (9)FESTO pneumatic muscle; (10)Maunting rack with weights

## 4.2. Experimental analysis of operational characteristic of PAM

Regardless of the chosen modelling approach, it is needed to understand the behavior of the system in different experimental conditions which are reflecting on potential working condition. Analogously to experiments of biological muscles, in view of statement explained in Chapter 2, that behavior of PAMs is very close to biological muscles, it is common practice that also PAMs are tested under similar experimental conditions.

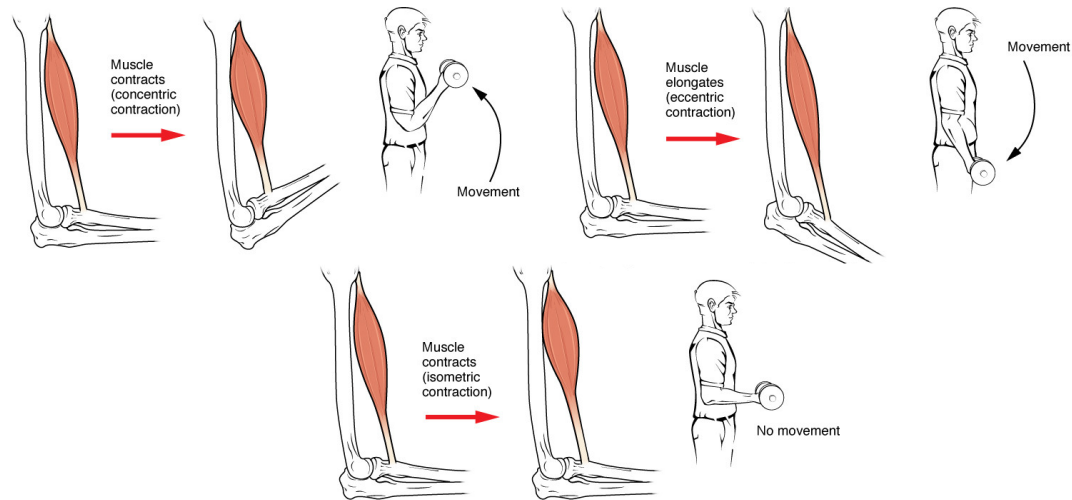


Figure 4.11: **Contraction types:** (1)Concentric contraction(top-left); (2)Eccentric contraction (top-right); (3)Isometric contraction(bottom)

Biological muscle can perform two different types of contraction (Figure 4.11). Isotonic contraction (shown at the top part of the figure), where tension develops to a point and then remains constant while the muscle changes its length. There are two types of isotonic contractions. Concentric contraction occurs when the muscle shortens, while eccentric contraction occurs when the muscle lengthens. During isometric contractions, the muscle itself does not change in length while the tension never exceeds the load that must be carried. This means that while the muscle itself does not shorten, the tension will never exceed the opposing force [71].

The nature of PAM actuator was analyzed under isotonic and isometric conditions. In order to get a mathematical model of the actuator, set of experiments, that accounts for the category of typical for analyzing a pneumatic muscle actuator, was performed. To describe the tension-length-pressure relationship of the fluidic muscle different testing configurations can be used: the length-pressure relationship under constant tension (isotonic experiments), static tension-length relationship under constant pressure (isobaric experiments) and force evaluation tests with fixed muscle length in response to pressure (isometric experiments). The pressure, analogous to the activation level of biological muscles is always an input to muscle mechanics.

### 4.2.1. Isotonic experiments

To carry out isotonic experiments different value of tensions were applied to the lower end of the muscle, by hanging different combination of weights which pull the muscle downwards. The force value was increased by approximately 100N from 0N to around 800N while the pressure at each nominal load force value is step-wise (0.5bar) increased from 0.15bar to 4.5bar and decreases again to initial value in order to analyze the hysteretic behavior of the muscle. The length and diameter of the fluidic muscle were measured in each case and the values of force, pressure, diameter, and length are recorded. The first muscle tested is the DMSP-40-100N. The typical obtained isotonic curves are presented in Figure 4.12, showing displacement in response to the internal pressure. At a constant force load, the contraction and diameter (Figure 4.13) of the muscle increases with the pressure inside the muscle in a nonlinear way. It can be also seen that higher weights at small pressures (up to 0.5bar) are stretching the muscle, and contractions are negative. This observation will be important in the next sections when mathematical models are analyzed.

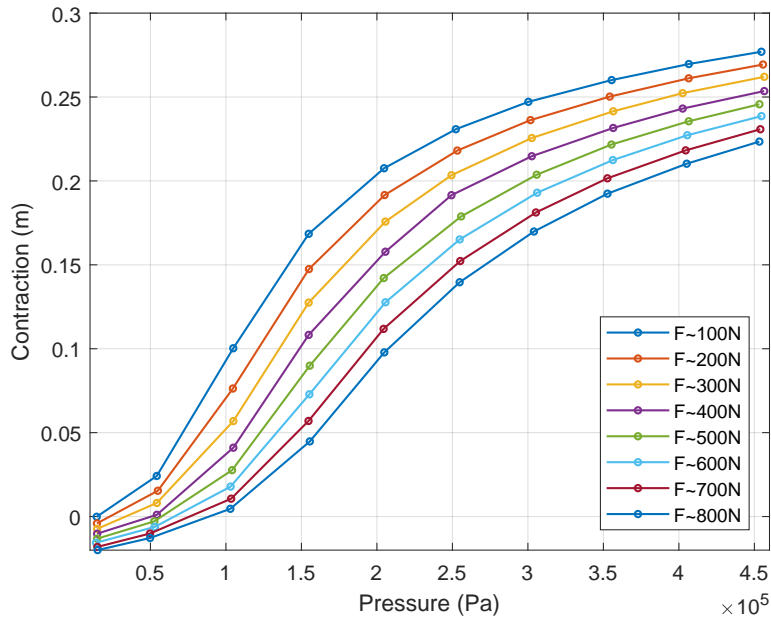


Figure 4.12: **Isotonic curves DMSP-40-1000N - Contraction**

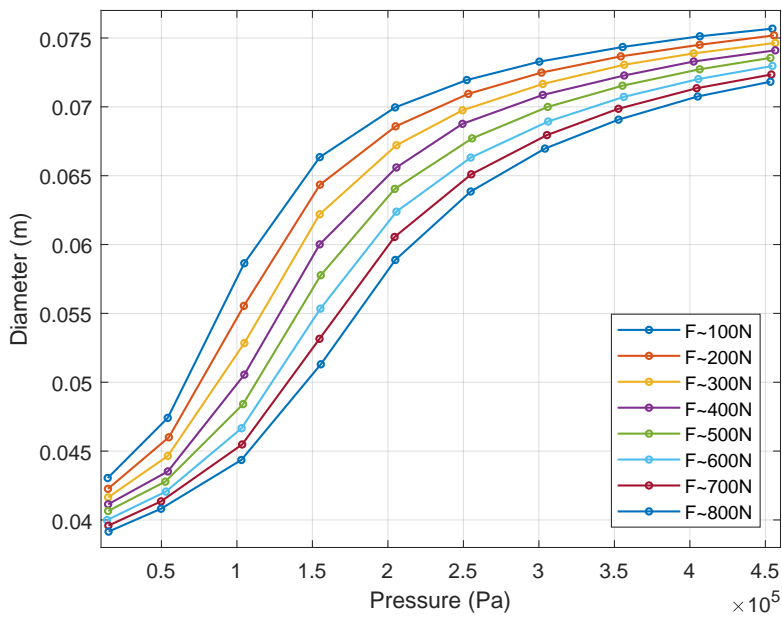


Figure 4.13: **Isotonic curves DMSP-40-1000N - Diameter**

The Figure 4.14 shows the isotonic curves with hysteresis. At a certain force load, the contraction is smaller when the internal muscle pressure increases than when it decreases. The width of the hysteresis loop decreases when the path length slightly decreases (with increasing load). Possible causes of the hysteresis are elastic energy storage during changing the form of the bladder and intern dry friction between the fibers of the muscle. Same properties are applying to its diameter, what is presented in Figure 4.15.

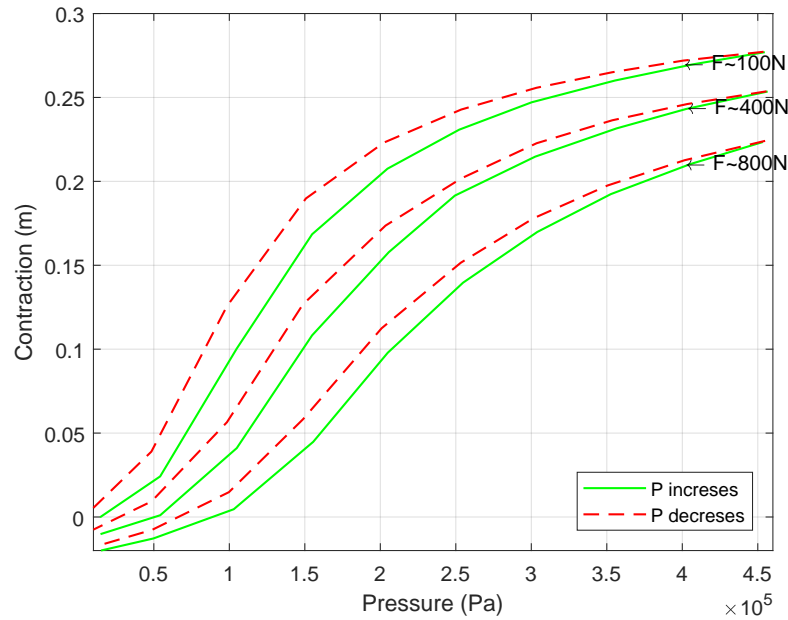


Figure 4.14: **Isotonic curves DMSF-40-1000N with hysteresis - Contraction**

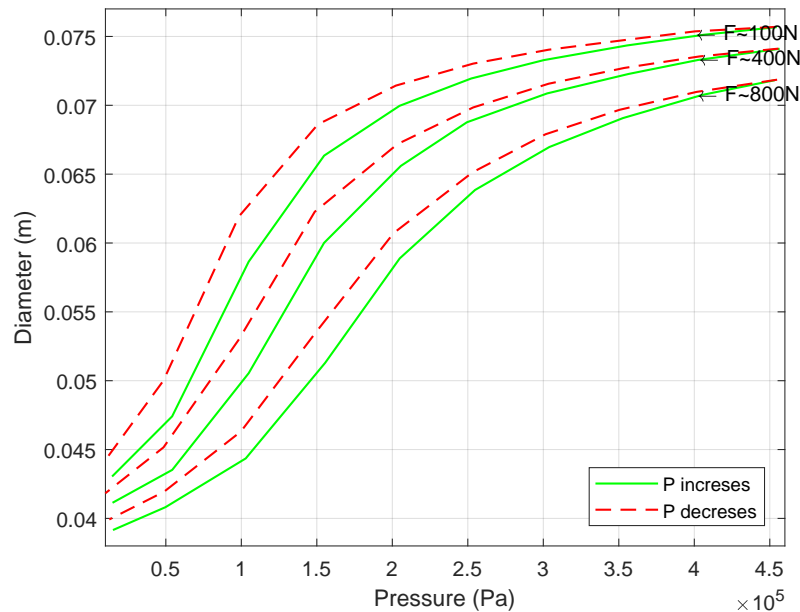


Figure 4.15: **Isotonic curves DMSF-40-1000N with hysteresis - Diameter**

The same experiments were done with the shorter muscle, DMSP-40-290N. The maximum contraction over nominal length is 25% for *FESTO* muscles. From this is clear that contraction of this muscle will have lower values, that can be seen from Figure 4.16, while values of diameter are similar since initial diameters of two tested muscles are same. It can be also seen that contractions over pressures are similar for all loads except for the load of 100N, that can cause problems in modeling of this muscle.

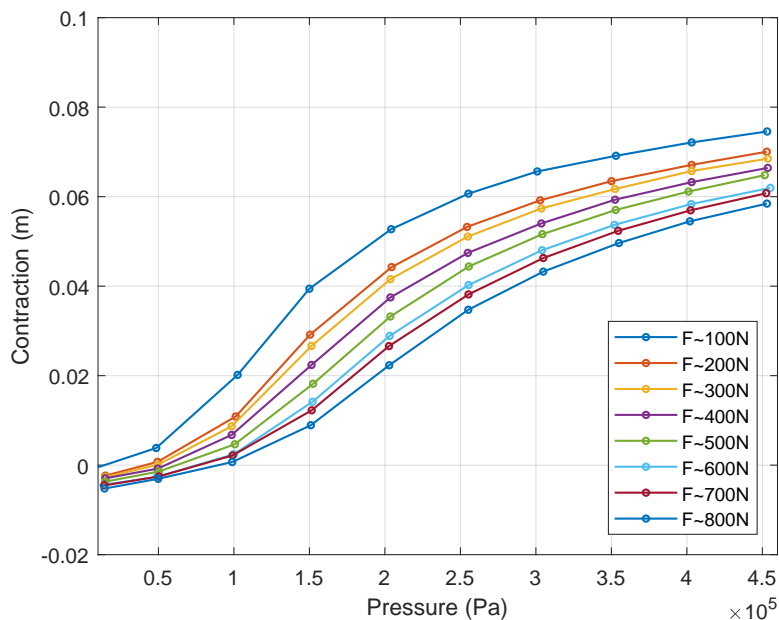


Figure 4.16: **Isotonic curves DMSP-40-290N - Contraction**

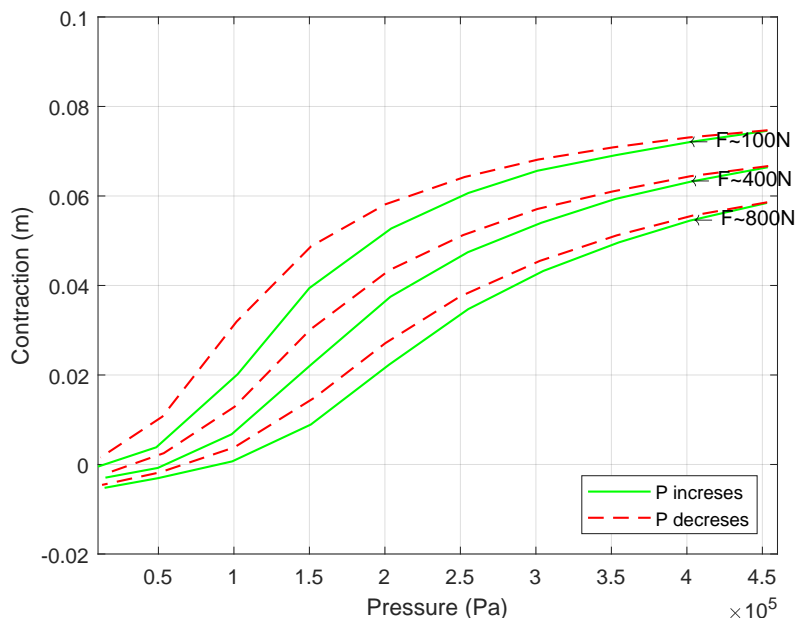


Figure 4.17: **Isotonic curves DMSP-40-290N with hysteresis - Contraction**

It is interesting now to see 3-Dimensional graphics (figures 4.18 and 4.19), which show the length-pressure-force relationship of actuator. In these figures, it can be observed how the nonlinear effects are clearer at lower pressure values.

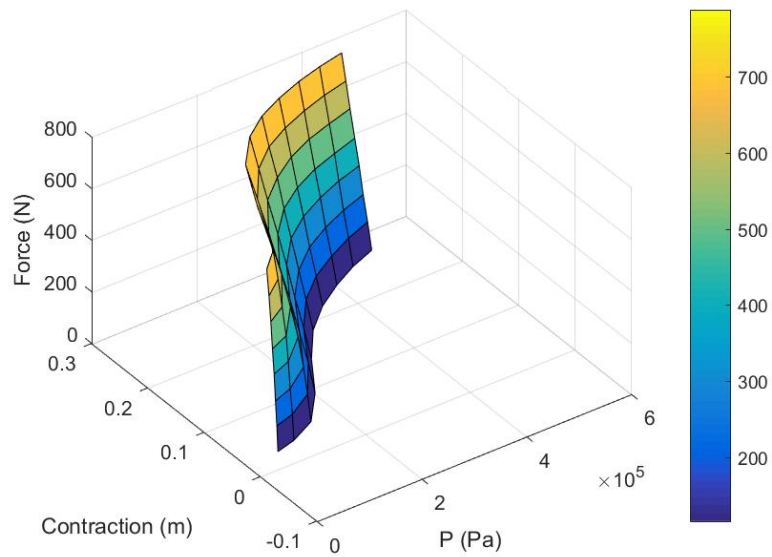


Figure 4.18: **3-D representation of experimental results DMSP-40-1000N**

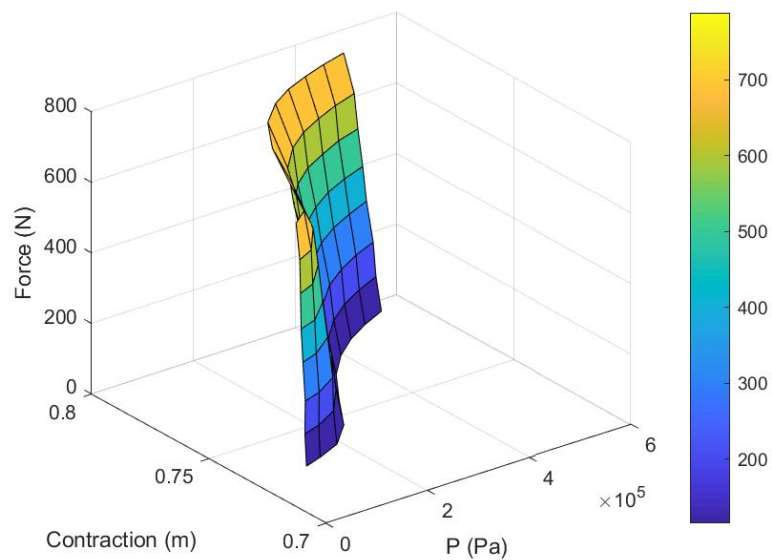


Figure 4.19: **3-D representation of experimental results DMSP-40-290N**

### 4.2.2. Isobaric experiments

These tests are carried out by maintaining the pressure in the muscle at constant levels from 1bar to 4bar, increasing the force by 100N from 0N to 800N and decreasing it again to the initial value. The length values were recorded. At a certain intern pressure, the contraction increases almost linearly with the increase of the load.

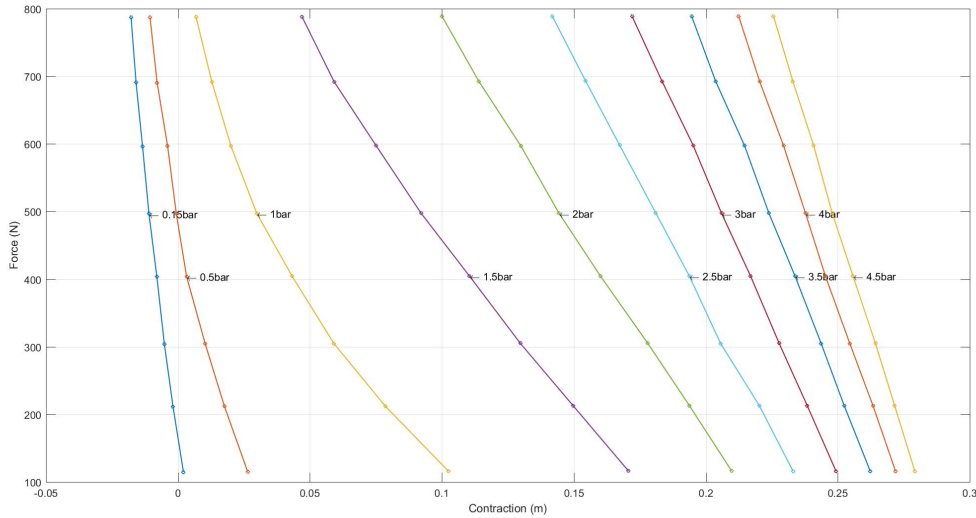


Figure 4.20: **Isobaric curves DMSP-40-1000N**

The isobaric experiments show the hysteresis effects of the *FESTO* muscles as well. The Figure 4.21 shows the isobaric curves for the DMSP-40-1000N.

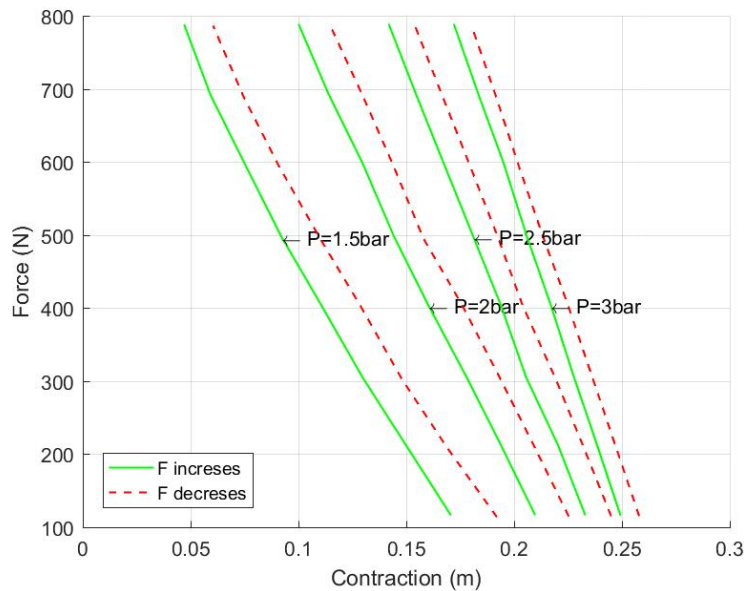


Figure 4.21: **Isobaric curves with hysteresis DMSP-40-1000N**

### 4.2.3. Isometric experiments

For analysis of isometric characteristic, the actuator needs to be fixed at the end, so that, although the pressure inside of the muscle increases, the muscle cannot contract itself. Instead of building a new setup, a numerical calculation method was adopted. To get all necessary data, interpolation of the length-pressure-force relationship was carried out through *MATLAB* function: *griddedInterpolant()*, with 'spline' interpolation method specified. The result of approximation satisfies needs for intended application but needs to be considered throughout calculation of the following mathematical model designs. Graphical representation of the mentioned procedure is shown in Figure 4.22:

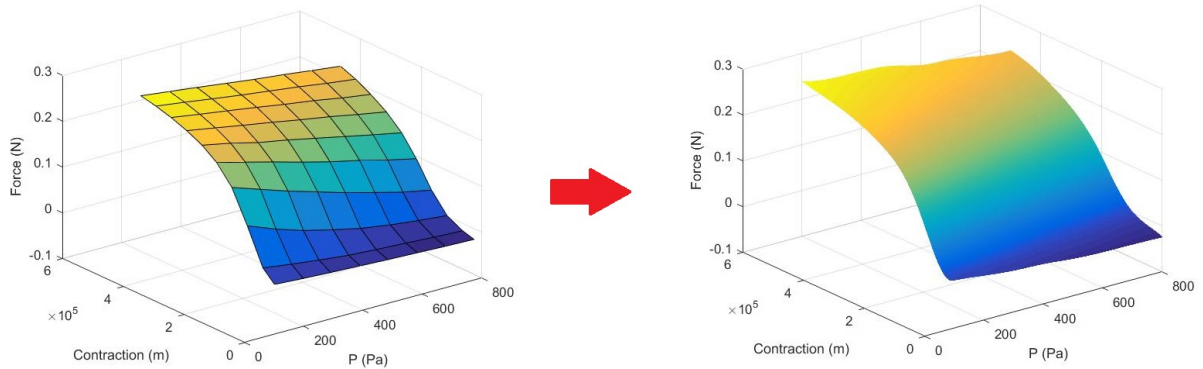


Figure 4.22: Interpolation of length-pressure-force relationship

To get isometric characteristic the muscle length value is fixed at 5 different values corresponding to different muscle contraction in range from 5cm to smallest of all maximum measured contraction from each attached weight, that is 22cm for applied force of 800N and the tension is calculated in combination with fixed pressures values as increments of 0.5bar. Isometric characteristic is presented in Figure 4.23:

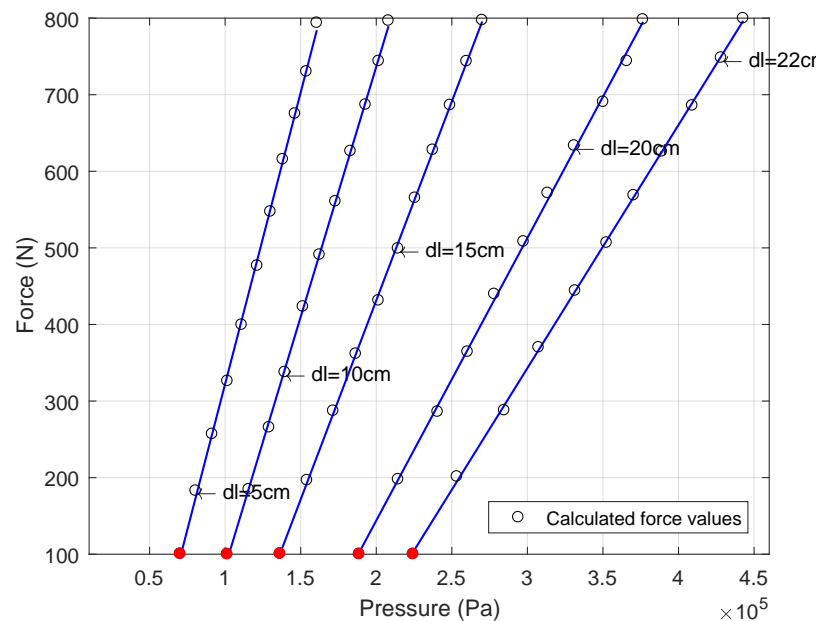


Figure 4.23: Isometric curves DMSP-40-1000N

### 4.3. Experimental implementation of different modeling methods

Deliberation of validity and justification is very important for adoption of existing models in a specific case. For this cause, some representatives of models described in Chapter 3 will be analyzed for experimental data of the actuators and their application. Benefits of chosen models will be explained, as well as flaws which they bring.

#### 4.3.1. Empirical "Virtual Area" Model

From the logic explained in Chapter 3, force realized at the actuator's end can be denoted as given pressure multiplied with virtual area  $A(\Delta L)$  which depends from the contraction that will be realized:

$$F = -p \frac{dV}{dl} \quad (4.1)$$

$$F(p, \Delta L) = pA(\Delta L) \quad (4.2)$$

As can be seen from this Figure 4.23, isometric force/pressure relationship can indeed be accurately approximated by the linear function. The slope of straight lines corresponds to the virtual area mentioned, which obviously decreases with the contraction (inversely, the real physical area of the muscle increases with the shortening, i.e., inflation). The force/pressure straight lines, however, don't pass through the origin, as indicated by the model (4.1, 4.2), rather crosses the  $x$ -axis at intercept points defining the pressure at which force becomes zero. This pressure is needed to inflate the muscle and to reach a given contraction, thereby deforming rubber/membrane core elements. The entire pressure work is consumed for the muscle deformation, and at zero force pressure and corresponding contraction, no mechanical force can further be exerted. This deformation energy was neglected in equations (4.1, 4.2). *FESTO*, comparing to other pneumatic muscles has significantly stronger bladder structure knitted, integrating both rubber tube and membrane, so the internal elastic deformation energy must be included, as discussed in Chapter 3, in the form:

$$F = -p \frac{dV}{dl} - V_b \frac{dW}{dl} \quad (4.3)$$

The internal deformation effect can be modelled by means of  $x$ -intercept pressure value. Assuming that this pressure depends on the contraction  $\Delta L$ , it may be written:

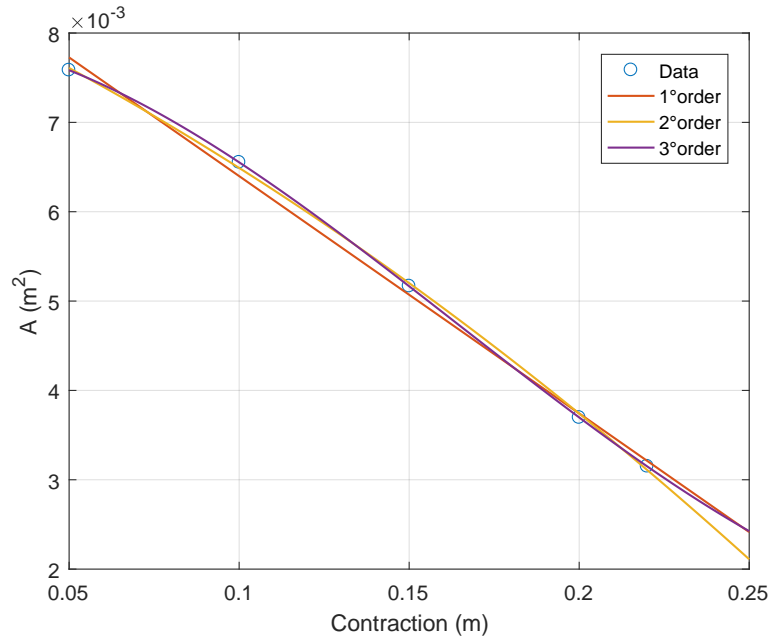
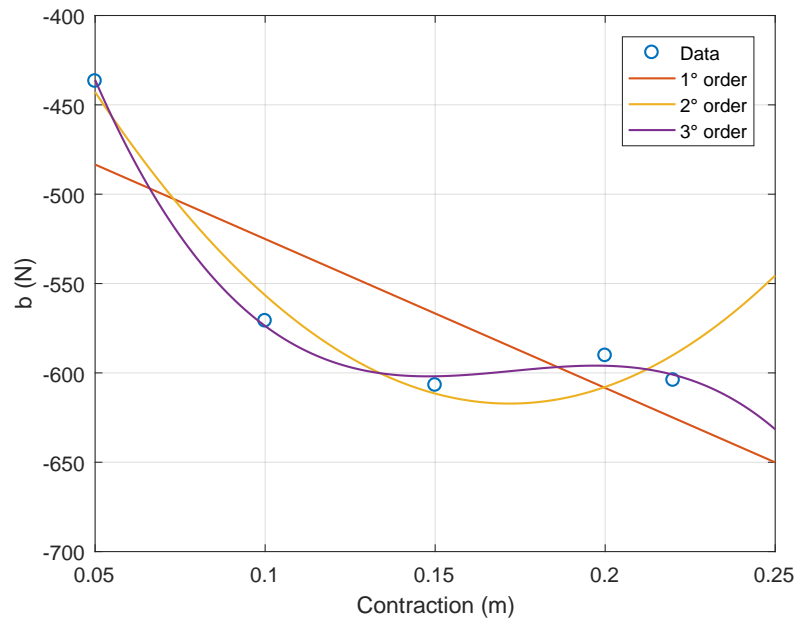
$$F = (p - p_0(\Delta L))A(\Delta) \quad (4.4)$$

This model can be transformed in the slope-intercept form:

$$F = pA(\Delta L) - p_0(\Delta L)A(\Delta L) = pA(\Delta L) + b(\Delta L) \quad (4.5)$$

Where  $b(\Delta L)$  represents a fictive negative force-intercept value at zero pressure. This model form has been applied for the identification of isometric force.

$A(\Delta)$  and  $b(\Delta L)$  are identified approximating the slopes of the straight lines and the  $x$ -intercept value by means of the polynomial in  $\Delta L$ . Interpolations of the first, second and third order were accomplished for both. Thereby the polynomial of the first, second and third order was used. The figures 4.24 and 4.25 show the results:

Figure 4.24: **Models for the virtual area DMSP-40-1000N**Figure 4.25: **Models for the radial expansion force DMSP-40-1000N**

As already mentioned, the virtual area  $A(\Delta L)$  can be accurately approximated by a linear function of contraction. The estimated virtual area is:

$$A(\Delta L) = a_1 \Delta L + a_0 = -0.0266 \Delta L + 0.0091 \quad (4.6)$$

The polynomial of 3rd order approximates properly the value  $b(\Delta L)$ :

$$b(\Delta L) = b_3 \Delta L^3 + b_2 \Delta L^2 + b_1 \Delta L + b_0 \quad (4.7)$$

$$b_3 = -1.0067 \cdot 10^5; \quad b_2 = 5.2111 \cdot 10^4; \quad b_1 = -8.8089 \cdot 10^3; \quad b_0 = -1.1329 \cdot 10^2 \quad (4.8)$$

Figure 4.26 presents the comparison between experimental results and model for the same data used to calculate model coefficients. It can be seen that model results are not fitting experimental ones perfectly. This mismatching is caused by two approximations that are applied, first one to get not experimentally measured isometric values, and second for fitting the function for  $A(\Delta L)$  and  $b(\Delta L)$ . Nevertheless, these inaccuracies are not significant, what can be proved with checking with other experimental data, used also in verification of other models, shown in the figures below (4.30, 4.31).

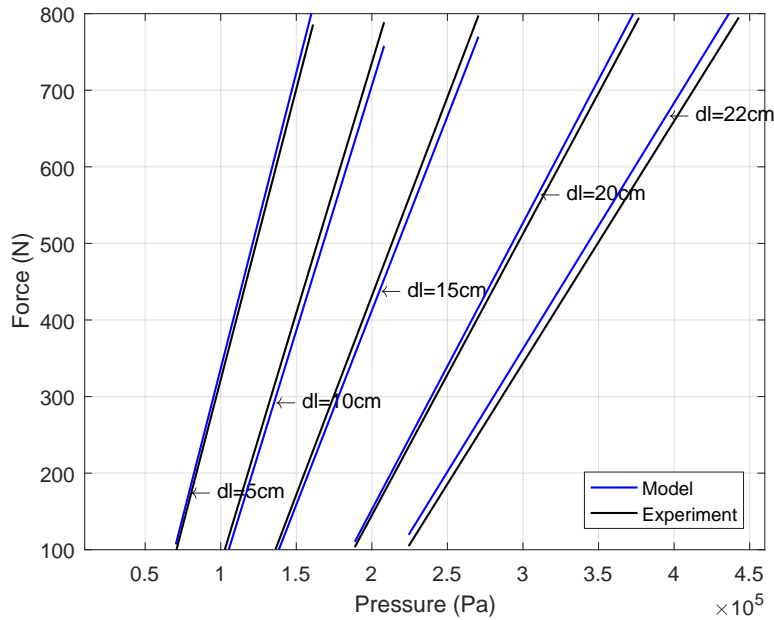


Figure 4.26: Comparison between experimental results and the model DMSP-40-1000N

The same interpolations were carried out to estimate the static virtual area of the shorter fluidic muscles. The figures 4.28, 4.27 and 4.29 illustrate it for DMSP-40-290N:

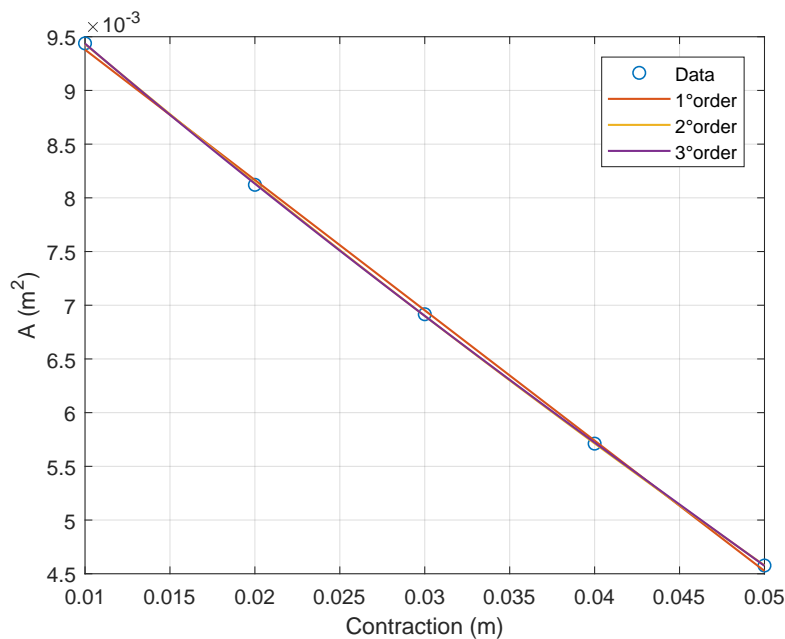
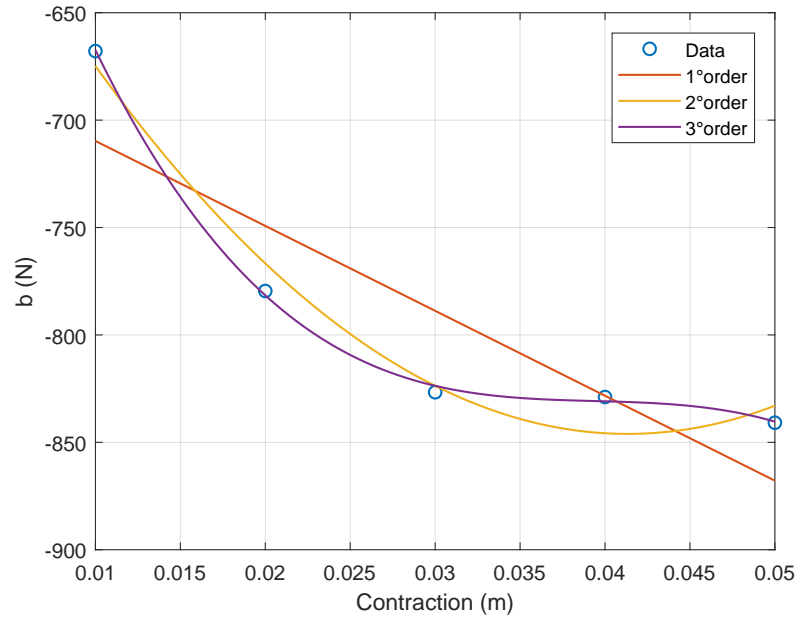
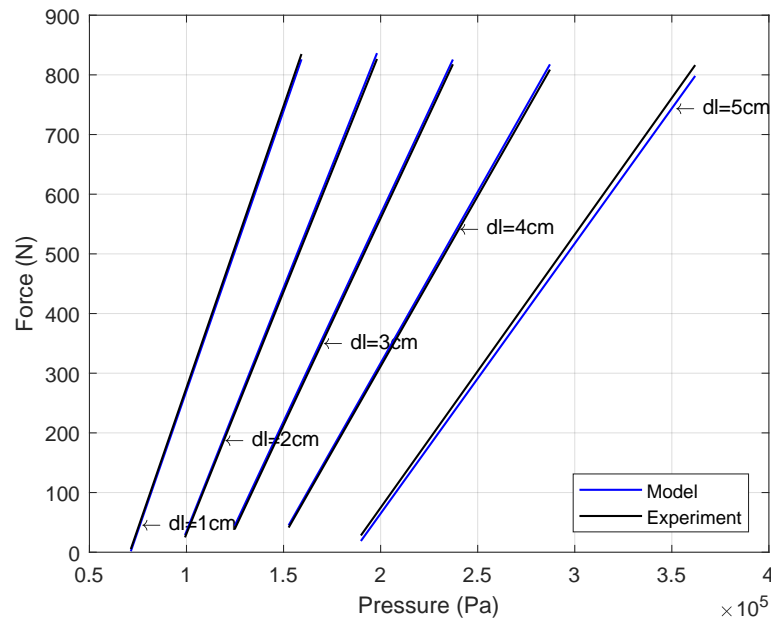


Figure 4.27: Models for the virtual area DMSP-40-290N

Figure 4.28: **Models for the radial expansion force DMSP-40-290N**Figure 4.29: **Comparison between experimental results and the model DMSP-40-290N**

From figures 4.27 and 4.28 can be seen that functions of the virtual area and radial expansion force have the almost same shape as for the longer muscle, but with different polynomial coefficients:

$$A(\Delta L) = a_1 \Delta L + a_0 = -0.1213 \Delta L + 0.0106 \quad (4.9)$$

The polynomial of 3rd order approximates properly the value  $b(\Delta L)$ :

$$b(\Delta L) = b_3 \Delta L^3 + b_2 \Delta L^2 + b_1 \Delta L + b_0 \quad (4.10)$$

$$b_3 = -6.19051 \cdot 10^6; \quad b_2 = 7.3168 \cdot 10^5; \quad b_1 = -2.9035 \cdot 10^4; \quad b_0 = -4.4399 \cdot 10^2 \quad (4.11)$$

Experimental results are compared with the model at following figures (4.30, 4.31):

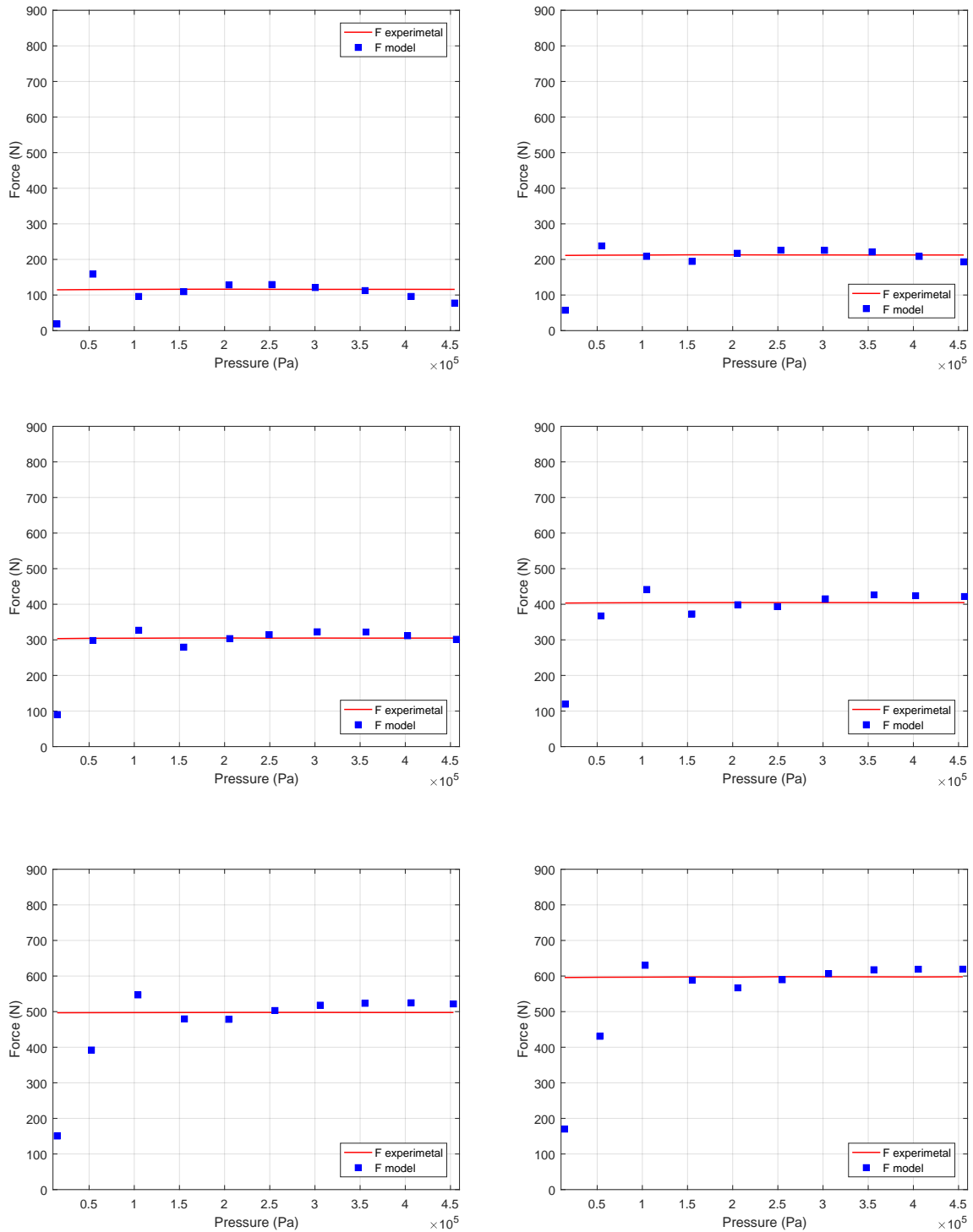


Figure 4.30: Comparison between experimental results and "Virtual Area" model: (1)10kg; (2)20kg; (3)30kg; (4)40kg; (5)50kg; (6)60kg

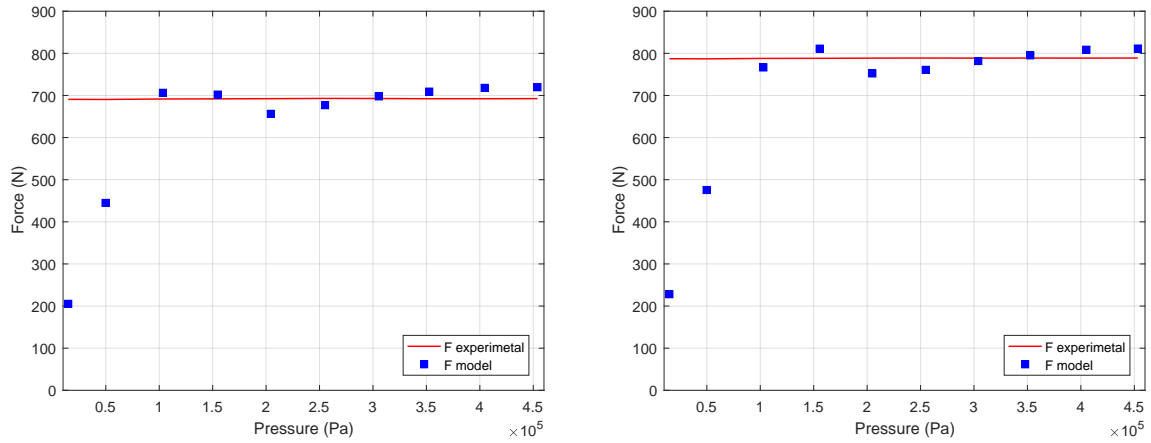


Figure 4.31: **Comparison between experimental results and "Virtual Area" model:** (1)70kg; (2)80kg

In the experiments, the force produced by the muscle and force calculated by model match considerably accurate, especially for relatively lighter loads (weights attached) for the pressures over  $0.5\text{bar}$ . In the model of the mechanical system (equation 4.2), the input is the pressure in the pneumatic muscle. The pressure multiplies the virtual area  $A(\Delta L)$  of the muscle obtained from the isometric experiments, the term  $b(\Delta L)$  which represents the energy loss by the elasticity of the rubber is added and the result is the force produced by the muscle. But the muscle is subject of an initial tension due to weights attached, causing increased dry friction between braids of the mesh. The movement (contraction) of the muscle begins when the value  $pA(\Delta L)$  overcomes this tension (recall negative contractions from subsection 4.2.1). During this occurrence, phenomena which are describing the model are still not established and that has the influence on the values of modeled force for pressures less than  $0.5\text{bar}$ , making them inaccurate.

### 4.3.2. Empirical "Spring" Model

As exposed in Chapter 3, the force acting on the muscle can be calculated from the equation:

$$F_{elastic} = K(P, L_S)L_S \tag{4.12}$$

Variable stiffness parameter  $K$  must be identified from experimental data. Observing the behavior of the unloaded muscle length according to the air pressure within the PAM, authors from [64] determined that the functional relationship between these two variables can be approximated by fitting the data into the second order polynomial function. Same can be noticed in the plot of DMSP-40-1000N presented in Figure 4.32:

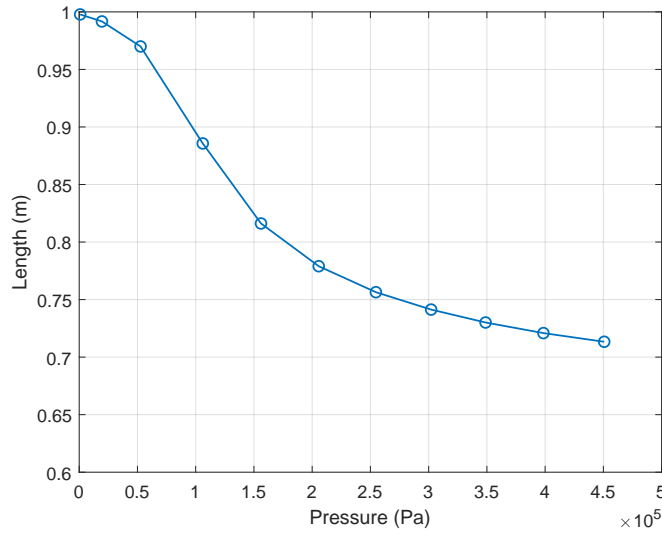


Figure 4.32: Plot of unstretched length against air pressure DMSP-40-1000N

Accordingly, the stiffness parameter  $K$  was explicitly taken as second-order polynomial function of  $L_S$  and  $P$ :

$$K = C_3P^2 + C_2PL_S + C_1L_S^1 + C_0 \tag{4.13}$$

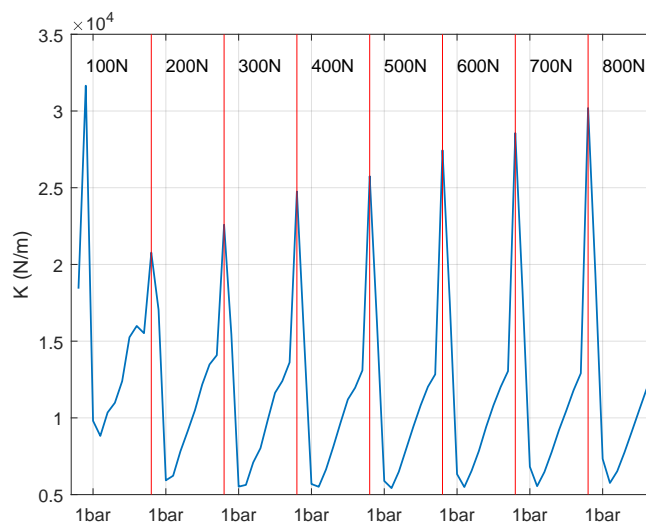


Figure 4.33: Stiffness parameter K over pressure/load combinations DMSP-40-1000N

Same characteristics are presented for DMSP-40-290N:

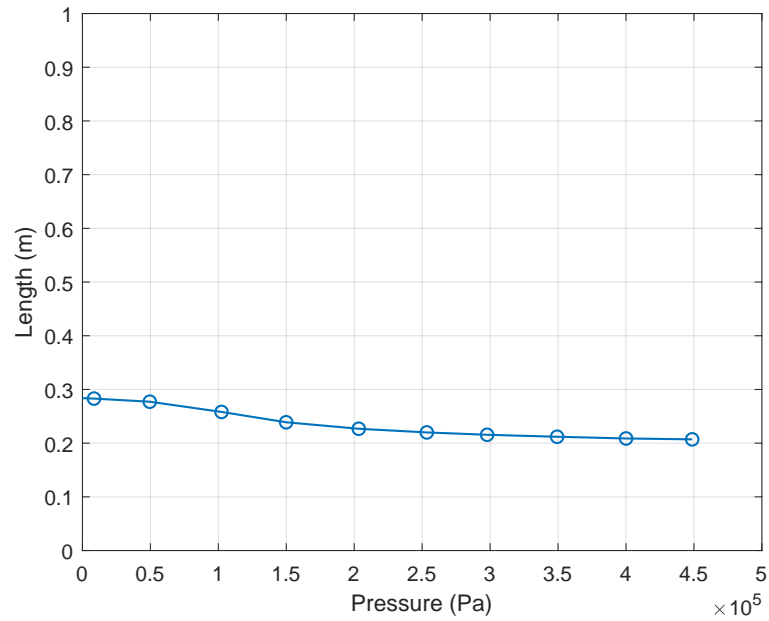


Figure 4.34: **Plot of unstretched length against air pressure DMSP-40-290N**

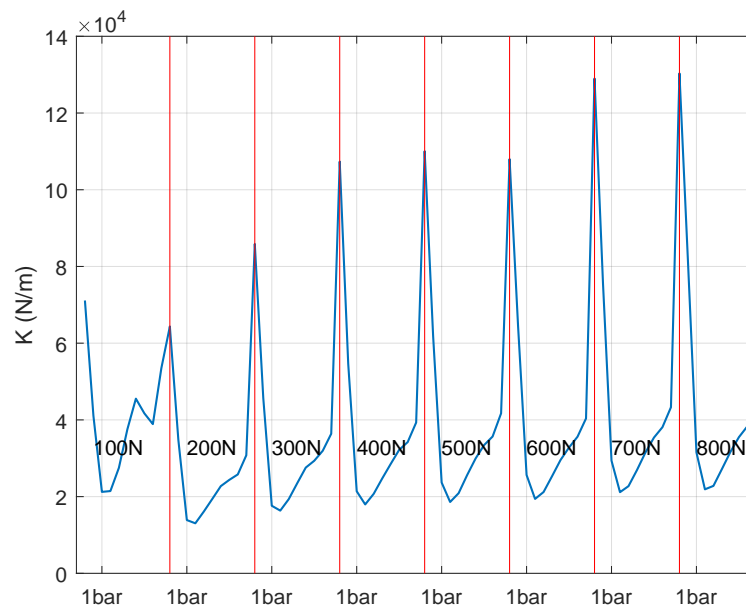


Figure 4.35: **Stiffness parameter K over pressure/load combinations DMSP-40-290N**

Studying function of parameter  $K$  calculated from experimental data, shown in Figure 4.33, it was decided to divide range of the air pressure while calculating coefficients for  $K$  into the operating conditions where the air pressure is  $0bar-1bar$  (considered as low-pressure range), and from  $1bar-4.5bar$  (considered the high-pressure range), so the best fit can be yield.

To determine the coefficients, regression over experimental steady-state force data is used to express the spring constant  $K$ . Constants coefficients  $C_0, C_1, C_2$  obtained in such way are presented in table 4.1:

Constant	$0bar-1bar$	$1bar-4.5bar$
$C_3$	$-1.4085 \cdot 10^{-6}$	$4.0050 \cdot 10^{-8}$
$C_2$	-0.9883	0.0138
$C_1$	$8.0126 \cdot 10^5$	$-5.2663 \cdot 10^4$
$C_0$	$2.3983 \cdot 10^4$	$5.2159 \cdot 10^3$

Table 4.1: Values of coefficient K for DMSP-40-1000N

The same procedure was carried out to estimate the coefficients of the polynomial function of stiffness coefficient  $K$  for shorter fluidic muscle. The figures 4.34 and 4.37 illustrate it for DMSP-40-290N. Constants coefficients  $C_0, C_1, C_2$ , calculated for this PAM, are presented in table 4.2:

Constant	$0bar-1bar$	$1bar-4.5bar$
$C_3$	$-5.1038 \cdot 10^{-6}$	$1.0624 \cdot 10^{-7}$
$C_2$	-32.6762	1.4412
$C_1$	$1.2782 \cdot 10^8$	$-5.8944 \cdot 10^5$
$C_0$	$8.5370 \cdot 10^4$	$1.0784 \cdot 10^4$

Table 4.2: Values of the coefficient K for DMSP-40-290N

Experimental results are compared with model at following figures (4.36, 4.37):

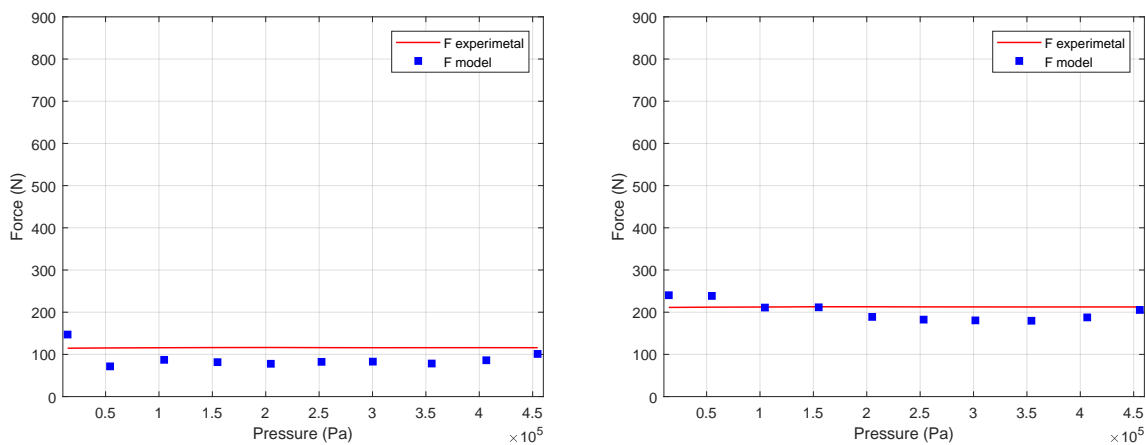


Figure 4.36: Comparison between experimental results and "Spring" model: (1)10kg; (2)20kg

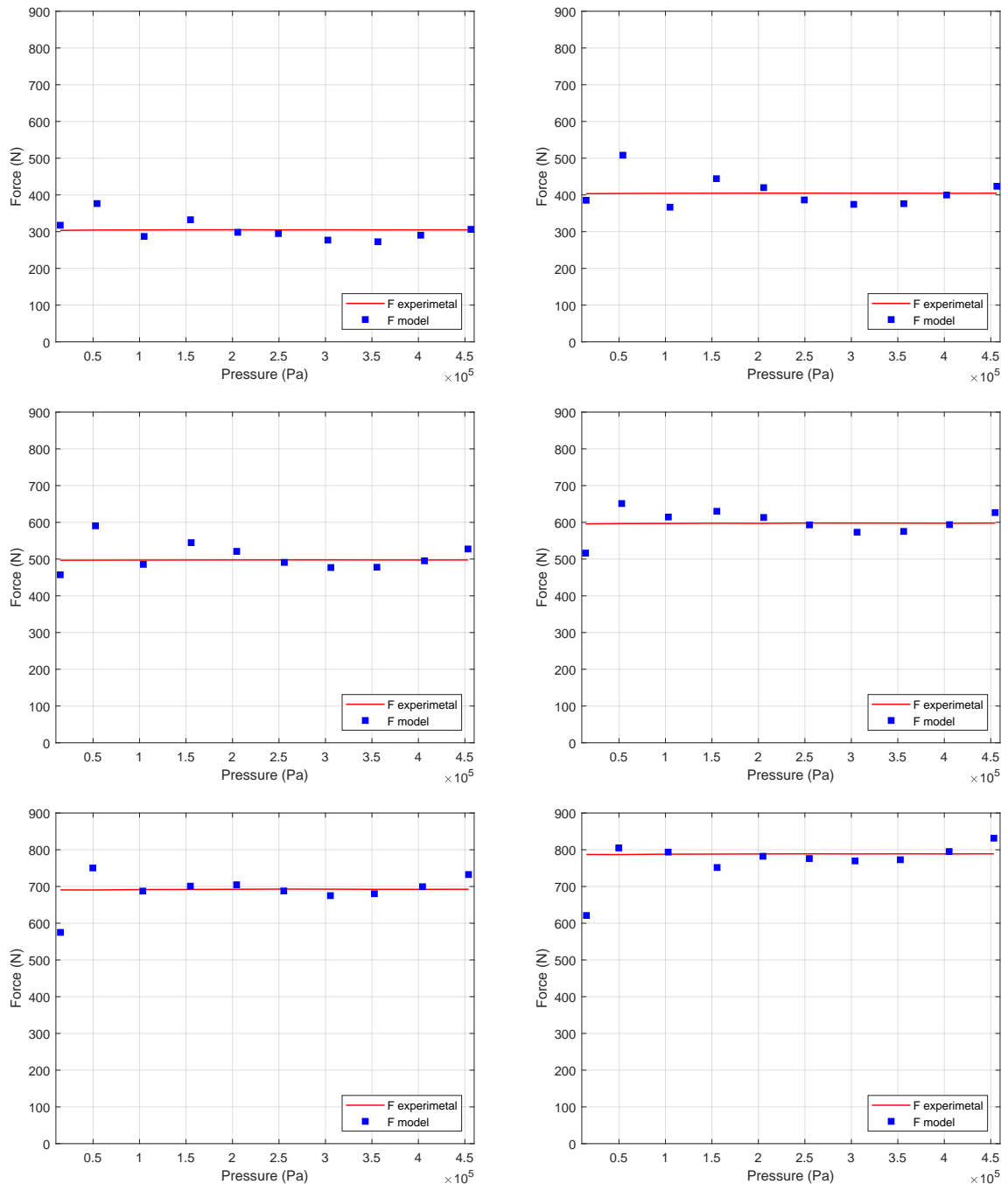


Figure 4.37: **Comparison between experimental results and "Spring" model:** (1)30kg; (2)40kg; (3)50kg; (4)60kg; (5)70kg; (6)80kg

This model also showed considerable accuracy in the matching of the experimental force produced by the muscle and force calculated by the model. Again, inaccuracy of modeled values for small pressures is present and can be also explained with the same explanation that muscle is initially stretched. Nevertheless, these errors are significantly smaller compared to values determined with the model before. One of the possible explanations for this is that this approach models the elasticity of the muscle, behaving like spring, what is also the reason of the muscle being stretched to a length longer than nominal. This explanation can be also one of the reasons why constant error exists for lowest load, what is expected observing function of the parameter  $K$ , that has a different shape for the load of  $10kg$  (Figure 4.33).

### 4.3.3. Geometrical models

Since geometrical models are the basis of many model developing, it was of interest to analyze which level of compatibility these showed applied to *FESTO* muscles. Starting from basic McKibben force formulation stated in Chapter 3:

$$F = \frac{Pb^2(\cos^2 \theta - 1)}{4\pi n^2} \tag{4.14}$$

And using geometrical relations presented with equations 4.14 and 3.5, another force expression stands:

$$F = \frac{p}{4\pi n^2} [3L^2 + b^2] \tag{4.15}$$

Constant values for number of braid turns  $n = 3.5$ , length  $b = 1.0877m$  and  $\theta_0 = 25.7^\circ$  were calculated using experimental data. Exploiting experimental data for DMSP-40-290N and DMSP-40-1000N in force equation 4.15, modeled "McKibben" force values are acquired. In behalf of better transparency the figures were limited so some of the plots were disregarded (figures 4.38 and 4.39):

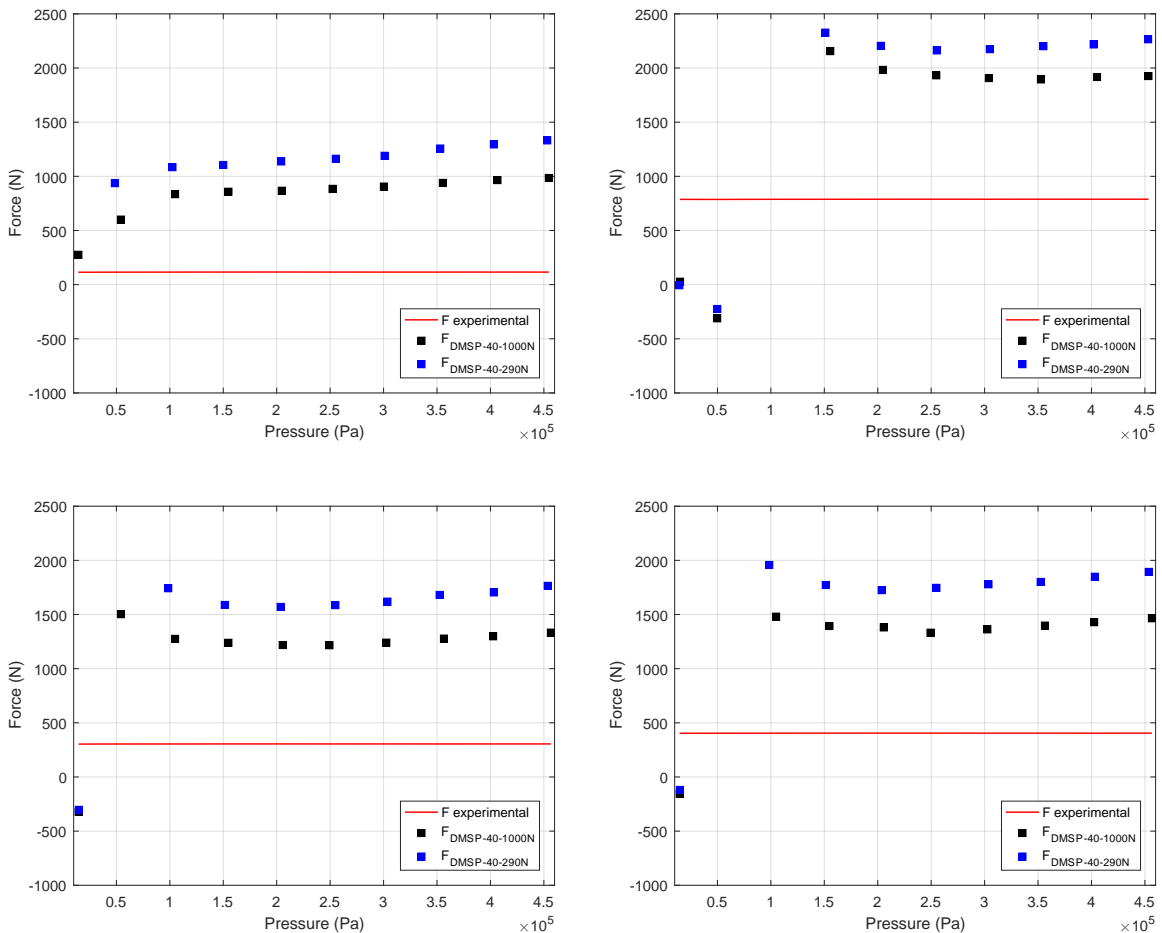


Figure 4.38: Comparison between experimental results and "McKibben" model: (1) 10kg; (2)20kg; (3)30kg; (4)40kg

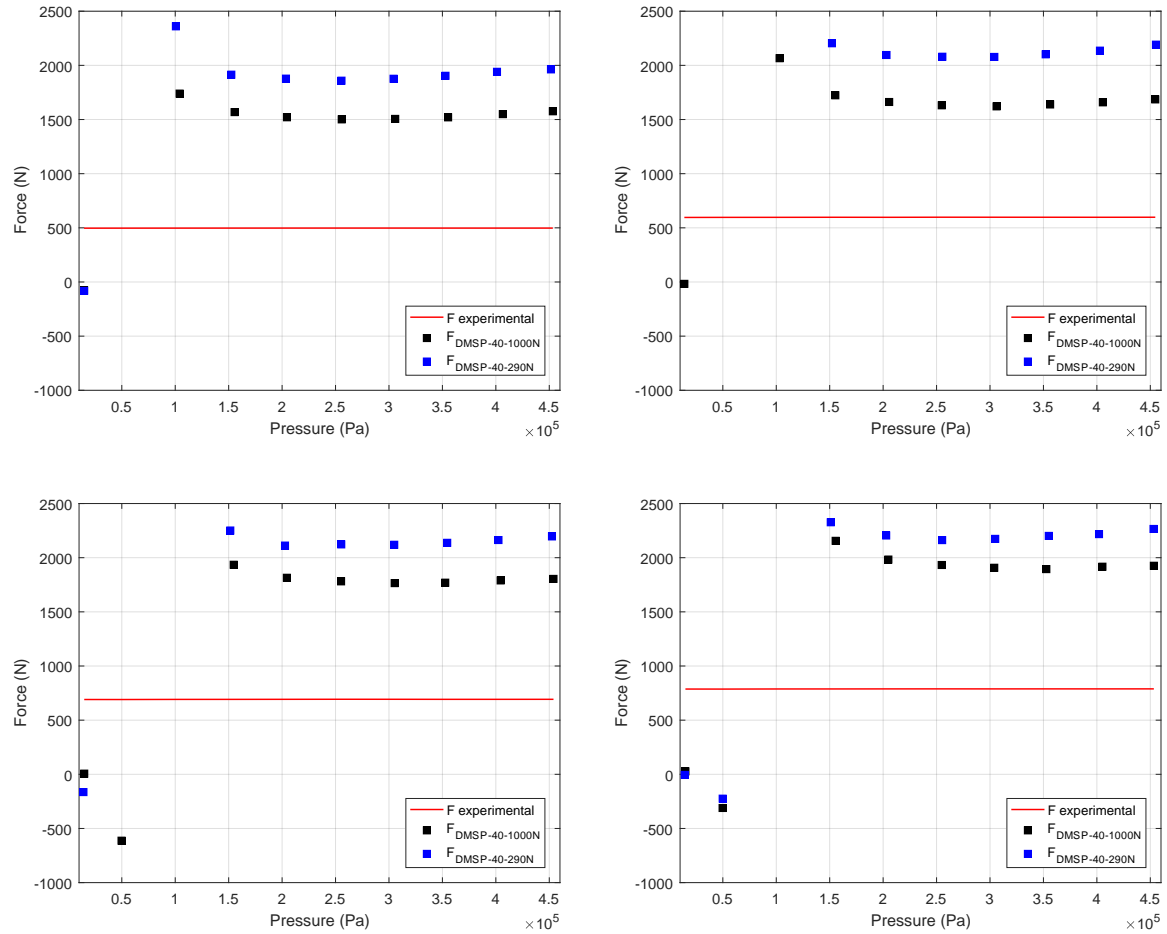


Figure 4.39: Comparison between experimental results and "McKibben" model: (1)50kg; (2)60kg; (3)70kg; (4)80kg

It is obvious that this model shows big inaccuracy in predicting force to be realized that is even bigger for shorter *FESTO* pneumatic muscle.

Exploring different papers more determined to identify precise values of PAMs parameters and their relationship, different value of initial braid angle then one determined trough McKibben geometrical equations was found  $\theta_0 = 30^\circ$  [72]. Model equation for force proposed by [57] is more sensitive to initial braid angle as a result of  $\alpha = \frac{3}{\tan^2 \theta_0}$  and  $\beta = \frac{1}{\sin^2 \theta_0}$ :

$$F = \pi \frac{D_0^2}{4} P [\alpha(1 - \varepsilon_l)^2 - \beta] \quad (4.16)$$

Novel calculated constants with  $\theta_0 = 30^\circ$  are:  $\alpha = 8.3095$  and  $\beta = 3.7698$ . Introducing these to equation 4.16 and calculating modeled force for experimental data, somewhat better results are indeed gained (figures 4.40, 4.41):

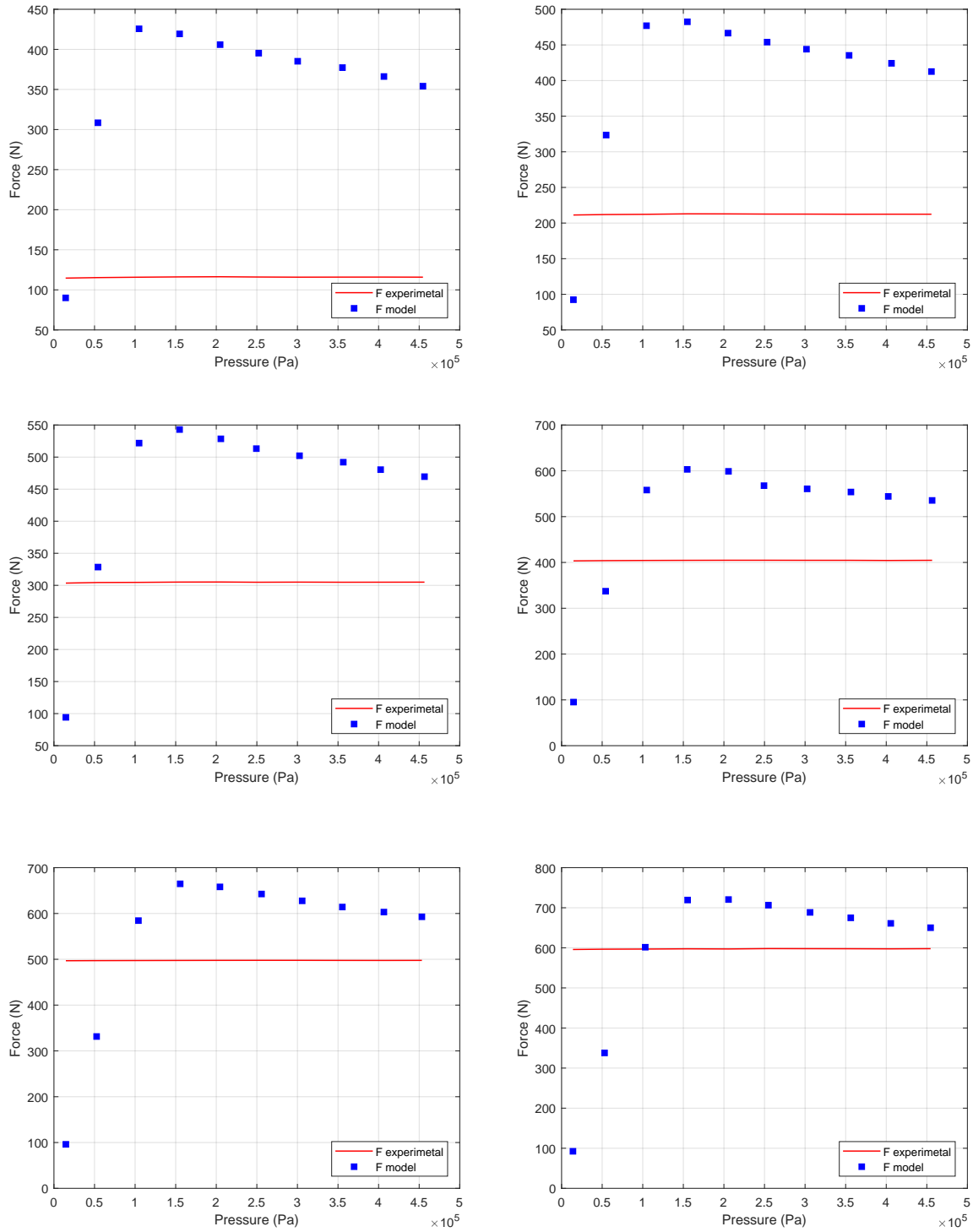


Figure 4.40: Comparison between experimental results and "McKibben II" model: (1)10kg; (2)20kg; (3)30kg; (4)40kg; (5)50kg; (6)60kg

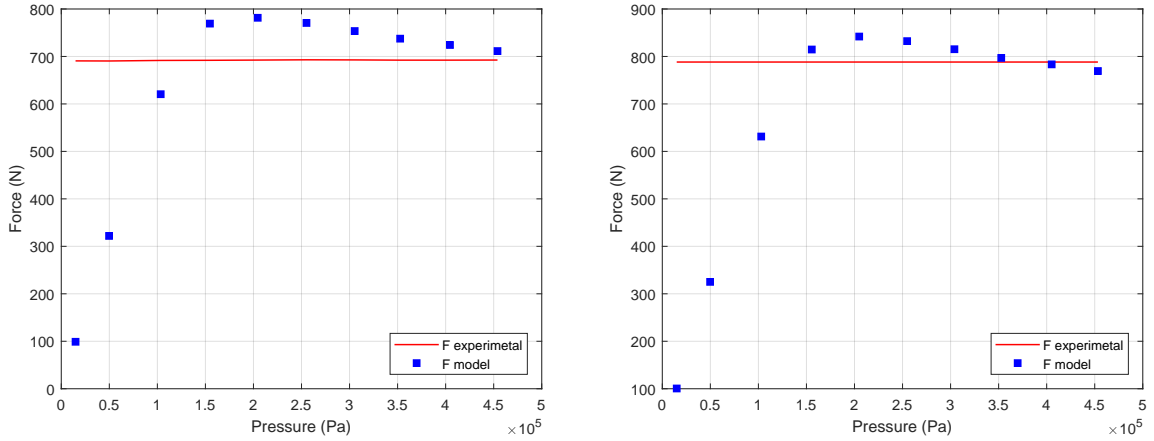


Figure 4.41: **Comparison between experimental results and "McKibben II" model:** (1)70kg; (2)80kg

Although this variation improved results, the acquired model is still not precise enough for most of the load cases. Beside that, this means that initial angle should be determined differently for muscle with different dimensions, which for the same brand of pneumatic muscle should be constant. Furthermore having this parameter deviated from the one gained through calculations proposed by McKibben model is giving an ambiguous relation between parameters and force to be modelled. This implies that input work produced by inlet pressure is not spent only for changing the included air volume causing axial movement of the muscle (contraction). Recalling that *FESTO* muscles have significantly stronger bladder structure knitted integrating both rubber tube and membrane, it is concluded that virtual work necessary to change the potential energy of the elastic membrane rubber has considerable influence on the force realized that is not included by this model.

Modeling that includes such considerations is described in Chapter 3, giving force formulation:

$$F = \frac{p}{4\pi n^2} [3L^2 + b^2] + E \left( \frac{L}{L_0} \right) \varepsilon_L \delta \pi D - E \left( \frac{L}{L_0} \right) \varepsilon_D \frac{2\delta L^2}{Dn^2\pi^2} \quad (4.17)$$

Modulus of elasticity of the membrane rubber must be identified by minimization. In [63], third order polynomial is used for approximation of the modulus of elasticity  $E(L)$  because as it said, determined experimentally it has been noticed that higher-order polynomials do not lead to better results, and on the other hand lower orders bring error. Diversely from this author modulus elasticity is identified as the function of relative length, so it can possibly be universal for muscles of different lengths:

$$E \left( \frac{L}{L_0} \right) = C_3 \left( \frac{L}{L_0} \right)^3 + C_2 \left( \frac{L}{L_0} \right)^2 + C_1 \frac{L}{L_0} + C_0 \quad (4.18)$$

Constant	DMSP-40-1000N	MSP-40-290N
$C_3$	$1.9739 \cdot 10^9$	$0.5256 \cdot 10^9$
$C_2$	$-6.3061 \cdot 10^9$	$-1.1613 \cdot 10^9$
$C_1$	$6.7062 \cdot 10^9$	$0.6621 \cdot 10^9$
$C_0$	$-23582 \cdot 10^9$	$-0.0074 \cdot 10^9$

Table 4.3: **Values of coefficient for  $E(L/L_0)$**

Fitting coefficients of the modulus of elasticity were calculated for both tested actuators and presented in table 4.3. The figures 4.42 and 4.43 are presenting comparison between model and experimental data from testing DMSP-40-1000N:

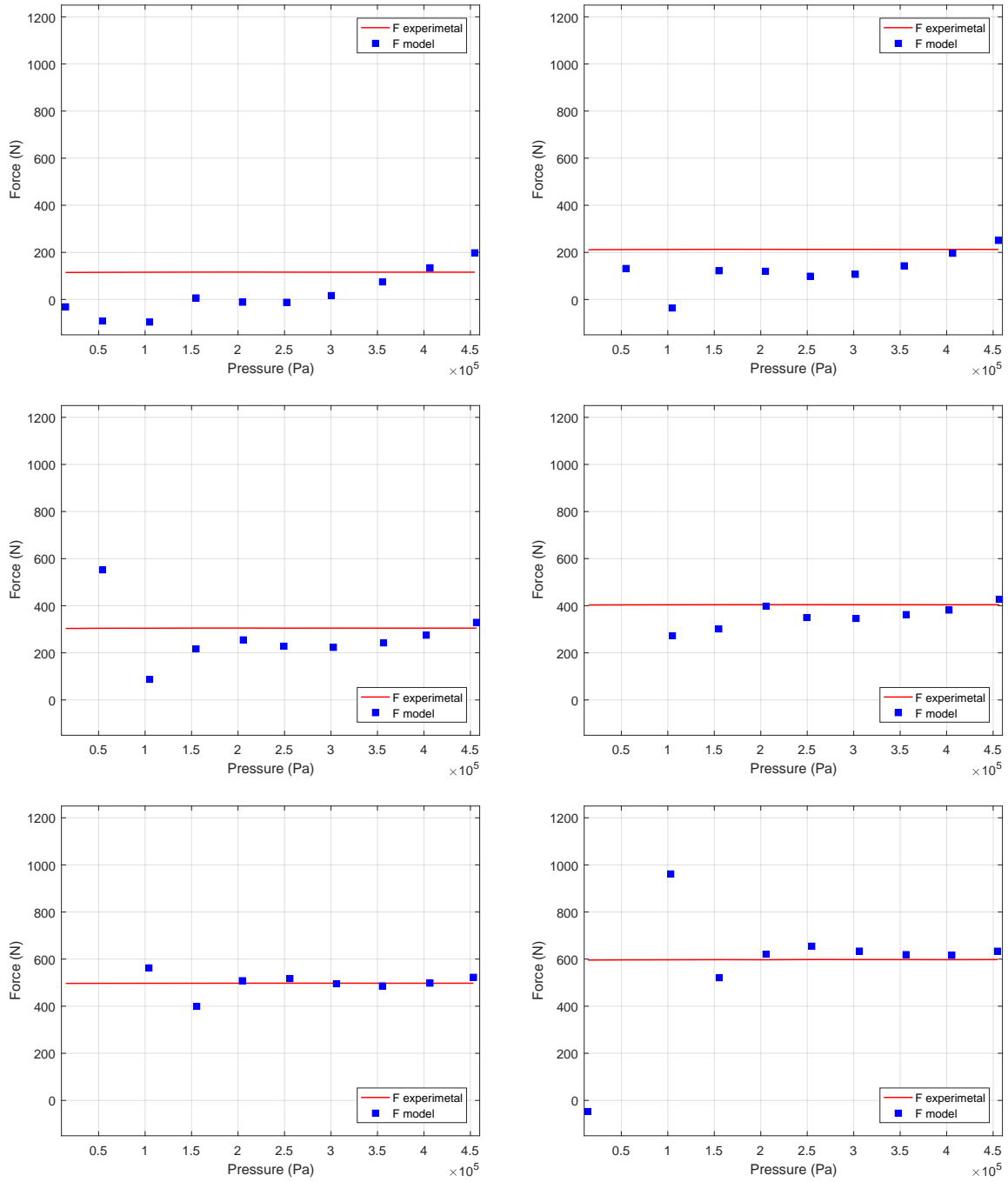


Figure 4.42: Comparison between experimental results and "Improved McKibben " model: (1)10kg; (2)20kg; (3)30kg; (4)40kg; (5)50kg; (6)60kg

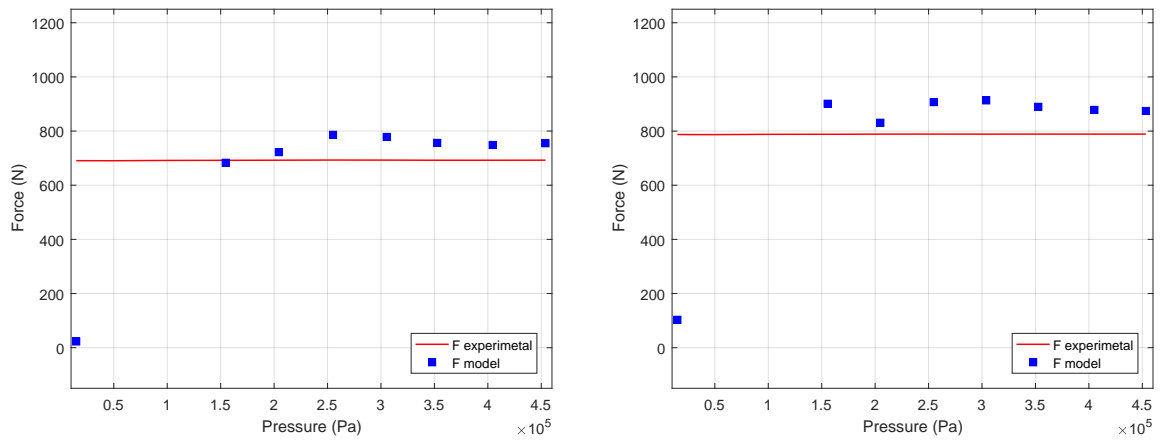


Figure 4.43: Comparison between experimental results and "Improved McKibben" model: (1)70kg; (2)80kg

The figures 4.44 and 4.45 are presenting comparison between model and experimental data from testing DMSP-40-290N:

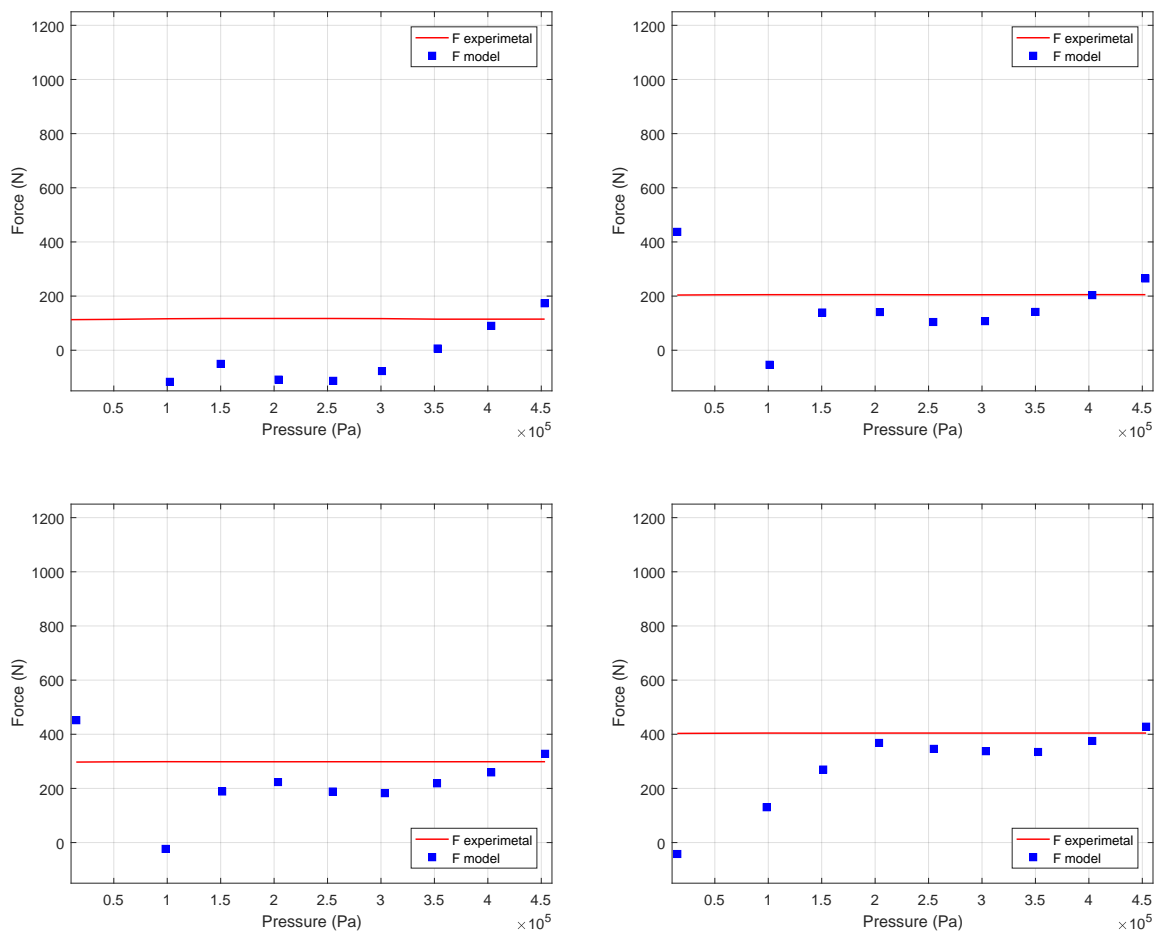


Figure 4.44: Comparison between experimental results and "Improved McKibben" model: (1)10kg; (2)20kg; (3)30kg; (4)40kg

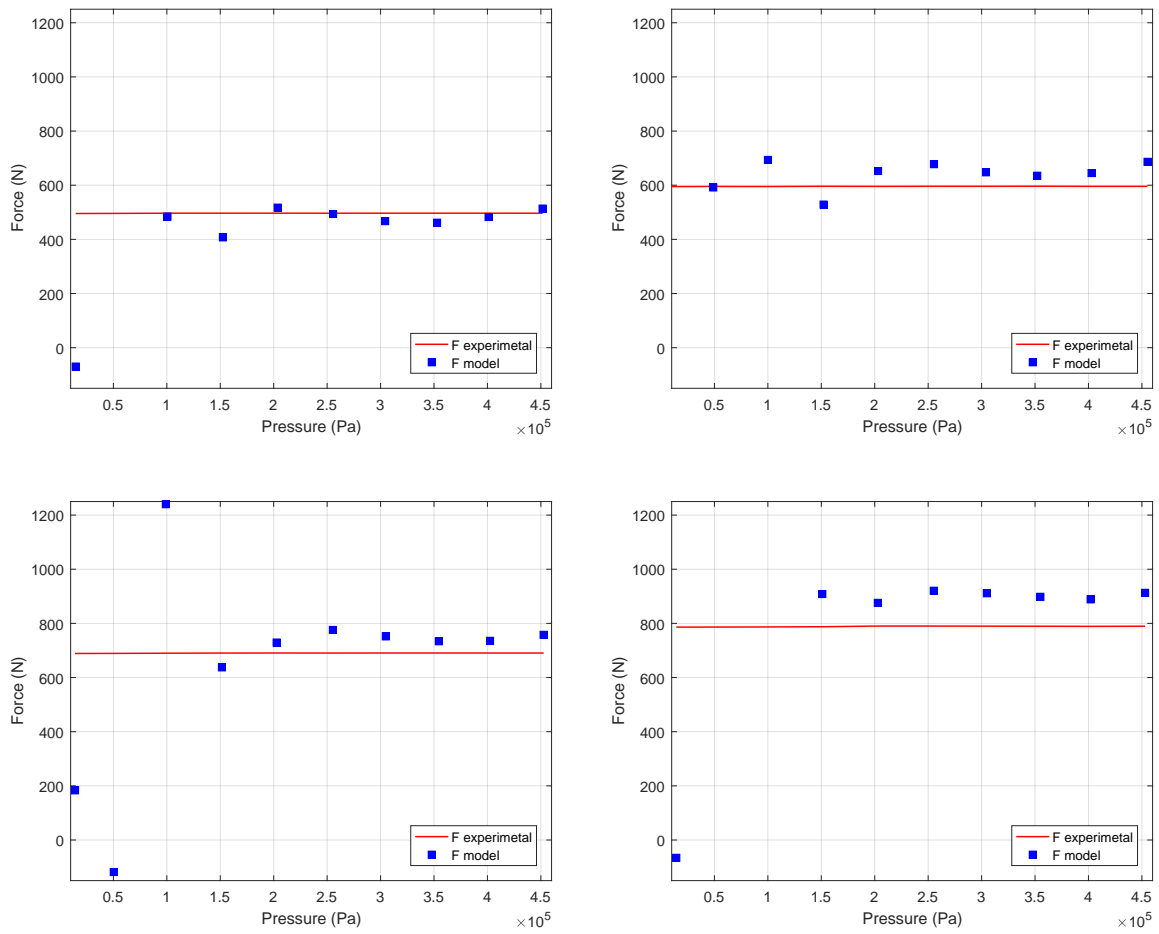


Figure 4.45: Comparison between experimental results and "Improved McKibben" model: (1)10kg; (2)20kg; (3)30kg; (4)40kg

For both actuators tested geometrical model is significantly improved, but still as in previous modeling approaches shows big inaccuracy for pressures lower than 1bar.

It is now interesting to observe how the model behaves if coefficients for identifying elastic modulus  $E \left( \frac{L}{L_0} \right)$  of DMSP-40-1000N are used to determine elastic forces of actuator DMSP-40-290N and vice versa. Cross-validation using parameters of long muscle to identify the model of short muscle is presented in flowing figures (4.46, 4.47):

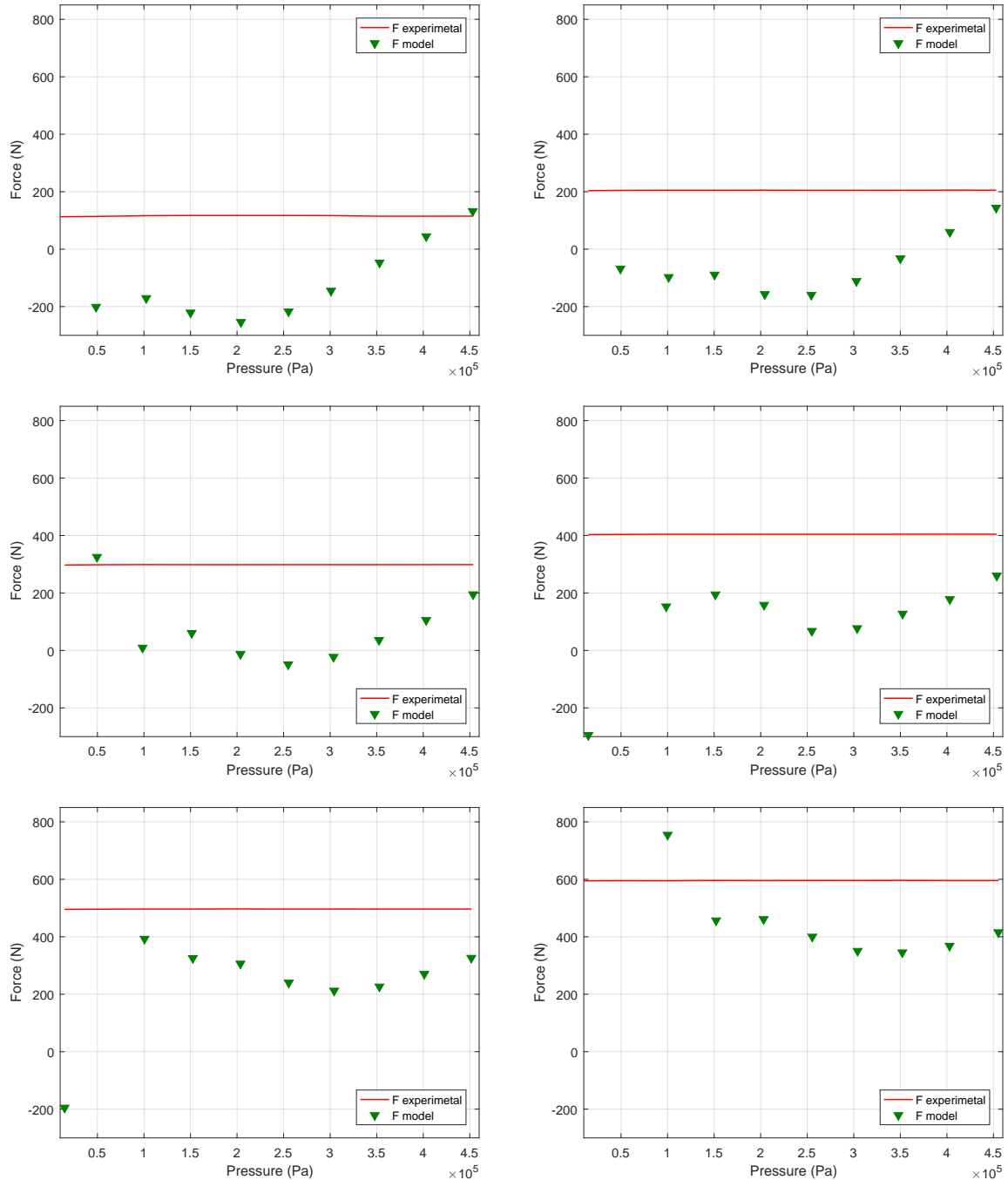


Figure 4.46: **Cross-validation "long-to-short"**: (1)10kg; (2)20kg; (3)30kg; (4)40kg; (5)50kg; (6)60kg

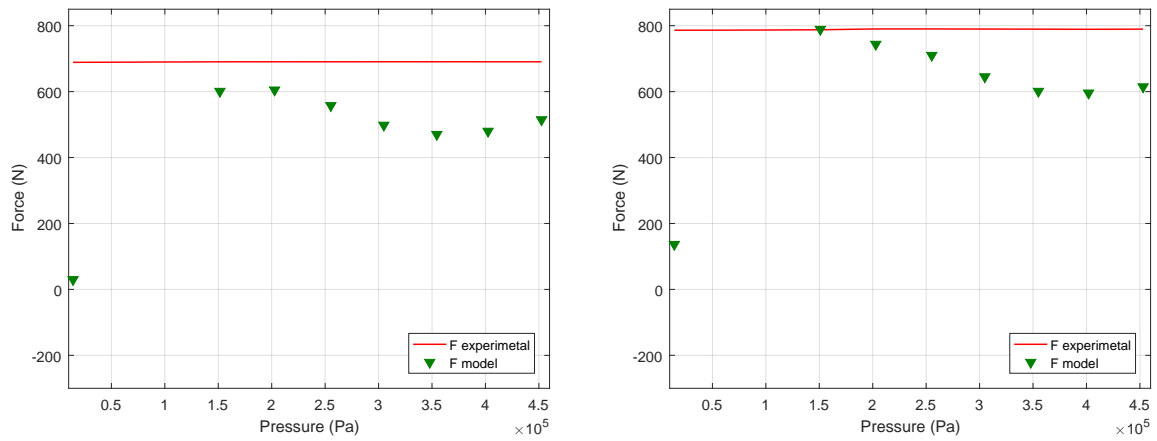


Figure 4.47: **Cross-validation "long-to-short"**: (1)70kg; (2)80kg

Cross-validation using parameters of short muscle to identify model of long muscle is presented in flowing figures (4.48, 4.49):

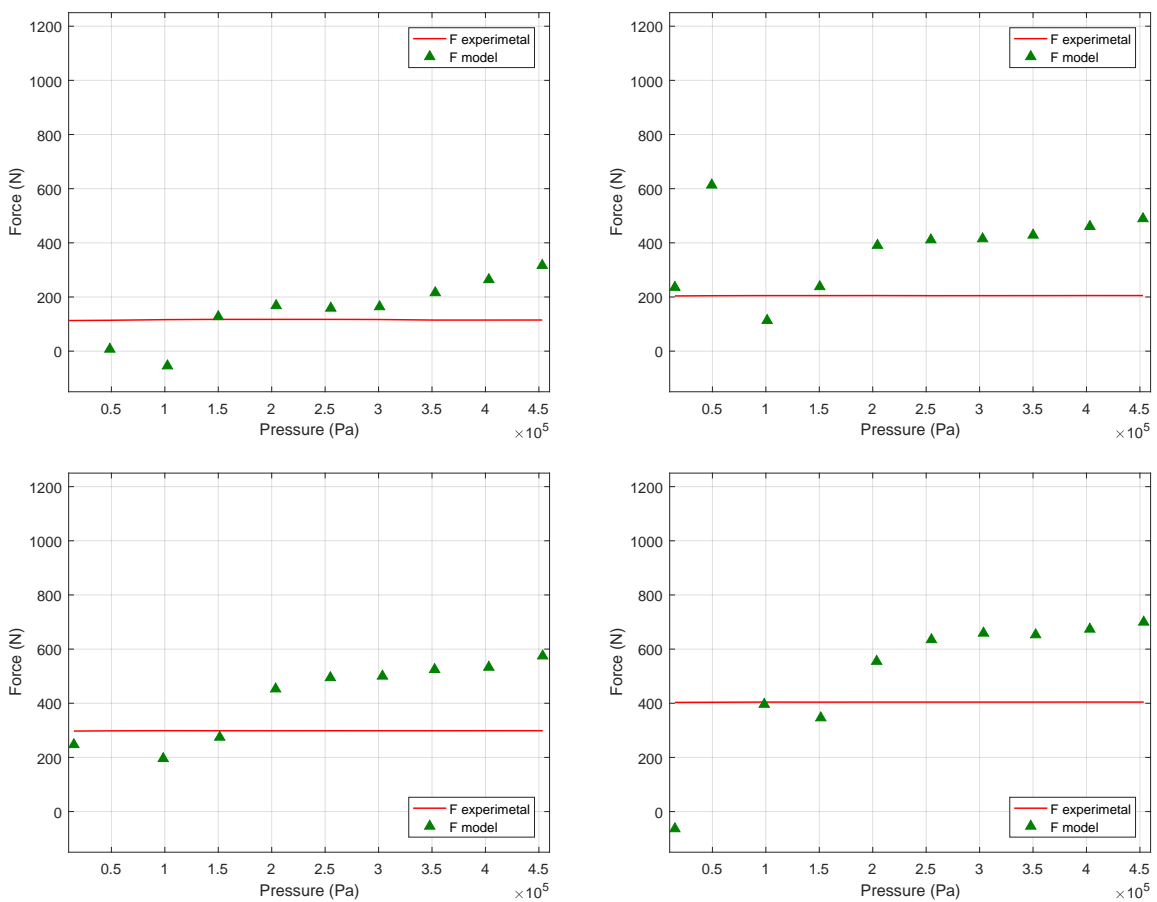


Figure 4.48: **Cross-validation "short-to-long"**: (1)10kg; (2)20kg; (3)30kg; (4)40kg

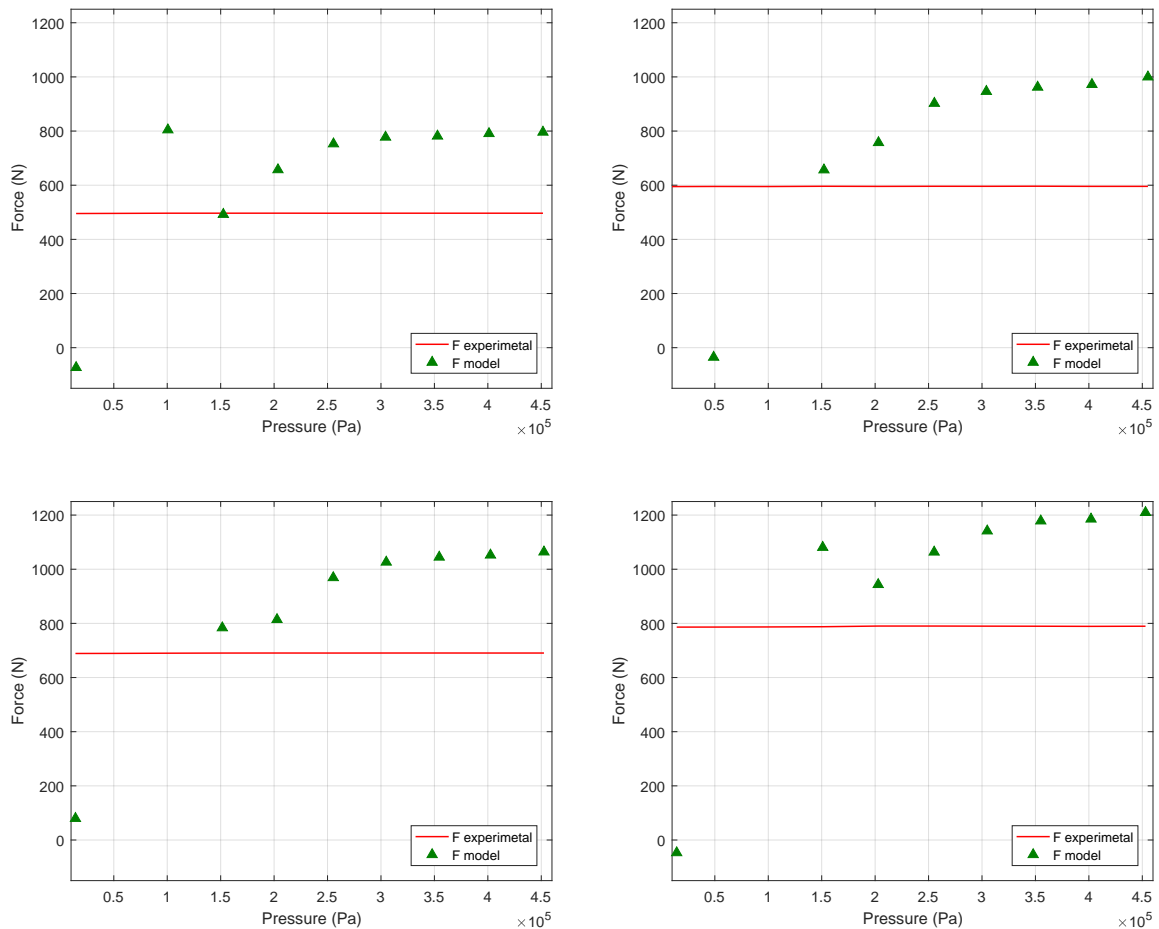


Figure 4.49: **Cross-validation "short-to-long"**: (1)50kg; (2)60kg; (3)70kg; (4)80kg

Comparing cross-validation of model results with validation results, it can be seen that bigger error of model exists if parameters from different muscle are used, what was expected. It can be also seen that the model of DMSP-40-290N acquired using modulus elasticity from DMSP-40-1000N shows negative error, meaning that the modeled force is lower than when using its parameters. On contrary, when using DMSP-40-290N's parameters for modeling DMSP-40-1000N actuator, the positive error is present.

Despite the fact that previously analyzed modeling methods have much better accuracy this model is more appropriate for the realization of our system, by means of control implementation. Having different types of PAMs, empirical models would require identifying parameters experimentally for every muscle itself, demanding a lot of time and test setup adapting. On the other hand, even if the cross-validation presented have not shown sizable relevance, it has still achieved better results than McKibben model itself and showed that some pattern in model outcomes when not using its own parameters exists, implying that relationship between these parameters can be found. Additionally, improved geometrical model even not precise, with a proper control algorithm, could give adequate results, what will be tested in Chapter 5.

From results given by tested models clear that they share the same problem: having huge errors for small values of inlet pressure, caused by increased dry friction between muscle braids and bladder while the muscle is pre-stretched with load hanged. Recalling improved equation 3.12 from Tondur [58], presented in Chapter 3, for increased accuracy in modeling taking in consideration non-cylindrical shape of actuator and compressibility of the air inside:

$$F_t = \pi \frac{D_0^2}{4} P [\alpha (1 - k \varepsilon_l)^2 - \beta] \quad (4.19)$$

Authors are also giving an expanded force expression that was derived by formulating a friction model that resist the actuator motion as a function of pressure and the surface area of the braids:

$$F = F_t - f \left( \frac{1}{n} \right) (\pi D_0 L_0) \times \frac{\sin \theta_0}{(1 - k \varepsilon_l) \sqrt{1 - \cos^2 \theta_0 (1 - k \varepsilon_l)^2}} \times P \text{sign}(\dot{x}) \quad (4.20)$$

Where  $f$  defines the dynamic dry friction coefficient, and  $\dot{x}$  is the motion velocity. Instead of using this complex expression and keep precision, in [57] is suggested using an empirical constant  $q$ , that incorporate the forces generated by the friction phenomena and the viscoelastic resistance of the elastomers that form the actuating section, in following way:

$$F_t = \pi \frac{D_0^2}{4} q P [\alpha (1 - k \varepsilon_l)^2 - \beta] \quad (4.21)$$

The unknown parameters  $k$  and  $q$  can be acquired from 4.21 by taking into consideration the extreme states of the force-displacement curve. Extreme states are states where PAM being loaded with specific weight is inflated with pressure to the point that it reaches its nominal length  $L = L_0$ . In this situation contraction is zero ( $\varepsilon_l = 0$ ). The second set of states involve pneumatic muscle being freely suspended, meaning  $F = 0$ , and therefore reaching the maximum displacements for pressures needed for the previous states. Utilizing this procedure to force expression 4.21, constant parameters can be calculated as:

$$q = \frac{4F_{max}}{\pi D_0^2 P_{test} (\alpha - \beta)} \quad (4.22)$$

$$k = \frac{L_0}{x_{max}} \left( 1 - \sqrt{\frac{\beta}{\alpha}} \right) \quad (4.23)$$

For pressures of our interest (lower than 1bar) parameters  $k$  and  $q$  are calculated and presented in table 4.4:

Constant	0.5bar	1bar
$k$	12.3268	3.3077
$q$	1.2838	1.3320

Table 4.4: Coefficients for improved geometrical model

Inserting calculated parameters into 4.21 equation together with experimental data modeled forces for different loads are calculated and presented in the figures 4.50 and 4.51:

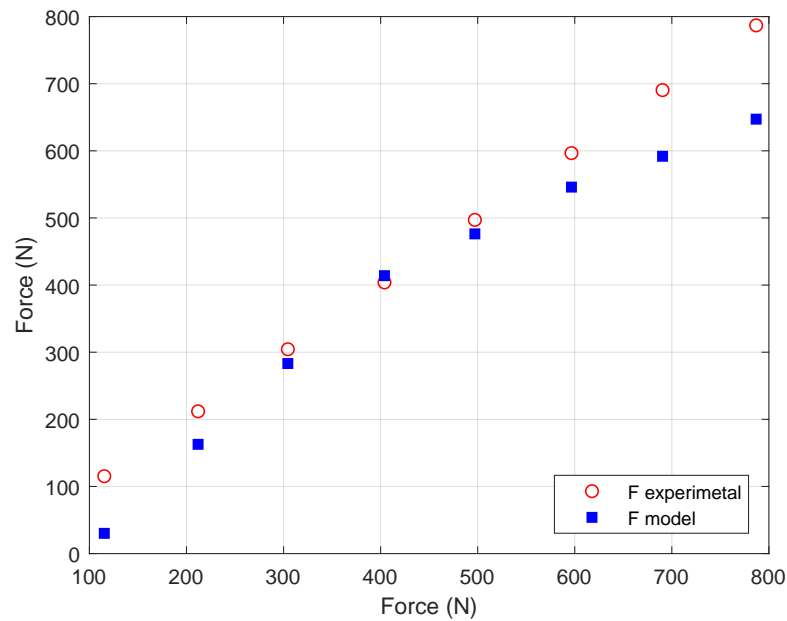


Figure 4.50: Comparison between experimental results and model at pressure 0.5bar

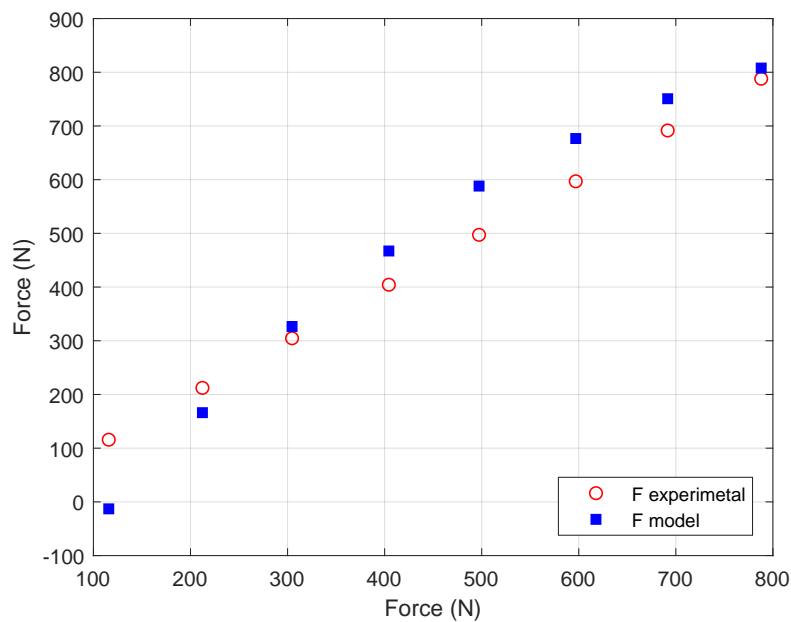


Figure 4.51: Comparison between experimental results and model at pressure 1bar

Comparing modeled forces at low pressures from any of models previously tested, this method gives extreme improvement to accuracy, however both the parameters  $k$  and  $q$  are considered constants for a specific test pressure and test actuator, and they need to be determined experimentally for every different working condition needed.

### 4.4. Dynamic experiments

After all the experiment done and the conclusions made about PAM under static conditions, imposed question is, is it justified to use such models in dynamic conditions. For purpose of comparing static and dynamic characteristics, dynamic tests were performed with constant loads and commanding pressure reference signals, as trajectories with various velocities and accelerations. Only the DMSP-40-1000N muscle was tested in the dynamic experiments. Velocities and acceleration used for these experiments are shown in table 4.5. Dynamic behavior of the contraction, diameter, and force as the response to dynamic, with different speed, change of input pressure is shown in the figures 4.52 and 4.53, while the influence of different loads attached on dynamic characteristic is presented in the figures 4.54 and 4.55:

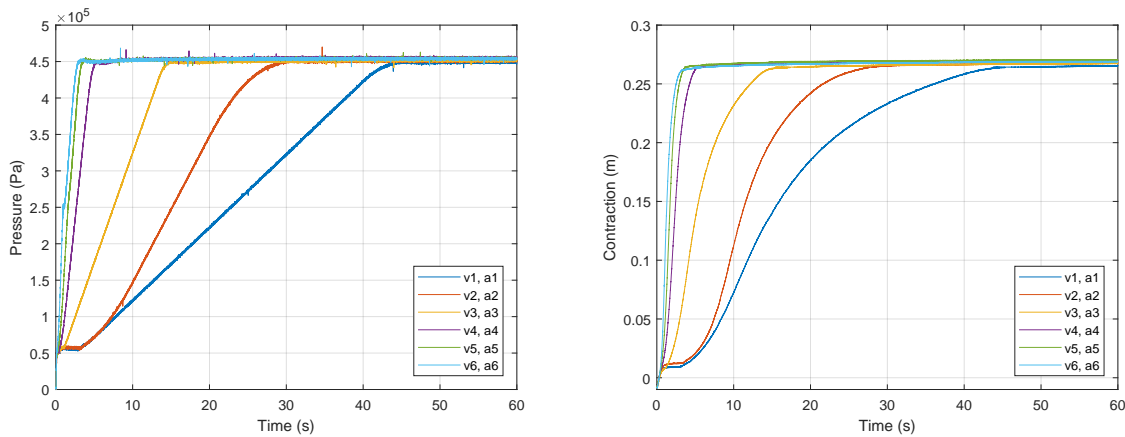


Figure 4.52: **Dynamic tests - velocity variation:** (1)Pressure; (2)Contraction

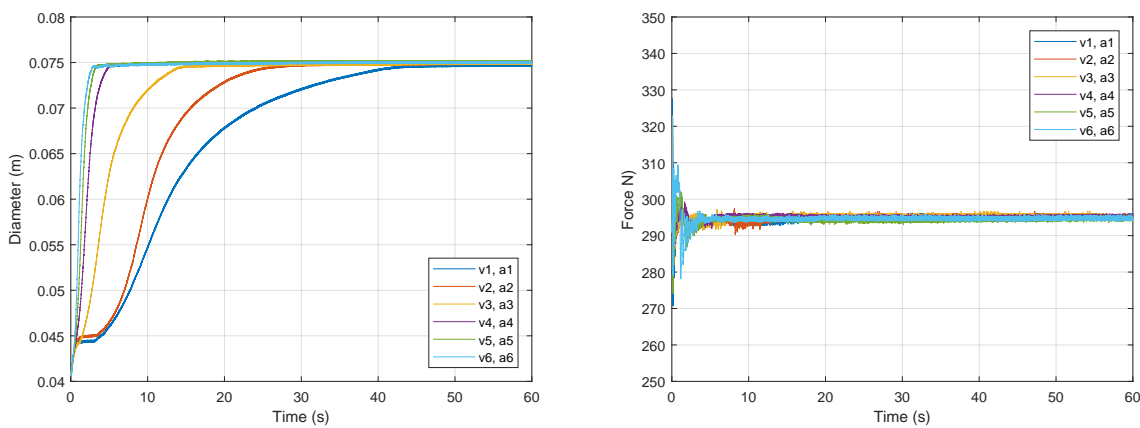


Figure 4.53: **Dynamic tests - velocity variation:** (1)Diameter; (2)Force

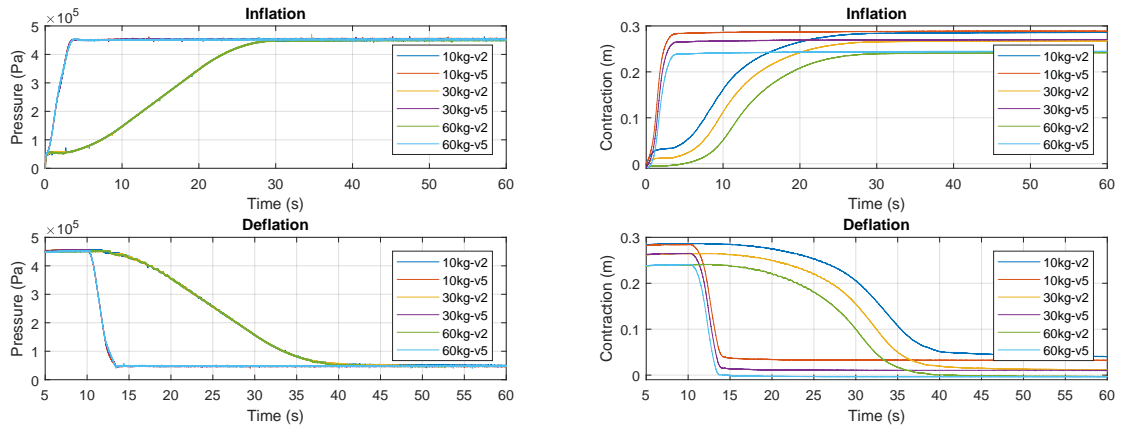


Figure 4.54: **Dynamic tests - load variation:** (1)Pressure; (2)Contraction

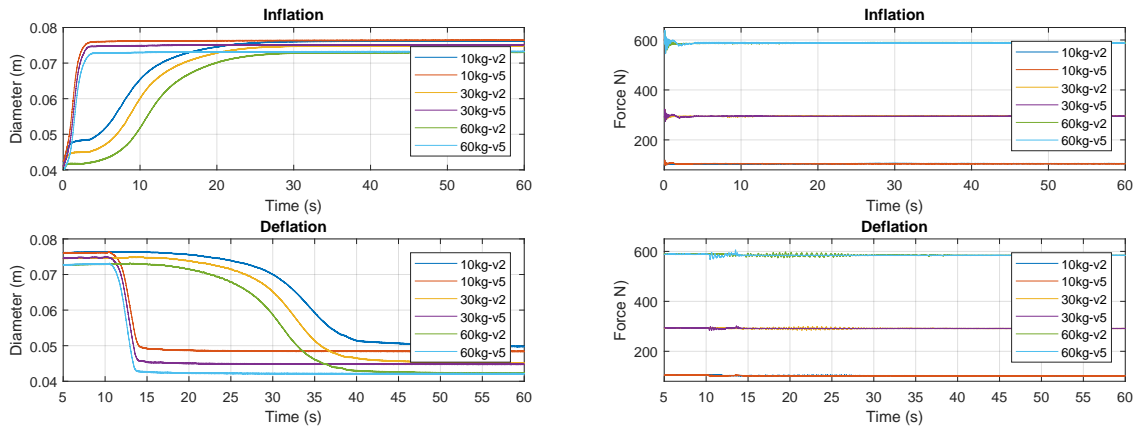


Figure 4.55: **Dynamic tests - load variation:** (1)Diameter; (2)Force

Index	$v[\text{bar/s}]$	$a[\text{bar/s}^2]$
1	0.1	0.02
2	0.2	0.02
3	0.3	0.2
4	1	0.8
5	2	2
6	4	6

Table 4.5: **Values of speed and acceleration of referent pressure trajectories**

For the better understanding of dynamic behavior, isolated working points are taken the same as in isotonic tests (pressure/load combination). Comparison between realized contractions from these experiments is presented in the figures 4.56, 4.57 and 4.58:

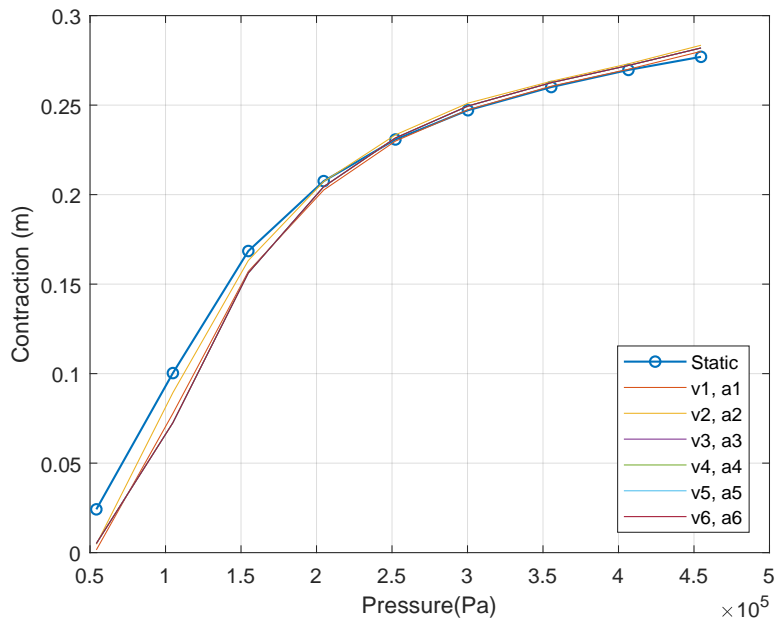


Figure 4.56: **Dynamic vs Static at load equals 10kg**

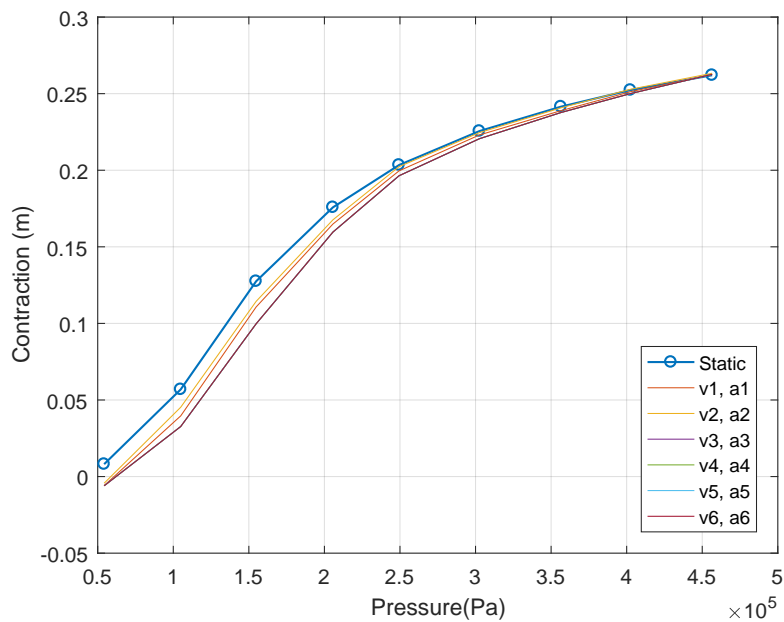


Figure 4.57: **Dynamic vs Static at load equals 30kg**

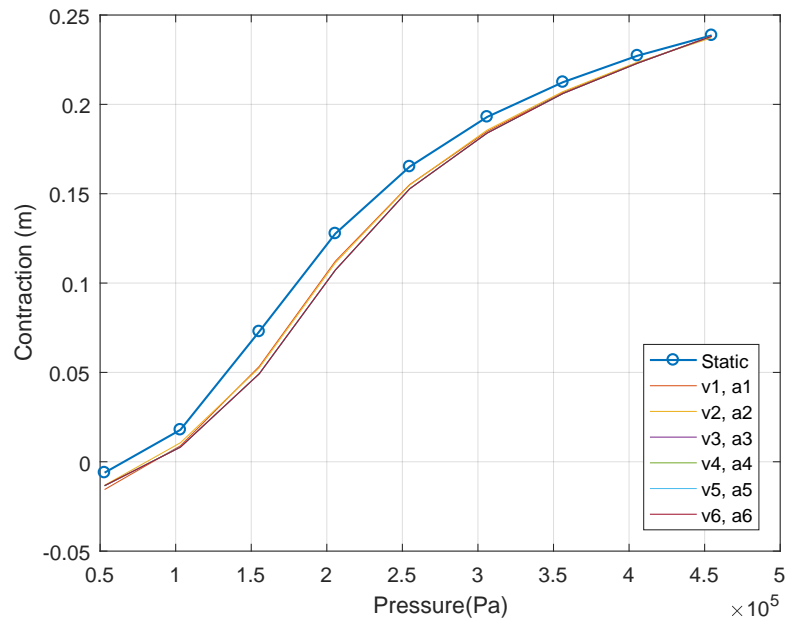


Figure 4.58: **Dynamic vs Static at load equals 60kg**

The dynamic contraction is slightly smaller as the static one, as expected. The dynamic force generated by the muscle is the smaller than the static one because there are energy losses caused by internal friction effects in the muscle during contraction/extension, as well as inertia forces caused by acceleration load at the end of the muscle. This explains also the difference between dynamic test using different velocities. It is interesting to see, with the lighter load (Figure 4.56) at higher pressures, dynamic contraction exceeds static characteristic because lighter weight has less influence on inertia in this range. Nevertheless, from these experiments, it may be concluded that the isotonic characteristic and the dynamic one is almost identical in exact working points. Therefore, it is obvious the static model approaches can be used to model the muscle at relatively slow realizable velocities and to design the controller.



Recalling, force model equation:

$$F = \frac{p}{4\pi n^2} [3L^2 + b^2] + E \left( \frac{L}{L_0} \right) \varepsilon_L \delta \pi D - E \left( \frac{L}{L_0} \right) \varepsilon_D \frac{2\delta L^2}{D n^2 \pi^2} \quad (5.1)$$

Blocks in Simulink model: FD, FL, and FMK are presenting force terms from perimetric elastic deformation, force term from elastic deformation in length direction and classical McKibben force respectively, and shown in next figures (5.2, 5.3 and 5.4):

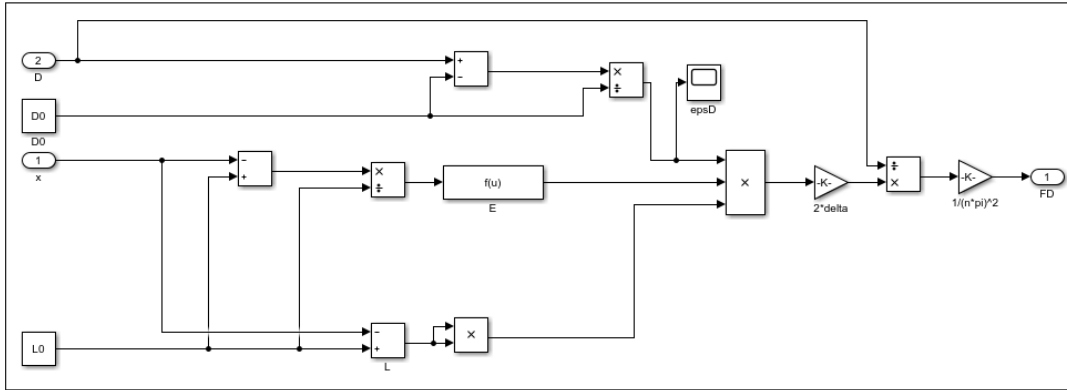


Figure 5.2: Simulink model of perimetric elastic deformation force

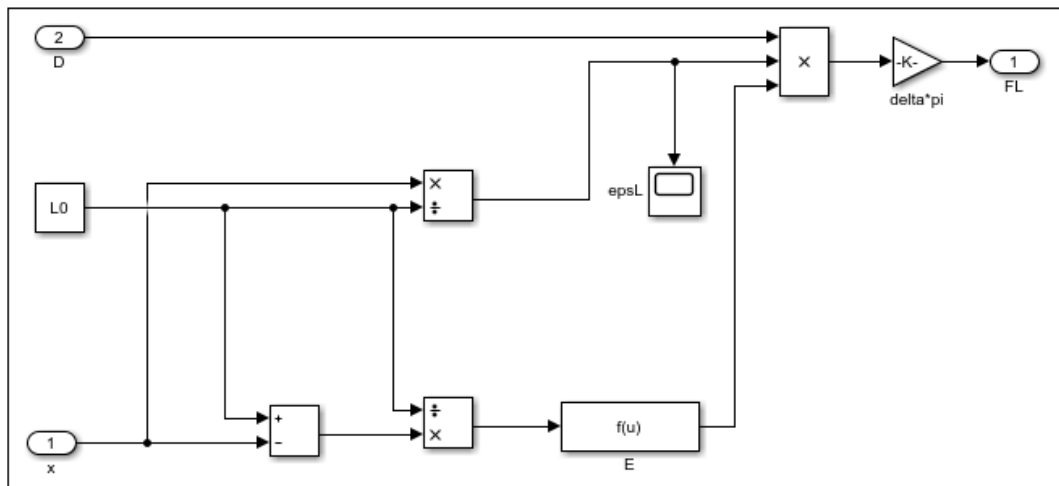


Figure 5.3: Simulink model of length direction elastic deformation force

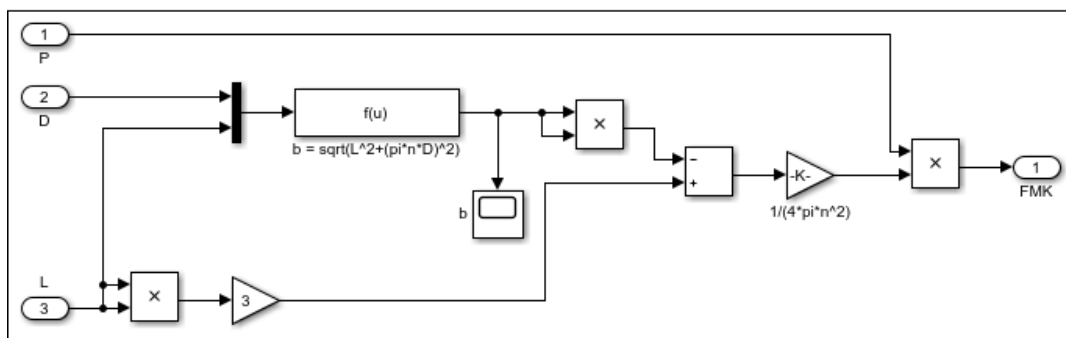


Figure 5.4: Simulink model of McKibben force

## 5.2. Model of the proportional valve

The output pressure of the valve in Pascals is proportional to the input in Volts with the factor of proportionality. The simplified model of the valve is:

$$\frac{P(s)}{U(s)} = K_v \quad (5.2)$$

This relation is only accurate in the range of frequencies inside the bandwidth of the valve. The cut-off frequency of the proportional valve was calculated as the frequency at which the amplitude of the output pressure decreases 3dB or analogously when the amplitude of the output pressure decreases to the 70.79% of the amplitude of the reference pressure signal.

The figure 5.5 shows the reference and output pressure signals when this condition is reached. The cut-off frequency of the proportional valve resulted to be  $w_p = 2.5Hz$ .

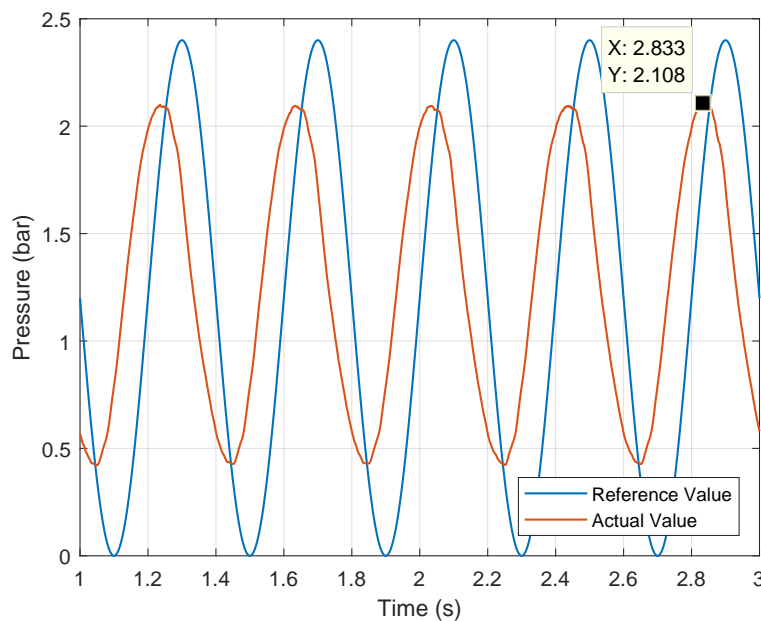


Figure 5.5: Reference and actual pressure at the cut-off frequency

A more accurate valve model is accomplished by considering it as a first order low pass filter with gain and cut-off frequency. The transfer function of this model is:

$$\frac{P(s)}{U(s)} = \frac{K_v \cdot w_p}{s + w_p} = \frac{2.5 \cdot 10^5}{s + 2.5} \quad (5.3)$$

## 5.3. Controller design

Pneumatic actuators have been used for many years and well adapted to repetitive tasks. In spite of this, several problems are still present in these systems concerned with the accuracy and difficulty of control, what is related to the compressibility of air in the muscle and although partial solutions have been found, the problems largely remain. In addition, the main difficulty of the control of PAM is due to their nonlinear behavior, what is actually a problem of modelling. Having many different complex methods used to control PAM, proves that lack of knowledge on forming the model exists. Therefore, a simple position control of the fluidic muscle, with a linear PID controller and Feed-Forward (FF), will be designed to show controllability properties of the model.

Combination **FF** + **PID** control have reactive and proactive nature. The Feed-Forward task is to, acting as a proactive controller, deliver an appropriate adjustment that either minimizes or eliminates the negative effects of a known disturbance. **FF** control requires integration of mathematical model into the control algorithm to determine the control actions, which makes it very sensitive to model accuracy, and this is the reason why this method has been chosen to show the validity of proposed modelling approach.

Having gravity constant  $g = 9.81(m/s^2)$ , and  $M$  mass of the muscle and weight attached together, the model of the mechanical system is:

$$F = M \cdot g + M \cdot \ddot{x} \quad (5.4)$$

And the approximation for force provided by the muscle model, given with equation 5.1:

$$F = \frac{p}{4\pi n^2} [3L^2 + b^2] + E \left( \frac{L}{L_0} \right) \varepsilon_L \delta \pi D - E \left( \frac{L}{L_0} \right) \varepsilon_D \frac{2\delta L^2}{D n^2 \pi^2}$$

Noticing that the last two terms are depending only on length, thus depending only on muscle's end displacement, it is decided to address these terms as disturbances and assign them to Feed-Forward control. When determining the **FF** signal, this function block is fed with the reference signal (contraction), directly canceling out elastic force effect in order to achieve a predefined process output. Only force term left is proportional to pressure, i.e., McKibben force, and assigned to **PID** controller to deal with.

Utilizing these considerations and equation 5.4 the transfer function of the system can be obtained. Furthermore, the complete model of the valve must be taken into account to design the **PID** controller. Otherwise, the gains obtained for the **PID**, without considering the low dynamics of the valve, would be much higher than needed and this would make the system unstable, which gives:

$$G(s) = \frac{K_v \cdot w_p}{M s^2 \cdot (s + w_p)} \quad (5.5)$$

The proportional-integral-derivative (**PID**) controller compares the measured position of the muscle ( $x$ ) with the desired position ( $x_0$ ). The difference  $\Delta x = x_0 - x$  or error is used to calculate the new input of the system ( $u_0$ ) that brings the output back to the desired position.

$$u_0(t) = K_p \cdot \Delta x(t) + K_i \int_0^t \Delta x(t) dt + K_d \frac{d(\Delta x(t))}{dt} \quad (5.6)$$

Or in the Lapace domain:

$$U_0(s) = \left( K_p + \frac{K_i}{s} + K_d \cdot s \right) \cdot \Delta X(s) \quad (5.7)$$

The **PID** regulator is designed by pole placement method. The gains are adjusted using the "Matlab Control System Designer" application so that the step response is adequate matches desired behavior realizable by the muscles (5.6, 5.8 and 5.7). The calculated gains are shown in table 5.1:

PID gains	
$K_p$	0.043
$K_i$	0.00040575
$K_d$	1.1398

Table 5.1: **PID** gains

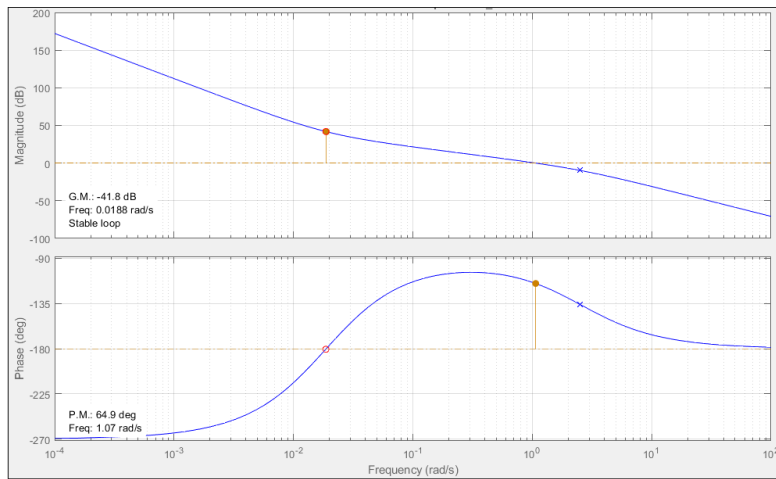


Figure 5.6: **Control System Designer:** Bode diagram of the closed loop system

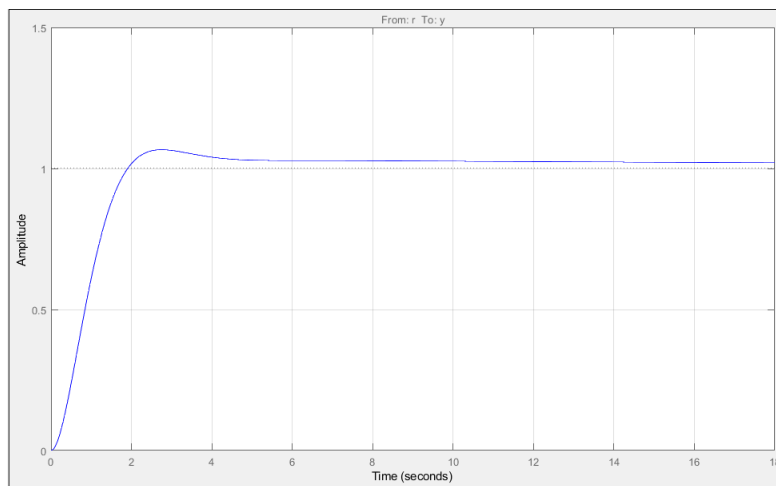


Figure 5.7: **Control System Designer:** Step Response of the closed loop system

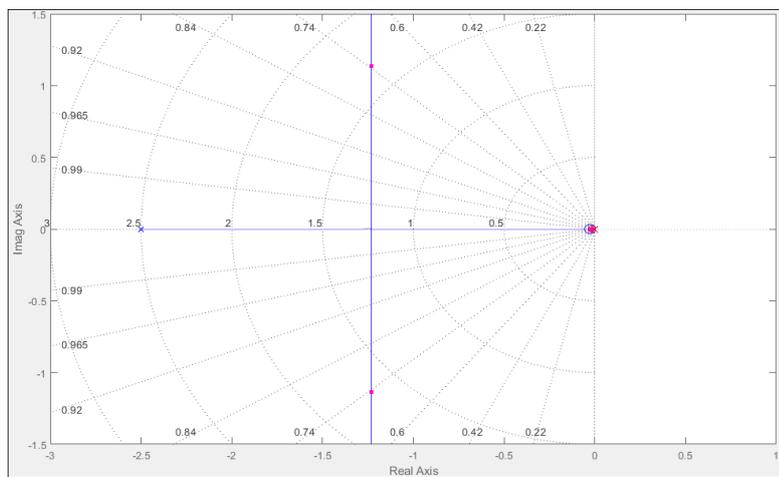


Figure 5.8: **Control System Designer:** Root Locus of the closed loop system

## 5.4. Evaluation

The closed loop system was tested by simulation in *MATLAB/Simulink* (figure 5.9):

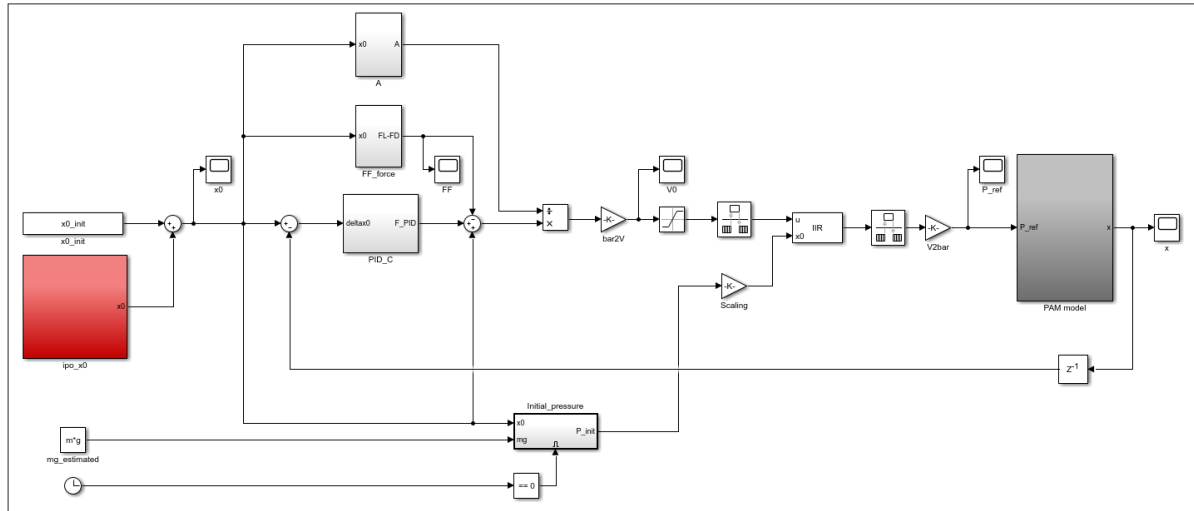


Figure 5.9: **Simulation block diagram of the closed loop system**

The reference signal (displacement) is obtained from an interpolator, in which the maximal value of the input signal, as well as rising time, and maximum velocity and acceleration of the signal can be tuned. The reference signal is also fed to **FF** block, realized same as the simulation of elastic forces in the model of **PAM**, producing **FF** force. Block "A" is used to convert force to pressure. Dynamic of the proportional valve is realized as a first order IIR filter, which for the purpose of simulation must have an initial value of the pressure (for testing displacements with an initial value different from zero), obtained through "initial\_pressure" block. The input to the block of the proportional valve is the electrical tension that is proportional to the output pressure of the valve to be input to block diagram of **PAM**'s model.

The system is simulated with the gains obtained 5.1, for the weights from scope equivalent to loads from "SMART-STRING" system's working range (used in experiments) and with a different velocities of reference position rise ( $v_1 = 0.01m/s$ ,  $v_2 = 0.03m/s$  and  $v_3 = 0.05m/s$ ). Maximal displacement value has been chosen as  $15cm$  so that the muscle contract over a wide range of reachable lengths, and also the reaction to smaller reference contraction of  $5cm$  with initial values were tested.

Reference and output position values for different velocities of position rise, and the reference displacement  $x=15cm$ , with simulated weight applied  $m=20kg$  are shown in Figure 5.10, then with  $m=40kg$  in Figure 5.12 and finally with  $m=80kg$  in Figure 5.14, while corresponding position errors are presented in the figures 5.11, 5.13 and 5.15:

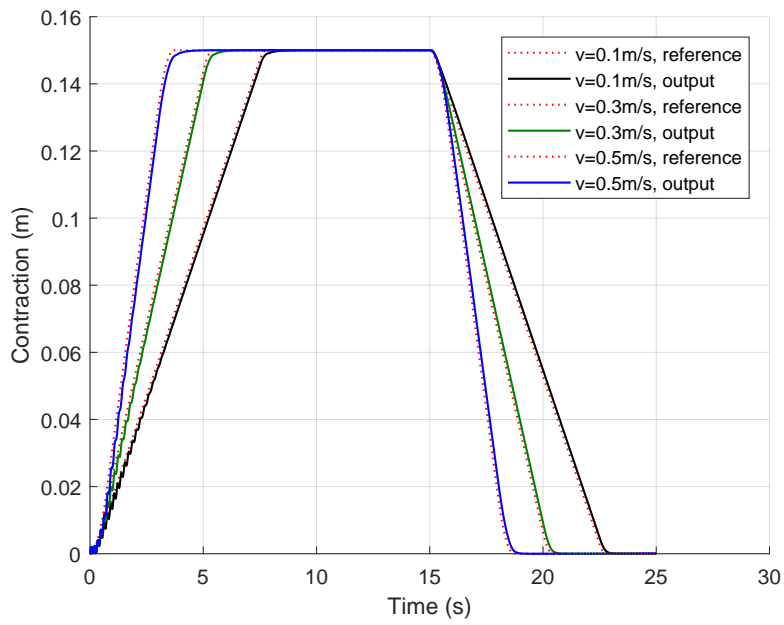


Figure 5.10: Reference and output position values with load of 20kg

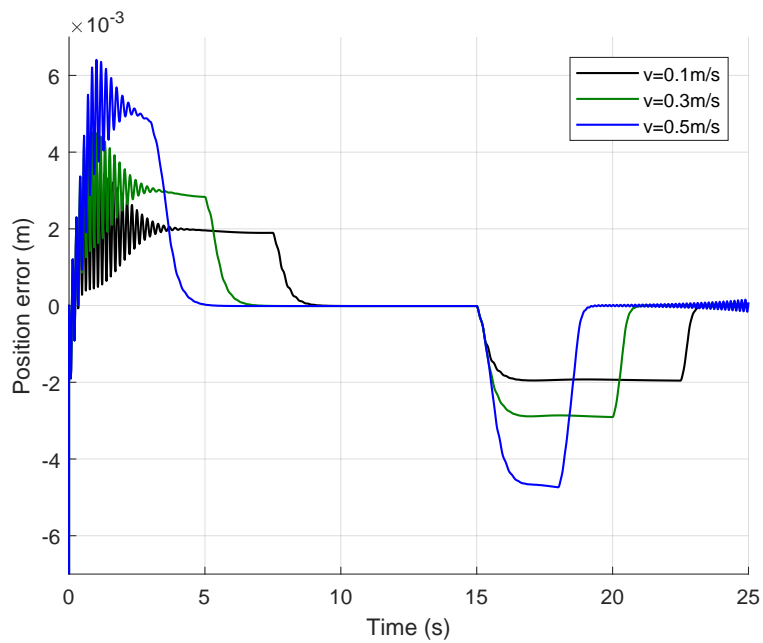


Figure 5.11: Position error values with load of 20kg

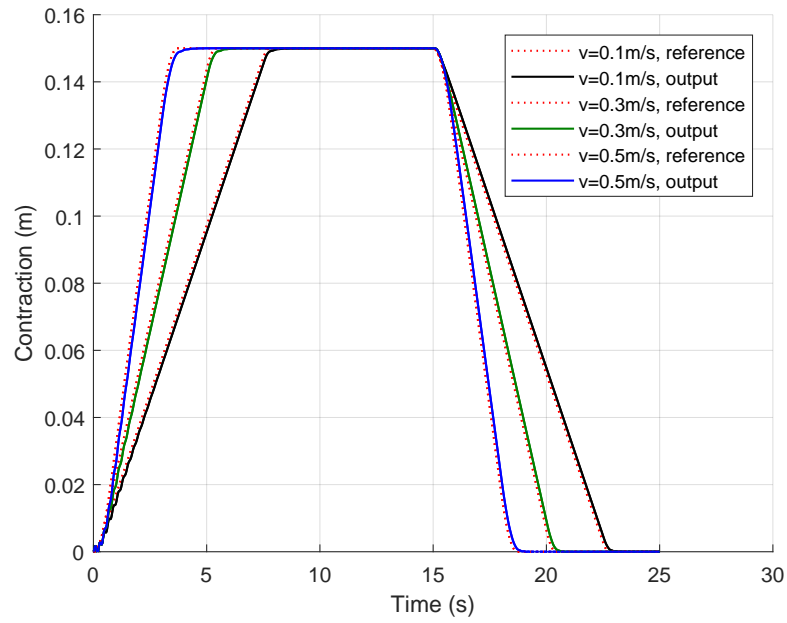


Figure 5.12: Reference and output position values with load of 40kg

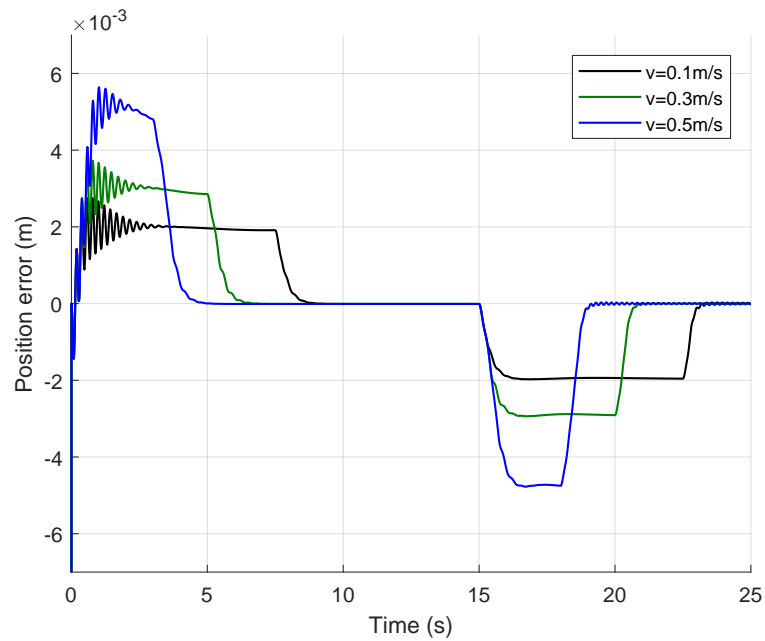


Figure 5.13: Position error values with load of 40kg

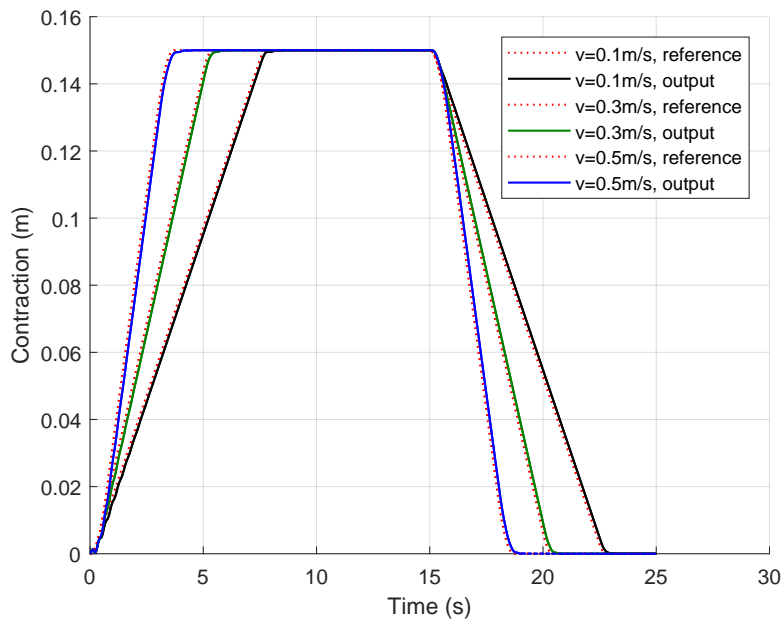


Figure 5.14: Reference and output position values with load of 80kg

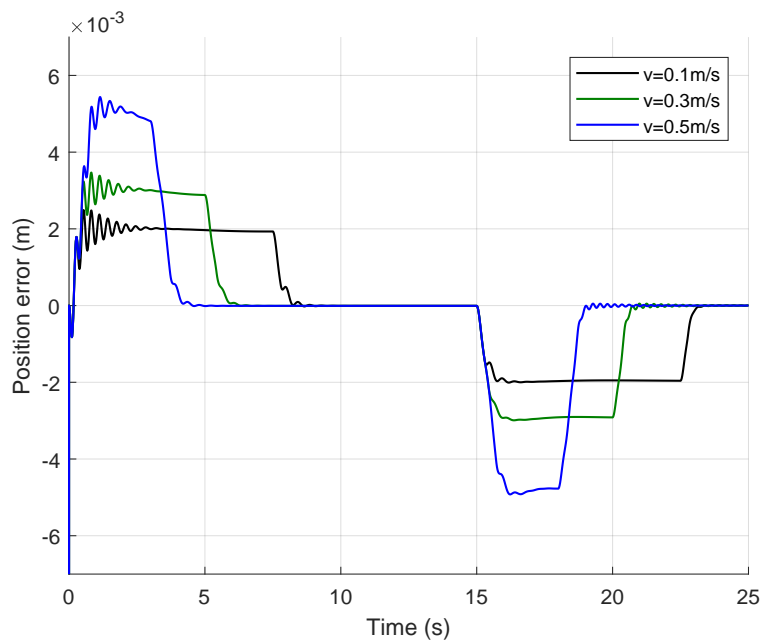


Figure 5.15: Position error values with load of 80kg

The figures 5.16 ÷ 5.21 show the reference and output position values for different velocities of position rise, and the reference displacement of  $x=5\text{cm}$ :

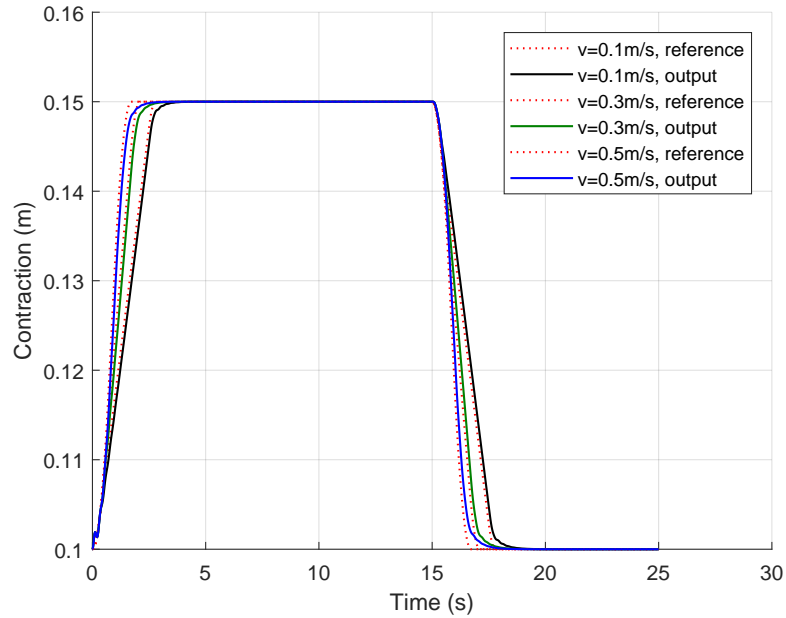


Figure 5.16: **Reference and output position values with load of 20kg**

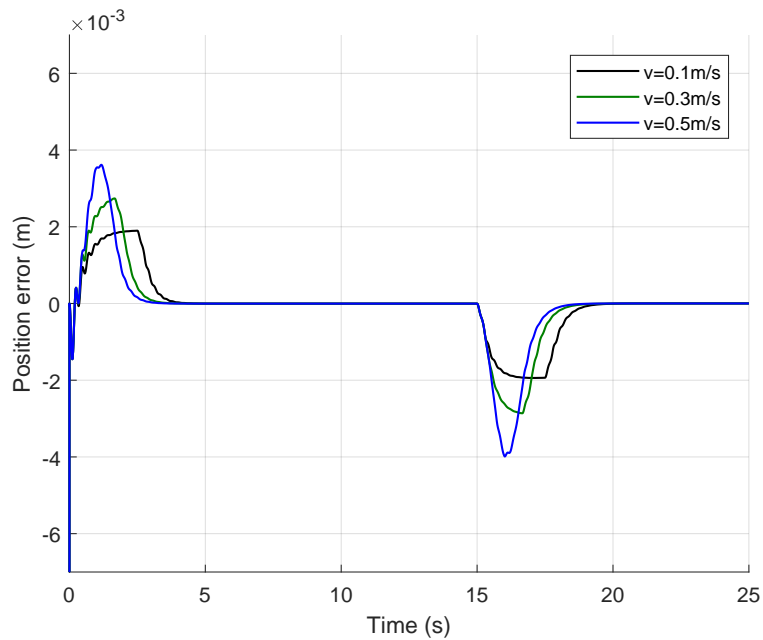


Figure 5.17: **Position error values with load of 20kg**

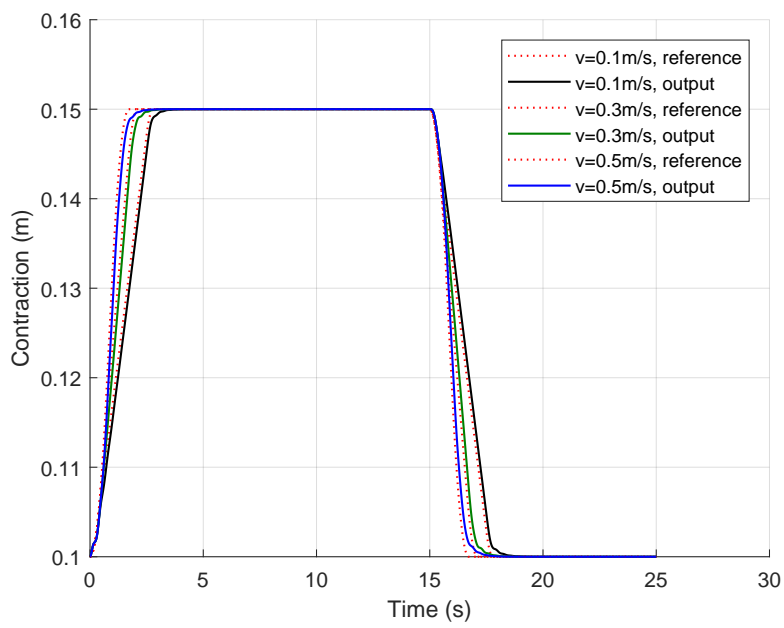


Figure 5.18: Reference and output position values with load of 40kg

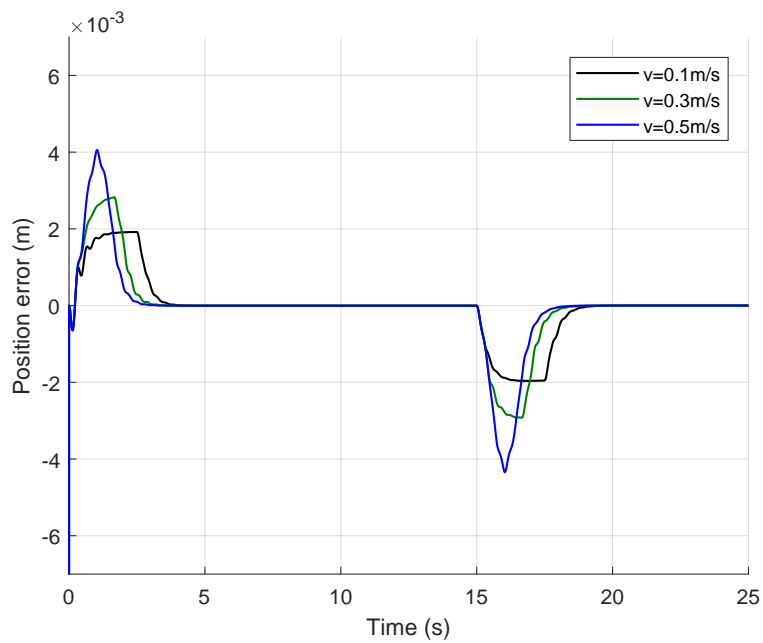


Figure 5.19: Position error values with load of 40kg

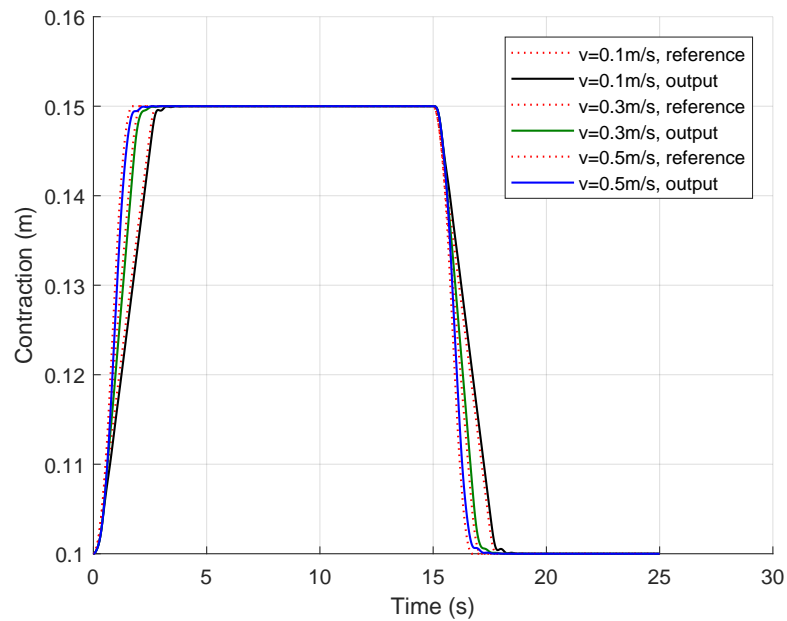


Figure 5.20: **Reference and output position values with load of 80kg**

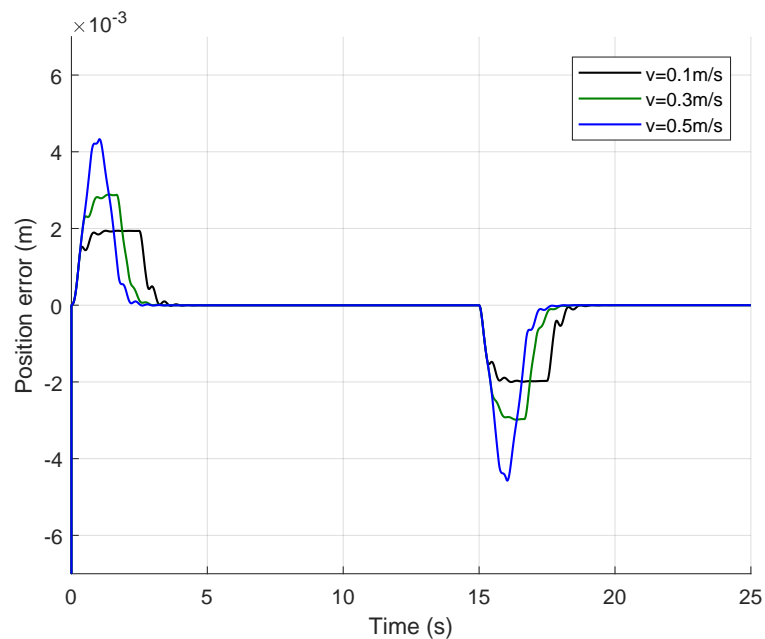


Figure 5.21: **Position error values with load of 80kg**

The above simulations demonstrate very good matching of reference and regulated motion, with relatively lower, nevertheless acceptable errors during a transition. This result validates the applicability and performance of the proposed control. The model for the pneumatic artificial muscle has been verified, meaning that controller can manage to overcome inaccuracy of model in the terms of force, giving us reason to further develop this modelling approach, dealing with problems that we might meet during implementation of the model experimentally (hysteresis effect and compressibility of the air), as well improving operating in range of small pressures.

# 6

## Conclusion

Fluidic muscles are powerful, light-weight and compliant actuators that have similarity with biological muscles, and which have found quite a number of applications in humanoid robotics, rehabilitation systems, and assistive systems, however their behaviour, presenting non linearities in all its operation range, is not sufficiently well known, thus making their field of application significantly limited. Many different modelling approaches were developed by authors, but in general, all available models are approximations based on empirical experience, and therefore no model can be applied to a different kind of PAMs. There are many parameters needed to be identified to obtain an accurate model, and all differing between particular actuators. Therefore, the main goal of this master thesis is the investigation of different mathematical models and development of general/universal mathematical model.

At the beginning of the thesis a general motivation and a specific problem which is aimed to be solved are stated (Chapter 1). We then introduce the theoretical background on the topics related to the problem (Chapter 2). Further, various modeling approaches found in the literature were described (Chapter 3). To find the relationship between force, length, and pressure, standard muscle quasi-static and dynamic testing experiments were performed (Chapter 4). In the same chapter, the described models are evaluated against the experimentally measured data, and the main findings are:

- A simple but accurate empirical model of the fluidic muscle force was derived using the energy conservation principle, where the muscle was considered as a one-way cylinder with variable diameter. Force can be expressed as the product of the relative pressure in the muscle and the virtual area, which was approximated as a fitting polynomial function, whose coefficients have to be identified experimentally together with the effects of the deformation energy approximated in the same way.
- Another empirical model was developed by representing fluidic muscle as loaded spring model. Realized force is proportional to the stiffness parameter that has to be identified experimentally. This model also demonstrated very good accuracy.
- Analyzing basic, and the most famous McKibben geometrical model it is noticed that this model is not valid for FESTO pneumatic muscles.
- Since membrane and braids of FESTO muscles are stiff and compressed together, elastic deformation virtual work cannot be disregarded with only geometrical approach. McKibben geometrical model was upgraded with these terms, significantly improving performance.
  - Cross-validation of identified elastic forces parameters is done, showing that utilization of the model is possible for different dimensions PAMs, that is a very important benefit.
- All of the tested models showed inaccuracy for small pressures, that is not a crucial problem, as our system is not operating in this working conditions. Additionally, the procedure for improving accuracy in low pressures operating range is proposed, however, this procedure can be accounted for unique pressure/actuator combination.

Finally, with the aim to validate the proposed model, a model-based control was designed and simulated in *MATLAB/Simulink*. A position controller was realized as, sensitive to model exactness, **PID+FF** controller. The closed-loop system was tested by simulation, varying load, and reference contraction velocity, and showed good trajectory tracking behavior (Chapter 5).

## 6.1. Future Research

The previous discussion provides directions for the future research.

The first direction is towards improving the proposed model to bigger comprehensiveness. In the thesis work, it is presented that the model shows a tendency toward universal model parameters. A relation between parameters of different muscles possibly can be found by introducing nonlinear strain/tension relation when determining deformation virtual work losses or by separating elastic energy to energy stored in rubber bladder and energy stored in fiber mesh.

Another direction for the future research is an incorporation of the proposed method with the phenomena which are not considered in this paper: the hysteresis effects of the muscle when inflating and deflating, caused by frictions between fibers and friction between rubber tube and fiber mesh.

Additionally, a robust controller which can manage the uncertainty of the model is necessary to be developed to improve the accuracy and repeatability of these actuators.

# Bibliography

- [1] G. Andrikopoulos, G. Nikolakopoulos, and S. Manesis. A survey on applications of pneumatic artificial muscles. In *2011 19th Mediterranean Conference on Control Automation (MED)*, pages 1439–1446, June 2011.
- [2] K. Kawamura, R. A. Peters, D. M. Wilkes, W. A. Alford, and T. E. Rogers. Isac: foundations in human-humanoid interaction. *IEEE Intelligent Systems and their Applications*, 15(4):38–45, Jul 2000.
- [3] V. Kepplin K. Berns, J. Albiez and C. Hillenbrand. Airbug - insectlike machine actuated by fluidic muscle. *CLAWAR 2001-Climbing and Walking Robots and the Support Technologies for Mobile Machines*, 2001.
- [4] F. Daerden, D. Lefeber, B. Verrelst, and R. Van Ham. Pleated pneumatic artificial muscles: actuators for automation and robotics. In *2001 IEEE/ASME International Conference on Advanced Intelligent Mechatronics. Proceedings (Cat. No.01TH8556)*, volume 2, pages 738–743 vol.2, 2001.
- [5] H. Witte, R. Hackert, K. E. Lilje, N. Schilling, D. Voges, G. Klauer, W. Ilg, J. Albiez, A. Seyfarth, D. Germann, M. Hiller, R. Dillmann, and M. S. Fischer. Transfer of biological principles into the construction of quadruped walking machines. In *Robot Motion and Control, 2001 Proceedings of the Second International Workshop on*, pages 245–249, 2001.
- [6] D. A. Kingsley, R. D. Quinn, and R. E. Ritzmann. A cockroach inspired robot with artificial muscles. In *2006 IEEE/RSJ International Conference on Intelligent Robots and Systems*, pages 1837–1842, Oct 2006.
- [7] B. Vanderborght F. Daerden B. Verrelst, R. Ham and D. Lefeber. The pneumatic biped "lucy" actuated with pleated pneumatic artificial muscles. In *Autonomous Robots*, volume 18, pages 201–213, 2005.
- [8] N. Kaesler G. Osborne M. Cowling, A. Jeffs and F. Wornle. Stumpy: A pneumatic muscle actuated bi-pedal robot. 2005.
- [9] P. Scarfe and E. Lindsay. Air muscles actuated low cost humanoid hand. In *Int. J. Advanced Robotic Systems*, pages 139–146, 2006.
- [10] E. Kubica D. Wight and D. Wang. Augmenting locomotion in an anthropomorphic system. In *The Journal of Systemics, Cybernetics and Informatics*, 2006.
- [11] A. Morioka K. Nakatani K. Suzuki K. Tsujita, T. Inoura and T. Masuda. Oscillator-controlled bipedal walk with pneumatic actuators. In *Journal of Mechanical Science Technology*, volume 21, pages 976–980, 2007.
- [12] R. Niiyama, A. Nagakubo, and Y. Kuniyoshi. Mowgli: A bipedal jumping and landing robot with an artificial musculoskeletal system. In *Proceedings 2007 IEEE International Conference on Robotics and Automation*, pages 2546–2551, April 2007.
- [13] R. Niiyama and Y. Kuniyoshi. A pneumatic biped with an artificial musculoskeletal system. In *in Proceedings of the 4th International Symposium on Adaptive Motion of Animals and Machines*, pages 80–81, 2008.
- [14] K. Tsujita, T. Kobayashi, T. Inoura, and T. Masuda. Gait transition by tuning muscle tones using pneumatic actuators in quadruped locomotion. In *2008 IEEE/RSJ International Conference on Intelligent Robots and Systems*, pages 2453–2458, Sept 2008.

- [15] I. Boblan and A. Schulz. A humanoid muscle robot torso with biologically inspired construction. In *in ISR 2010, 41st International Symposium on Robotics and ROBOTIK*, pages 80–81, 2010.
- [16] R. Niiyama, S. Nishikawa, and Y. Kuniyoshi. Athlete robot with applied human muscle activation patterns for bipedal running. In *2010 10th IEEE-RAS International Conference on Humanoid Robots*, pages 498–503, Dec 2010.
- [17] G. Andrikopoulos and S. Manesis. A study of the behavior of pneumatic artificial muscles in industrial applications controlled by programmable logic controllers. In *in 2010 International Congress on Computer Applications and Computational Science (CACs 2010), Singapore*, 2010.
- [18] R. Neumann A. Hildebrandt, O. Sawodny and A. Hartmann. Cascaded control concept of a robot with two degrees of freedom driven by four artificial pneumatic muscle actuators. In *American Control Conference*, pages 680–685, 2005.
- [19] S. Wongsiri and S. Laksanacharoen. Design and construction of an artificial limb driven by artificial muscles for amputees. In *International Conference on Energy and the Environment*, 2003.
- [20] S. Laksanacharoen. Cascaded control concept of a robot with two degrees of freedom driven by four artificial pneumatic muscle actuators artificial muscle construction using natural rubber latex in thailand. In *Thailand and Material Science and Technology Conference*, number 3, 2004.
- [21] H. Kobayashi and K. Hiramatsu. Development of muscle suit for upper limb. In *Robotics and Automation, 2004. Proceedings. ICRA '04. 2004 IEEE International Conference on*, volume 3, pages 2480–2485 Vol.3, April 2004.
- [22] H. Herr and R. Kornbluh. New horizons for orthotic and prosthetic technology: artificial muscle for ambulation. In *SPIEs Smart Structures and Materials*, volume 5385, pages 1–9, 2004.
- [23] Jiping He, E. J. Koeneman, R. S. Schultz, H. Huang, J. Wanberg, D. E. Herring, T. Sugar, R. Herman, and J. B. Koeneman. Design of a robotic upper extremity repetitive therapy device. In *9th International Conference on Rehabilitation Robotics, 2005. ICORR 2005.*, pages 95–98, June 2005.
- [24] M. Perez B. Shepard E. Koeneman J. Koeneman S. Balasubramanian, R. Wei and J. He. Rupert. an exoskeleton robot for assisting rehabilitation of arm functions. In *Virtual Rehabilitation*, pages 163–167, 2008.
- [25] D. Nagem C. Vimieiro, B. G. do N. and M. Pinotti. Development of a hip orthosis using pneumatic artificial muscles. In *TMSI (Technology meets Surgery International)*, 2005.
- [26] J. Czerniecki D. Ferris and B. Hannaford. An ankle foot orthosis powered by artificial pneumatic muscles. In *J. Appl. Biomec*, volume 21, pages 189–197, 2005.
- [27] G. Sawicki D. Ferris, K. Gordon and A. Peethambaran. An improved powered ankle-foot orthosis using proportional myoelectric control. In *Gait and Posture*, volume 23, page 425–428, 2005.
- [28] G. Sawicki K. Gordon and D. Ferris. Mechanical performance of artificial pneumatic muscles to power an ankle-foot orthosis. In *Journal of Biomechanics*, volume 39, 2006.
- [29] A. Gupta and M. K. O'Malley. Design of a haptic arm exoskeleton for training and rehabilitation. *IEEE/ASME Transactions on Mechatronics*, 11(3):280–289, June 2006.
- [30] N. Tsagarakis and D. Caldwell. Development and control of a physiotherapy and training exercise facility for the upper limb using soft actuators. In *International Conference on Advanced Robotics*, page 1092–1097, 2003.
- [31] A compliant exoskeleton for multi-planar upper limb physiotherapy and training. In *International Journal of the Robotics Society of Japan, Advanced Robotics*, 2007.
- [32] S. Kousidou N. Costa D. Caldwell, N. Tsagarakis and I. Sarakoglou. "soft" exoskeletons for upper and lower body rehabilitation - design. In *International Journal of Humanoid Robotics*, volume 4, page 549–573, 2007.

- [33] M. Takaiwa T. Noritsugu and D. Sasaki. "soft" exoskeletons for upper and lower body rehabilitation - design. In *Asia Int. Symposium on Mechatronics*, 2008.
- [34] T. Thanh and T. Phuc. Neural network control of pneumatic artificial muscle manipulator for knee rehabilitation. In *Science Technology Development*, volume 11, 2008.
- [35] S. KleeBarillas M. Knestel, E. Hofer and R. Rupp. The artificial muscle as an innovative actuator in rehabilitation robotics. In *The International Federation of Automatic Control*, 2008.
- [36] T. Deaconescu and A. Deaconescu. Pneumatic muscle actuated isokinetic equipment for the rehabilitation of patients with disabilities of the bearing joints. In *International MultiConference of Engineers and Computer Scientists (IMECS 2009)*, page 1823–1827, 2009.
- [37] D. Surdilovic, J. Zhang, and R. Bernhardt. String-man: Wire-robot technology for safe, flexible and human-friendly gait rehabilitation. In *2007 IEEE 10th International Conference on Rehabilitation Robotics*, pages 446–453, June 2007.
- [38] H. F. Schulte. The characteristics of the mckibben artificial muscle. *The Application of External Power in Prosthetics and Orthotics*, pages 94–115, 1961.
- [39] Bertrand Tondu. Modelling of the mckibben artificial muscle: A review. *Journal of Intelligent Material Systems and Structures*, 23(3):225–253, 2012.
- [40] Y. S. Zhang. The course of the development of mckibben pneumatic artificial muscles. *Chinese Hydraulics and Pneumatics*, 40(3):232–241, 2008.
- [41] F. Daerden. *Conception and Realization of Pleated Pneumatic Artificial Muscles and their Use as Compliant Actuation Elements*. PhD thesis, Vrije Universiteit Brussel, Belgium, 1999.
- [42] Daerden F. and Lefeber D. Pneumatic artificial muscles: actuators for robotics and automation. *European Journal of Mechanical and Environmental Engineering*, 47(1):10–21, 2002.
- [43] Y. C. Fung and R. Skalak. Biomechanics: Mechanical properties of living tissues. *Journal of Applied Mechanics*, 49(2):464–465–241, 1982.
- [44] G. K. Klute, J. M. Czerniecki, and B. Hannaford. Mckibben artificial muscles: pneumatic actuators with biomechanical intelligence. In *1999 IEEE/ASME International Conference on Advanced Intelligent Mechatronics (Cat. No.99TH8399)*, pages 221–226, September 1999.
- [45] Ching-Ping Chou and B. Hannaford. Measurement and modeling of mckibben pneumatic artificial muscles. *IEEE Transactions on Robotics and Automation*, 12(1):90–102, February 1996.
- [46] Th. Beullens. Hydraulic or pneumatic drive device. *US Patent No. 4 841 845*, 1989.
- [47] J. M. Yarlott. Fluid actuator. *US Patent No. 3 645 173*, 1972.
- [48] G. B. Immega. Romac muscle powered robots. *Technical report MS86-777, Society of Manufacturing Engineers, Dearborn*, 1986.
- [49] G. B. Immega. Romac actuators for micro robots. *IEEE Micro Robotics and Teleoperators Workshop, Hyannis, Massachusetts*, 1987.
- [50] M. Kukolj. Axially contractible actuator. *US Patent No. 4 733 603*, 1988.
- [51] A. H. Morin. Elastic diaphragm. *US Patent No. 2 642 091*, 1953.
- [52] H. A. Baldwin. Realizable models of muscle function. *Proceedings of the First Rock Biomechanics Symposium, New York*, page 139–148, 1969.
- [53] H. M. Paynter. Hyperboloid of revolution fluid-driven tension actuators and methods of making. *US Patent No. 4 721 030*, 1988.
- [54] P.Lopez B. Tondu. Modelling and control of mckibben artificial muscle robot actuators. *IEEE Control Systems Magazine*, 20:15–38, April 2000.

- [55] FESTO. Fluidic Muscle DMSP, [www.festo.com/cat/sr\\_rs/data/doc\\_engb](http://www.festo.com/cat/sr_rs/data/doc_engb), 2017.
- [56] Miha Pipan. Experimental validation of change of volume in pneumatic artificial muscle during excitation. *International Journal of Industrial Engineering and Management (IJIEM)*, 6(1):1–6, 2015.
- [57] G. Andrikopoulos, G. Nikolakopoulos, and S. Manesis. Novel considerations on static force modeling of pneumatic muscle actuators. *IEEE/ASME Transactions on Mechatronics*, 21(6):2647–2659, Dec 2016.
- [58] B. Tondu and P. Lopez. Modeling and control of mckibben artificial muscle robot actuators. *IEEE Control Systems*, 20(2):15–38, Apr 2000.
- [59] M. Doumit, A. Fahim, and M. Munro. Analytical modeling and experimental validation of the braided pneumatic muscle. *IEEE Transactions on Robotics*, 25(6):1282–1291, Dec 2009.
- [60] Y. Tian, K. Wang, J. Yi, Z. Wang, and M. Z. Q. Chen. Introduction to modeling of the mckibben pneumatic artificial muscle with end constraints. In *2016 IEEE International Conference on Information and Automation (ICIA)*, pages 1624–1629, Aug 2016.
- [61] M. Tóthová and J. Pitel. Dynamic model of pneumatic actuator based on advanced geometric muscle model. In *2013 IEEE 9th International Conference on Computational Cybernetics (ICCC)*, pages 8–87, July 2013.
- [62] Glenn K. Klute and Blake Hannaford. Accounting for elastic energy storage in mckibben artificial muscle actuators. *Journal of Dynamic Systems, Measurement and Control, Transactions of the ASME*, 122(2):386–388, 6 2000.
- [63] Mirco Martens and Ivo Boblan. Modeling the static force of a festo pneumatic muscle actuator : A new approach and a comparison to existing models. 2017.
- [64] Kanchana Crishan Wickramatunge and Thananchai Leephakpreeda. Study on mechanical behaviors of pneumatic artificial muscle. *International Journal of Engineering Science*, 48:188–198, 2010.
- [65] The heat of shortening and the dynamic constants of muscle. *Proceedings of the Royal Society of London B: Biological Sciences*, 126(843):136–195, 1938.
- [66] B. Tondu and S. D. Zagal. Mckibben artificial muscle can be in accordance with the hill skeletal muscle model. In *The First IEEE/RAS-EMBS International Conference on Biomedical Robotics and Biomechatronics, 2006. BioRob 2006.*, pages 714–720, Feb 2006.
- [67] D. B. Reynolds, D. W. Repperger, C. A. Phillips, and G. Bandry. Modeling the dynamic characteristics of pneumatic muscle. *Annals of Biomedical Engineering*, 31(3):310–317, Mar 2003.
- [68] MATLAB. *version 9.3.0.713579 (R2017b)*. The MathWorks Inc., Natick, Massachusetts, 2017.
- [69] Juan Gómez and Enrique Baeyens. Identification of block-oriented nonlinear systems using orthonormal bases. 14:685–697, 09 2004.
- [70] A. Mbarek, H. Messaoud, and G. Favier. Robust predictive control using kautz model. In *10th IEEE International Conference on Electronics, Circuits and Systems, 2003. ICECS 2003. Proceedings of the 2003*, volume 1, pages 184–187 Vol.1, Dec 2003.
- [71] Wikipedia contributors. Muscle contraction - Wikipedia, the free encyclopedia, 2018. [Online; accessed 26-June-2018].
- [72] Jun Zhong, Jizhuang Fan, Yanhe Zhu, Jie Zhao, and Wenjie Zhai. Static modeling for commercial braided pneumatic muscle actuators. *Advances in Mechanical Engineering*, 6:425217, 2014.

# Glossary

CDPR Cable-Driven Parallel Robot. [3](#)

FF Feed-Forward. [71](#), [72](#), [74](#), [82](#)

IPK Institute for Production Systems and Design Technology. [3](#)

PAM Pneumatic Artificial Muscle. [2](#), [3](#), [5](#), [7–13](#), [15](#), [19–21](#), [23](#), [25–28](#), [33](#), [36](#), [37](#), [39](#), [41](#), [49](#), [51](#), [54](#), [62](#), [63](#), [65](#), [71](#), [74](#), [81](#), [89](#)

PID Proportional-Integral-Derivative. [71](#), [72](#), [82](#)



# List of Figures

1.1	Biorobotic applications of PAMs	2
1.2	Medical applications of PAMs	3
1.3	STRING-MAN configuration	4
1.4	Integrated Wire-Robot – PAMs active weight balancing module	4
2.1	Operation at constant load	8
2.2	Operation at constant pressure	8
2.3	PAM's isobaric force contraction diagrams	9
2.4	Biological skeletal muscle shapes	9
2.5	Relationship between force and length for various animals and a McKibben actuator	10
2.6	Agonist-antagonist connection of biological muscles	10
2.7	Agonist-antagonist connection of artificial muscles for linear motion	11
2.8	Agonist-antagonist connection of artificial muscles for rotational motion	11
2.9	Braided muscles	12
2.10	Sleeved muscle	12
2.11	Pleated muscle	13
2.12	Yarlott muscle	13
2.13	ROMAC muscle	14
2.14	Kukolj's muscle	14
2.15	Morin muscle	14
2.16	Baldwin muscle	15
2.17	Paynter's muscle	15
2.18	Kleinwachter torsion device	15
2.19	Pneumatic muscle manufactured by FESTO	16
2.20	Cross-section of FESTO fluidic muscle	16
2.21	Some applications of FESTO pneumatic muscle recommended from producer	17
3.1	Schematic of geometrical relations of braided muscle	20
3.2	Schematic of geometrical relations of braided muscle with frustum cone endings	21
3.3	Upgraded geometrical relations schematics	22
3.4	Schematic of deformation strains of membrane	24
3.5	Edge surfaces	25
3.6	Spring model of PAM	25
3.7	Hill model	26
3.8	Three-element model	27
3.9	Hammerstein model block diagram	28
4.1	Experimental setup draft	30
4.2	Fluidic Muscles DMSP-40 manufactured by <i>FESTO</i>	31
4.3	Manufactured rack for mounting weights	31
4.4	Force sensor	32
4.5	Proportional valve	32
4.6	Position sensor	33
4.7	Inductive sensors with 3D printed extensions	33
4.8	Expansion box	34
4.9	dSPACE Board box	34
4.10	Experimental setup	35
4.11	Contraction types	36
4.12	Isotonic curves DMSP-40-1000N - Contraction	37

4.13 Isotonic curves DMSP-40-1000N - Diameter . . . . .	37
4.14 Isotonic curves DMSP-40-1000N with hysteresis - Contraction . . . . .	38
4.15 Isotonic curves DMSP-40-1000N with hysteresis - Diameter . . . . .	38
4.16 Isotonic curves DMSP-40-290N - Contraction . . . . .	39
4.17 Isotonic curves DMSP-40-290N with hysteresis - Contraction . . . . .	39
4.18 3-D representation of experimental results DMSP-40-1000N . . . . .	40
4.19 3-D representation of experimental results DMSP-40-290N . . . . .	40
4.20 Isobaric curves DMSP-40-1000N . . . . .	41
4.21 Isobaric curves with hysteresis DMSP-40-1000N . . . . .	41
4.22 Interpolation of length-pressure-force relationship . . . . .	42
4.23 Isometric curves DMSP-40-1000N . . . . .	42
4.24 Models for the virtual area DMSP-40-1000N . . . . .	44
4.25 Models for the radial expansion force DMSP-40-1000N . . . . .	44
4.26 Comparison between experimental results and the model DMSP-40-1000N . . . . .	45
4.27 Models for the virtual area DMSP-40-290N . . . . .	45
4.28 Models for the radial expansion force DMSP-40-290N . . . . .	46
4.29 Comparison between experimental results and the model DMSP-40-290N . . . . .	46
4.30 Comparison between experimental results and "Virtual Area" model I . . . . .	47
4.31 Comparison between experimental results and "Virtual Area" model II . . . . .	48
4.32 Plot of unstretched length against air pressure DMSP-40-1000N . . . . .	49
4.33 Stiffness parameter K over pressure/load combinations DMSP-40-1000N . . . . .	49
4.34 Plot of unstretched length against air pressure DMSP-40-290N . . . . .	50
4.35 Stiffness parameter K over pressure/load combinations DMSP-40-290N . . . . .	50
4.36 Comparison between experimental results and "Spring" model I . . . . .	51
4.37 Comparison between experimental results and "Spring" model II . . . . .	52
4.38 Comparison between experimental results and "McKibben" model1 . . . . .	53
4.39 Comparison between experimental results and "McKibben" model II . . . . .	54
4.40 Comparison between experimental results and "McKibben II" model I . . . . .	55
4.41 Comparison between experimental results and "McKibben II" model II . . . . .	56
4.42 Comparison between experimental results and "Improved McKibben" model - DMSP-40-1000N I . . . . .	57
4.43 Comparison between experimental results and "Improved McKibben" model - DMSP-40-1000N II . . . . .	58
4.44 Comparison between experimental results and "Improved McKibben" model - DMSP-40-290N I . . . . .	58
4.45 Comparison between experimental results and "Improved McKibben" model - DMSP-40-290N II . . . . .	59
4.46 Cross-validation "long-to-short" I . . . . .	60
4.47 Cross-validation "long-to-short" II . . . . .	61
4.48 Cross-validation "short-to-long" I . . . . .	61
4.49 Cross-validation "short-to-long" II . . . . .	62
4.50 Comparison between experimental results and model at pressure 0.5bar . . . . .	64
4.51 Comparison between experimental results and model at pressure 1bar . . . . .	64
4.52 Dynamic tests - velocity variation - Pressure/Contraction . . . . .	65
4.53 Dynamic tests - velocity variation - Diameter/Force . . . . .	65
4.54 Dynamic tests - load variation - Pressure/Contraction . . . . .	66
4.55 Dynamic tests - load variation - Diameter/Force . . . . .	66
4.56 Dynamic vs Static at load equals 10kg . . . . .	67
4.57 Dynamic vs Static at load equals 30kg . . . . .	67
4.58 Dynamic vs Static at load equals 60kg . . . . .	68
5.1 Simulink model of the FESTO pneumatic muscle . . . . .	69
5.2 Simulink model of perimetric elastic deformation force . . . . .	70
5.3 Simulink model of length direction elastic deformation force . . . . .	70
5.4 Simulink model of McKibben force . . . . .	70
5.5 Reference and actual pressure of the valve at the cut-off frequency . . . . .	71

---

5.6 Control System Designer - Bode diagram . . . . .	73
5.7 Control System Designer - Step Response . . . . .	73
5.8 Control System Designer - Root Locus . . . . .	73
5.9 Simulation block diagram of the closed loop system . . . . .	74
5.10 Reference and output position values - 20kg/15cm . . . . .	75
5.11 Position error values - 20kg/15cm . . . . .	75
5.12 Reference and output position values - 40kg/15cm . . . . .	76
5.13 Position error values - 40kg/15cm . . . . .	76
5.14 Reference and output position values - 80kg/15cm . . . . .	77
5.15 Position error values - 80kg/15cm . . . . .	77
5.16 Reference and output position values - 20kg/5cm . . . . .	78
5.17 Position error values - 20kg/5cm . . . . .	78
5.18 Reference and output position values - 40kg/5cm . . . . .	79
5.19 Position error values - 40kg/5cm . . . . .	79
5.20 Reference and output position values - 80kg/5cm . . . . .	80
5.21 Position error values - 80kg/5cm . . . . .	80



# List of Tables

4.1	Values of coefficient K for DMSP-40-1000N . . . . .	51
4.2	Values of the coefficient K for DMSP-40-290N . . . . .	51
4.3	Values of coefficient for E(L/L0) . . . . .	56
4.4	Coefficients for improved geometrical model . . . . .	63
4.5	Values of speed and acceleration of referent pressure trajectories . . . . .	66
5.1	PID gains . . . . .	72